Mathematical and computational modelling of skin biophysics – A review.

Georges Limbert [a, b]

[a] national Centre for Advanced Tribology at Southampton (nCATS) | Bioengineering Science Research Group, Faculty of Engineering and the Environment, University of Southampton, Southampton SO17 1BJ, United Kingdom
[b] Biomechanics and Mechanobiology Laboratory, Biomedical Engineering Division, Department of Human Biology, Faculty of Health Sciences, University of Cape Town, Anzio Road, Observatory 7925, South Africa

Abstract

The objective of this paper is to provide *a* review on some aspects of the mathematical and computational modelling of skin biophysics, with special focus on constitutive theories based on non-linear continuum mechanics from elasticity, through anelasticity, including growth, to thermoelasticity. Microstructural and phenomenological approaches combining imaging techniques are also discussed. Finally, recent research applications on skin wrinkles will be presented to highlight the potential of physics-based modelling of skin in tackling global challenges such as ageing of the population and the associated skin degradation, diseases and traumas.

Keywords: skin, biological soft tissue, biophysics, modelling, finite element, microstructure, continuum mechanics, elasticity, viscoelasticity, plasticity, growth, thermoelasticity, damage, contact, tribology, homogenisation, multiscale, *stratum corneum*, epidermis, dermis, hypodermis, surface instability, wrinkle.

Invited review

Accepted for publication in **Philosophical Transactions of the Royal Society of London Part A** (June 21 2017)

Structure of the paper

1. Introduction

Besides the brain, no other organ of the human body plays such a central role in our everyday biological *and* social life than the skin. The skin is the first line of defence of our body against the external environment, and therefore, acts as a primary and essential physical interface. This interface controls many types of exchanges between our inner and outside worlds which take the form of mechanical, thermal, biological, chemical and electromagnetic processes. These processes typically do not operate in isolation but are rather parts of a very dynamic system featuring complex non-linear feedback mechanisms [1, 2]. At a secondary, but nonetheless very important exchange level, the skin is not only a sort of social sign post that tells a story about us, but also a fundamental active social instrument that is pivotal in how we socially interact with our fellow humans, through conscious and unconscious communication cues [3]. The skin is also a biochemical plant that synthesises vital compounds like vitamin D, hosts vital immunologic biochemical and cellular processes, and contains a rich sensory biophysical network that informs us in real-time of any haptic cues or potentially threatening physical insults and noxious agents [1, 3].

Considering the place of the skin in our life and its multiple physiological functions, from genesis to death, understanding its complex physiology and biophysics in health, disease and trauma has become, particularly in the last two decades, a broad research arena. Interdisciplinary scientists, engineers and clinicians join forces to improve health, quality of life, design products that are easier and more comfortable to use or help us to slow down the signs of ageing by developing innovative surgical cosmetic procedures and skin care pharmaceutical compounds.

As in many branches of life sciences, be it in academia or industry, physics-based modelling of the skin has become an integral part of research and development. Nowadays, advanced numerical simulations, typically relying on finite element [4] and/or meta-modelling techniques [5], are used in the rational design of products intended to interact with the skin, from razors and incontinence nappies through respiratory masks and medical surfaces to running shoes, vehicle interiors and tactile electronic surfaces. At a more fundamental level, and as hypothesis-driven research tools, mathematical and computational models of the integument are developed to shed light on the biophysical complexity of skin physiology and to unravel particular mechanobiological aspects associated with diseases and the ageing process. This focus is particularly relevant for medical, pharmaceutical and cosmetic sciences.

Jor *et al.* [6] provided an excellent review discussing the current (as of 2013) and future challenges of the computational modelling and experimental characterisation of skin mechanics. These authors highlighted the need for tight integration of modelling, instrumentation and imaging. They also recommended that focus should be directed toward the development of *in vivo* quantitative characterisation techniques so that research could be more seamlessly translated into the clinical setting. Recently, Li [7] conducted a short review of modelling approaches for the description of *in vitro* biomechanical properties of the skin. He concluded that major research efforts should be devoted to the development of constitutive models of skin capable of accounting for viscoelastic effects, damage and fracture. Although Jor *et al.* [6] and Li [7] reviewed some popular constitutive models of the skin, no attempt was made to provide an extensive, detailed and *unified* review of formulations capable of representing the finite strain and anisotropic behaviour of skin, from elasticity through anelasticity to damage and growth.

Here, it is proposed to address this current shortcoming. The objective of this paper is to provide *a* review on some aspects of the mathematical and computational modelling of skin biophysics with special focus on theories based on the powerful constitutive framework offered by non-linear continuum mechanics [8-10]. As in any review paper, there is a natural bias towards the topics covered which stems from the author's personal research but, here, it is hoped that the treatment of the subject is sufficiently general and high-level to appeal to a broad range of scientists and engineers, particularly those involved in interdisciplinary skin research. The ambition is to present *a* selection of state-of-the-art skin models that are presently used in academic and industrial research, inform about the attractive prospects offered by biophysical modelling, highlight less well-known areas where the modelling of skin can address important scientific questions and practical engineering challenges. Ultimately, the aim is to stimulate cross-fertilising of ideas and techniques, to encourage researchers from diverse scientific background to engage dialogue within their communities and outside, particularly with clinicians and biologists. More generally, the review should also be of interest to researchers involved in the modelling of biological soft tissues.

2. Basic structural anatomy and biophysical characteristics of the skin

2.1 Structural anatomy

In mammalian species, the skin is part of the integumentary system that includes the skin itself as the largest organ of the body in terms of surface, and various appendages such as hair, nails and hooves, nerve receptors and glands. In humans, the skin—which can be considered as a membrane—accounts for up to 16% of an adult's total body weight whilst covering an average surface area of about 1.6 m^2 [11]. As alluded to in the **Introduction section**, the skin is a very complex biological system featuring a multitude of coupled physical processes acting in concert, or sequentially, as for instance, in the case of wound healing where a cascade of biochemical and mechanobiological events is triggered by an injury [12]. From the mechanical and material science point of view, the skin is primarily a multiphasic and multiscale structure which, as a result, encompasses a rich set of mechanical properties and constitutive behaviours [13, 14]. The biological nature of this structure renders these properties very dynamic, particularly over a life time, and like most biological tissues, there is a strong variability according to body site, individuals, age, sex, ethnicity and exposure to specific environmental conditions [15, 16]. At the meso-macroscopic level, skin is generally considered as a multi-layer assembly made up of three main distinct structures: the epidermis, dermis and hypodermis (**Figure 1**) [11, 14, 17, 18].

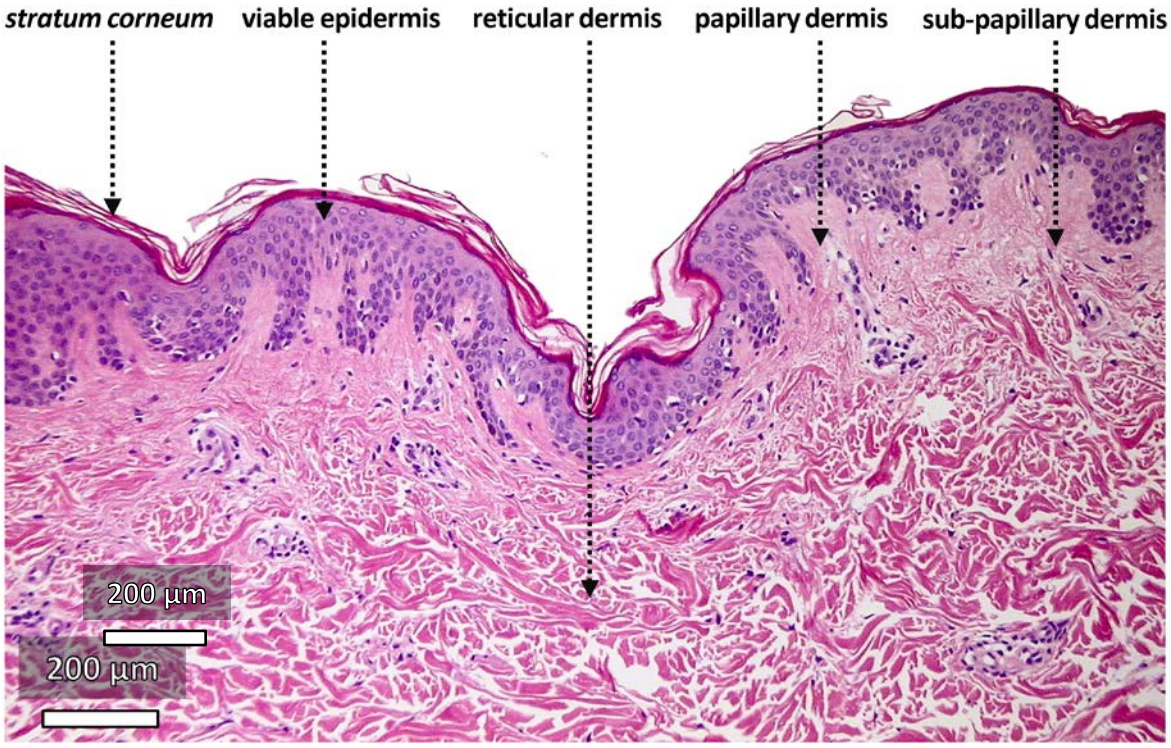

Figure 1. Histological section of haematoxylin and eosin stained back human skin sample obtained from a 30 years-old healthy White Caucasian female volunteer following biopsy (10 x magnification, image resolution: 1600 x 1200 pixels, imaged using a modified Nikon E950 camera). Image courtesy of Dr. Maria-Fabiola Leyva-Mendivil (University of Southampton, UK).

The epidermis—which is avascular—is a terminally differentiated stratified squamous epithelium about 200 µm thick. 95% of the cells contained in the epidermis are keratinocytes which undergo mitosis at the 0.5-1 µm thick epidermal basement membrane (also known as *basal lamina*) [19]. From this basement membrane which separates the epidermis from the dermis, the cells subsequently migrate from towards the skin surface, forming four main well delineated layers during their transit, namely the *stratum basale* (also called the *stratum germinativum*), the *stratum spinosum*, the *stratum granulosum* and *the stratum corneum*. This latter layer consists of a one to three cell-thick layer of dead keratinocytes representing a 15 to 30 thickness µm. The epidermis includes other cells such as melanocytes, Langerhans's cells and Merkel cells [11]. The complex formed by the living epidermis at the exclusion of the *stratum corneum* is called the living or viable epidermis.

The ***stratum corneum*** is the prime line of defence against external threats be they mechanical, thermal, chemical, electromagnetic or biological. In particular, the mechanical properties of the *stratum corneum* are key in conditioning transmission of loads and subsequent deformations of the other underlying skin layers across several spatial scales [20, 21]. These purely mechanical aspects are essential for certain biophysical processes such as the stimulation of mechano-receptors that transduce mechanical energy into neural signalling (e.g. tactile perception [22] and pain [23]) or mechanobiological transduction involved in metabolic processes (e.g. homoeostatic regulation of the skin barrier function [24]).

Any variation in the mechanical properties of the stratum corneum—like those occurring daily as a results of fluctuations in internal and external environmental conditions (e.g. relative humidity, temperature) [25]—is likely to affect the material mechanical response and also the subsequent altered external surface topography. This has obvious consequences for the tribological response of the skin [21].

The **living epidermis** is connected to the underlying dermis through a three-dimensional (3D) interlocking wavy interface, called the dermal-epidermal junction (DEJ) which is the *basal lamina* evoked earlier. Papillae are the protrusions of the papillary dermis into the epidermis (**Figure 1**). These finger-like structures increase the contact surface area between the reticular dermis and the living epidermis, and are thus believed to favour biochemical mass exchanges between these layers e.g. transport of oxygen or nutrients [19, 26, 27]. The DEJ controls the transit of biomolecules between the dermis and epidermis according to their dimension and charge. It allows the passage of migrating and invading cells under normal (i.e. melanocytes and Langerhans cells) or pathological (i.e. lymphocytes and tumour cells) conditions [27]. The behaviour of keratinocytes is influenced by the DEJ via modulation of cell polarity, proliferation, migration and differentiation.

As principally constituted of a dense array of crimped stiff collagen fibres, the **dermis** is the main load-bearing structural component of the skin when subjected to tension-inducing loads (e.g. in-plane tension, out-of-plane indentation and suction). It is 15 to 40 times as thick as the epidermis [11] and much thinner on the eyelids than on the back. The dermis can be decomposed into three main layers: the papillary layer juxtaposed to the epidermis, the sub-papillary layer underneath and the reticular layer which is connected to the underlying subcutaneous tissue. The papillary layer is defined by the rete ridges protruding into the epidermis and contains thin collagen fibres, a rich network of blood capillaries, sensory nerve endings and cytoplasms. The sub-papillary layer which is the zone below the epidermis and papillary layer features similar structural and biological components to the papillary layer. Besides a dominant content of types I and III collagen (respectively 80 and 15% of total collagen content), the reticular layer is innervated and vascularised, contains elastic fibres (e.g. elastin) and the dermal matrix made of cells in the interstitial space. Cells present in the reticular dermis include fibroblasts, plasma cells, macrophages and mast cells.

Collagen fibres account for approximately 70% of the weight of dry dermis. Collagen fibres in the papillary and sub-papillary dermis are thin (because of their low aggregate content of fibrils) and sparsely distributed while reticular fibres are thick, organised in bundles and densely distributed. Fibrils are typically very long, 100 to 500 nm in diameter featuring a cross striation pattern with a 60 to 70 nm spatial periodicity. The diameter of thick collagen bundles can span 2 to 15 μm. Birefringence techniques are promising tools to characterise the orientation and supramolecular organisation of collagen bundles in skin [28].

The **dermal matrix** is composed of an extra-cellular matrix, ground substance which is a gel-like amorphous phase mainly constituted of proteoglycans and glycoproteins (e.g. fibronectin) as well as blood and lymph-derived fluids which are involved in the transport of substances crucial to cellular and metabolic activities. Proteoglycans are composed of multiple glycosaminoglycans (i.e. mucopolysaccharides) interlaced with back bone proteins. Dermal fibroblasts produced glycosamine which is rich in hyaluronic acid and therefore plays an essential role in moisture retention.

Unlike collagen fibres, **elastic fibres** are extremely elastic and can fully recover from strains in excess of 100% [29]. Their diameter ranges between 1 and 3 μm. Their mechanical entanglement with the collagen network of the dermis is what gives the skin its resilience and recoil ability. This is evidenced by the correlation between degradation of elastin/abnormal collagen synthesis associated with ageing and the apparent stiffening of the dermis [30]. The diameter of elastic fibres in the dermis is inversely proportional to their proximity to the papillary layer where they tend to align perpendicular to the DEJ surface.

The **subcutaneous tissue** is the layer between the dermis and the fascia which is a band of connective tissue, primarily collagen, that attaches, stabilises, encloses, and separates muscles and other internal organs. The thickness of subcutaneous tissue is highly variable intra- and inter-individually. This layer is mainly composed of adipocytes. Its role is to provide mechanical cushioning, heat generation and insulation as well as a reserve of nutrients.

A very important aspect of skin mechanics is that, *in vivo*, skin is in a state of complex in-plane heterogeneous tension patterns which depend on individuals, their age, body location and position. This was first evidenced by French anatomist and military surgeon Baron Guillaume Dupuytren (1777-1835) who, incidentally, also gave his name to a proliferative connective tissue disorder, the Dupuytren's contracture. In 1834, Dupuytren examined the chest of a man who had stabbed himself with a round-tipped awl in a failed suicide attempt, and noticed that the inflicted wounds were elliptical and not circular [31-33]. Later, in 1838, French surgeon and medical historian Joseph-François Malgaigne (1806-1865) reported that this type of elliptical wound patterns were oriented differently according to body location. Although these two surgeons had discovered the existence of tension lines *in vivo*, it was the Austrian anatomist Karl Langer (1819-1887) [31-33] who provided a sound explanation and comprehensive anatomical basis by conducting a large number of punctures on cadavers, using a round awl, and meticulously mapping the direction and dimensions of the created elliptical wounds on the body. Because these experiments were conducted on cadavers with extremities in extension, Langer observed that tension lines varied with the position of the cadaver. Real *in vivo* conditions are also likely to differ from cadaveric conditions because of *rigor mortis* which stiffens muscles and joints. Moreover, tension lines are also dependent upon skin dysfunctions and diseases such as the Elhers-Danlos syndrome.

2.2 Mechanical properties of the skin

In light of the skin anatomy described above, and, as will be discussed in the next section in more details, depending on the spatial scale considered, the skin can be viewed as a structure or material (i.e. a homogeneous structure). Here, in this brief review of mechanical properties, we will mainly focus on the latter. Due to its characteristic dimensions and interfacial nature, the skin is often described as a membrane in the general sense. From the mechanical point of view, it would be more accurate to describe it as a multi-layer shell structure because it possesses a non-negligible bending stiffness despite mainly sustaining membrane strains.

Due to its significant thickness compared to that of the *stratum corneum* and viable epidermis, combined with its high content in collagen fibres, the dermis is the main contributor to the tensile mechanical properties of the skin. The intricate fibrous collagen architecture of the dermis and its close mechanical connectivity to elastin fibres lead to anisotropic and non-linear macroscopic mechanical properties which is consistent with the strain stiffening effect typically observed in biological soft tissues under tension [8].

Here, it is important to point out and recognise that the *measured* mechanical anisotropy of the skin is not only due to the structural characteristics of the skin layers and their microstructural constituents but is also the result of its mechanical interplay with the Langer lines. In-plane anisotropy of the skin is correlated with the distribution and orientation of Langer lines [34] while out-of-plane (or across-the-thickness) anisotropy is due to the distinct mechanical properties and complex 3D structure of the skin layers. This presents a number of challenges for the experimental characterisation of the mechanical properties of skin [6, 35] as well as their mathematical and computational realisation. Intuitively, one would expect that the inclusion or not of pre-stress/pre-strain in a mathematical or computational model of the skin would significantly influence its mechanical response. Flynn et al. [36, 37] determined a relation between the *in vivo* relaxed skin tension lines (RSTL) on a human face and the directional dependency of the skin stiffness using a combination of contact measurement techniques and inverse finite element methods. These authors demonstrated the need to account for these tension lines in the characterisation of the anisotropic properties of the human skin. Recently, Deroy *et al.* [38] developed a non-destructive and non-invasive experimental protocol based on elastic surface wave propagation to determine the orientation of skin tension lines. The method was validated on canine cadaveric specimens. The Cutiscan CS 100® (Courage-Khazaka Electronic GmbH, Köln, Germany) is a device offering the possibility of qualitatively measuring mechanical anisotropy of the skin *in vivo* [39].

A variety of methods have been used to measure the mechanical properties of skin: e.g. uniaxial and biaxial tensile tests [34, 40-42], multiaxial tests [13, 43], application of torsion loads [44], indentation [45], suction [39, 46-49] and bulge testing [50]. More recent techniques have focused on the experimental characterisation of the mechanical properties of the epidermis [51-53] which are particularly relevant for cosmetic and pharmaceutical applications. Beside intra- and inter-individual biological variability as well as sensitivity to environmental conditions, the nature of these experimental techniques combined with their operating spatial scale (e.g. macroscopic or cellular levels) are the main reasons there is a such a wide variability in mechanical properties reported in the literature. Differences for the mechanical properties of the skin or those of its individual layers can span several order of magnitude (see **Table 1** in [20]).
Given its complex hierarchical structure, and like most soft tissues, the skin exhibits a wide range of viscoelastic phenomena including creep, relaxation, hysteresis [16, 40, 54, 55] and strain rate dependency [42].

3. Modelling of the skin

3.1 General considerations

The review of the structural and macroscopic mechanical properties of the skin in the previous section have highlighted three main characteristics, namely, non-linear behaviour, structural non-homogeneity and mechanical anisotropy. The first task in any constitutive modelling endeavour is to assess the "why" of the constitutive model. Why do we need a model? What are the answers we are looking for? What are the hypotheses we want to assess? Do we want to be *predictive* or simply *descriptive*? What are the operating conditions we need to account for? Can we practically design a physical experiment or a series of experiments that will inform the mathematical formulation of the constitutive equations and allow us to extract constitutive parameters so we can exploit the constitutive model?
The formulation of any constitutive model must be designed in the light of the intended application, which means that the model will have to rely on a number of (simplifying) assumptions that will discard certain aspects of the physical system (e.g. heterogeneous microstructure, time-dependent behaviour, large strains) whilst accounting for others. For example, for studying the transport of drug through the skin it would be highly relevant to account for the geometry and porous nature of the microstructure of the relevant skin layers. If biochemical aspects such as molecular water binding to collagen were of interest, then models and techniques capable of representing these atomic/molecular scale phenomena would be appropriate. In these conditions, using a finite strain model would be "overkill" as only very small strains would be expected. If one were to investigate the failure of skin in traumatic situations (e.g. vehicle accident) it would be essential to avail oneself with a model capable of describing the large strain and failure behaviour of the tissue.

3.2 Classification of constitutive models

Mathematical and computational models of the skin can be classified into three main categories: ***phenomenological***, ***structural*** and ***structurally-based phenomenological*** models.

Phenomenological models are based on the assumption that the skin is a homogeneous material where the microstructure and multiple phases as well their associated mechanical properties are ignored These phenomenological models aim to capture the overall—generally macroscopic—behaviour of the tissue without accounting for the individual behaviour of its elemental constituents and their mutual interactions [56]. Typically, if one considers mechanical behaviour only, a phenomenological model is a set of mathematical relations that describe the evolution of stress as a function of strain [8]. Provided the formulation is appropriate, it is generally always possible to fit such a constitutive law to a set of experimental data. However, the main drawback of this approach is that the resulting constitutive parameters often do not have a direct physical interpretation, and the model effectively acts as a "black box" without the flexibility of integrating and studying mechanistic structural effects.
Structural models of the skin represent the tissue as a composite material made of an *explicitly* defined assembly of key microstructural elements (e.g. collagen fibres arranged in bundles with a certain degree of crimp and dispersion, within a matrix mainly composed of proteoglycans). The way these structural elements interact can also be specified by developing appropriate equations (e.g. mutual shear interactions of collagen fibrils and fibres or small-range electromagnetic interactions between proteoglycans and collagen fibres [57]).

In this approach, not only the mechanical properties of the individual basic structures need to be determined or known but also the way they are geometrically arranged to form the macroscopic tissue, and how they interact mechanically, thermally or through any other type of physics. The overall mechanical properties of the tissue are the result of this—generally nonlinear— coupling between geometry and mechanics. Structural models can be viewed as geometrical assemblies of phenomenological models. For this reason, one could argue that, strictly speaking, structural models are not fully structural, and that classification as a structural or phenomenological model is a matter of spatial scale. Only if models are built *ab initio* from the first principles of quantum chemistry could one talk about structural models. In that respect, the constitutive parameters of phenomenological models describing the behaviour of elemental microstructural components may also not have a direct physical interpretation but, typically, they do. For example, if collagen fibres are part of the formulation, their elastic modulus, waviness and degree of dispersion around a main orientation are indeed constitutive parameters with have a direct physical interpretation. One of the main drawbacks of structural models lays in the necessity to have accurate information about the geometrical and material characteristics of each elemental building block as well as their mutual spatial and interfacial arrangement. This presents obvious experimental characterisation challenges which, however, are progressively overcome as technologies in this field improve, and new techniques emerge. Moreover, in a computational finite element environment, structural models spanning several orders of magnitude in terms of length scale require significantly high mesh density to explicitly capture the geometry of the structural constituents. Inevitably, despite tremendous advances in the computing power of modern processors, this can lead to prohibitively computationally expensive analyses and lengthy run times.

A judicious compromise between strictly phenomenological and structural models is a third-class of models, formulated by combining certain characteristics of phenomenological models to those of structural ones. These models could be denoted under the general appellation of ***structurally-based phenomenological models*** or ***structurally-based continuum models***. The continuum composite approach of Spencer is a good example of that idea [58]. In this type of constitutive formulation for fibre-reinforced composite materials, fibres are not explicitly modelled at the geometric level but their mechanical contribution to the overall (i.e. continuum) behaviour is implicitly accounted for by strain energy density terms directly related to microstructural metrics (e.g. stretch along the fibre direction). Nowadays, models adopting this type of constitutive hypotheses dominate the published literature as they have been very successful at representing the biomechanics of many biological tissues [9, 10]. The mathematical formulation of these models can be viewed as mutltiscale in the general sense as it accounts for structural geometrical/mechanical features/effects arising from a smaller spatial scale than that at which the gross physical response is represented in a continuum sense. Multiscale formulations in the homogenisation theory/computational mechanics sense are also possible but require more advanced finite element formulations for practical calculations [59, 60].

It appears that over the last fifteen years there has been a significant thrust in the biomechanics community to delve into this under-researched topic that is skin biophysics. This possibly stems from the academic potential to deliver novel research with high impact which is intimately correlated to the drive to address growing research needs in many industrial sectors such as personal care and consumer products, cosmetics and biomedical devices. Like what happened in the communities of orthopaedic, dental and cardiovascular clinicians, the new generations of reconstructive surgeons and dermatologists are progressively acknowledging and embracing the potential and key role that computational modelling can play in improving and optimising treatment procedures. An attractive feature of computational models is the ability to quantify physical parameters required to obtain a specific outcome. For example, Prof. Kuhl's group at Stanford University has pioneered the development of mechanobiological adaptation models for skin to optimise the outcome of reconstructive surgery procedures in children [61-67] (see **Supplementary Material section 1.10**).

3.3 Image-based microstructural models of the skin: principles and applications

Given the hierarchical nature of the structure of biological tissues, especially the skin, capturing certain key aspects of their microstructure in computational models opens up the possibility of conducting hypothesis-driven research about the links between their structure and function [8] in a very systematic and mechanistic way. One can isolate and study the influence of certain microstructural and/or material parameters on the global response of the system [20, 21, 68] to formulate hypotheses and theories that can further our fundamental understanding of skin physiology and also assist in the design of physical experiments.

According to the classification of models presented in the previous section, image-based models could be best described as computational (micro)structural models where the constitutive model used for representing the material behaviour of each substructure could be a phenomenological, structural or structurally-based phenomenological model. Image-based modelling has become ubiquitous in many research domains where capturing complex multiphasic structures at various length scales is essential for conducting physics-based numerical analyses [69]. In the context of biological tissues and structures, any type of imaging modalities (1D, 2D, 3D, 4D) can be used including digital optical photography [20], computed tomography [70], magnetic resonance imaging [71] and laser confocal microscopy [72].
Developing an image-based computational model is the process of acquiring the geometry of a physical system through a single or a combination of imaging modalities, bring it into the digital world under the form of a picture or a series of pictures, conduct image-processing on these files to identify and isolate regions of interest (i.e. segmentation) (e.g. distinct skin layers) and mesh these digital regions into finite elements so that the partial differential equations governing the physics considered could be solved using the finite element method (**Figure 2**).

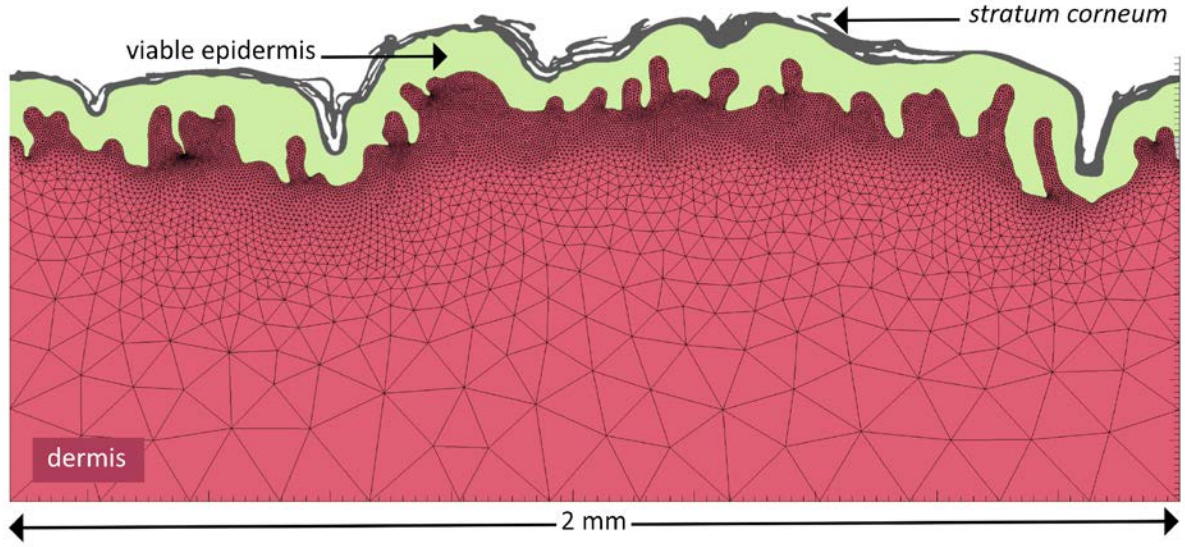

Figure 2. Image-based microstructural finite element model of a cross section of human abdominal skin obtained from a 30 years-old healthy white Caucasian female patient following biopsy [adapted from Leyva-Mendivil et al. [20]]. Series of digital images of histological sections that had been stained with haematoxylin and eosin were acquired using Nikon E950 camera (Nikon UK Ltd, Kingston Upon Thames, UK) mounted on an optical microscope at 10 times magnification (digital sensor resolution 1600 x 1200 pixels). Each histological section was imaged several times by moving the plate. The series of images were subsequently stitched together in a software environment (GIMP, www.gimp.org) by aligning each image with the next one, ensuring correct overlapping and alignment. The resulting composite image was then exported as a single PNG file into the image processing environment of ScanIP ® 6.0 (Simpleware, Synopsys, Exeter, UK) where three regions of interest (stratum corneum, viable epidermis and dermis) were identified and segmented using a simple threshold-based algorithm. The three masks corresponding to the segmented anatomical regions were then meshed using bilinear triangular finite elements within ScanIP®. To capture the geometrically-complex microstructures as well as the large aspect ratio between the largest and smallest dimensions, whilst ensuring a minimum number of finite elements, an adaptive mesh refinement algorithm was used. Because of their high densities, the meshes of the *stratum corneum* and viable epidermis layer are not plotted.

Image-based microstructural finite element models of the skin can provide unique insights into the interplay between material and structural properties of the skin even when considering 2D geometries. Leyva-Mendivil et al. [20] unveiled and quantified structural folding mechanisms driven by the mechanics of the *stratum corneum* in combination with its intricate surface topography when the skin is subjected to plane-strain compression (**Figure 3**). It was shown that *macroscopic* strains may significantly be modulated at the *microscopic* (i.e. local) level. The convoluted shape of the *stratum corneum* can effectively acts as a strain reducer. These authors subsequently used a similar approach to show that the *macroscopic* coefficient of friction between the skin and a rigid slider moving across its surface is noticeably higher that the *local* coefficient of friction applied as an input parameter to the finite element analyses [21].

This demonstrated that the deformation-induced component of skin friction is significant unlike what has been widely assumed in the tribology community [73-77] where adhesion-induced friction is deemed to be the dominant contributor to macroscopic friction. Similar observations were made in a similar computational contact homogenisation study by Stupkiewicz *et al.* [78]: geometrical effects alone can have a significant impact on the macroscopic frictional response of elastic contacts. To date, despite much experimental and modelling studies investigating shear stress at the surface of the skin in relation to skin injuries and pressure ulcers [51, 53, 79], very little efforts have been made to develop methodologies to gain a more accurate and mechanistic understanding of how shear stresses are induced at the level of skin microrelief asperities and how they propagate from the skin surface to the deeper layers where they are likely to mechanically stress living cells. Ultimately, excessive stress or strain can lead to cell damage and death, which, at a meso/macroscopic level translates into tissue damage and loss of structural integrity. An image-based finite element study was recently conducted by Leyva-Mendivil *et al.* [68] to investigate these aspects and demonstrated again the importance of accounting for skin microstructure in this type of study.

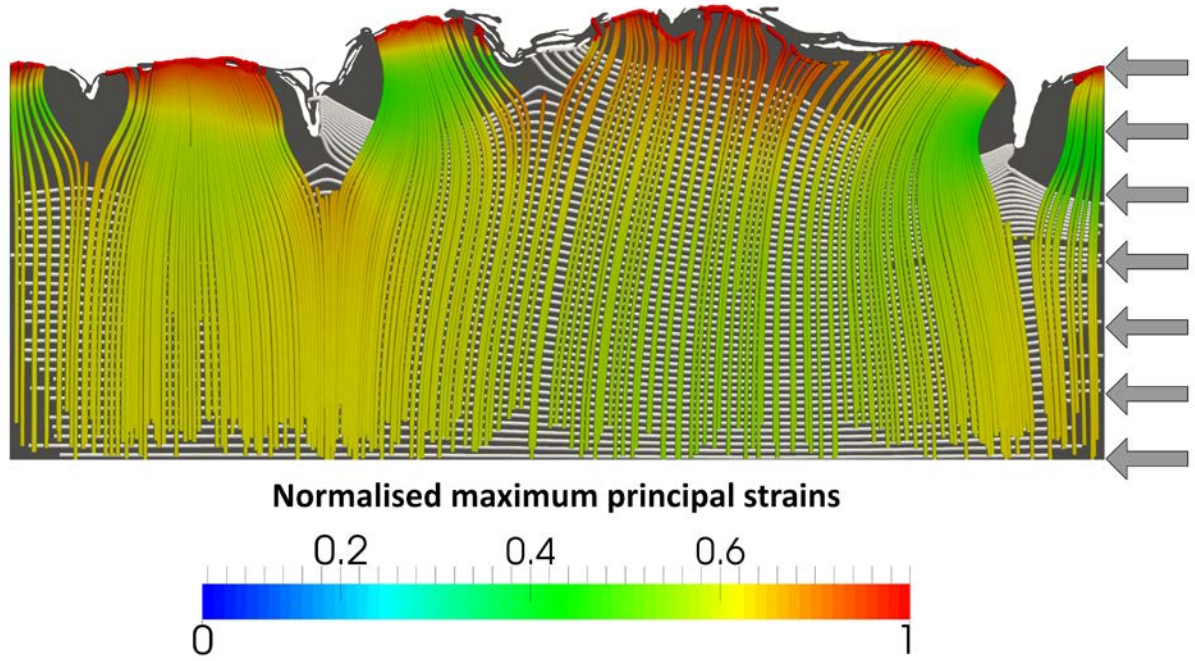

Figure 3. Streamline plots representing the maximum (coloured) and minimum (white) principal strain vectors in a finite deformation 2D plane-strain image-based finite element model of the skin subjected to 20% in-plane compression (adapted from [20]). Grey arrows indicate the direction and location of the applied load. Streamlines, which are here overlaid over the *undeformed* geometry of the cross section of skin, allow direct visualisation of load/strain paths within the skin as a result of any type of applied load. They are therefore very valuable, for example, to understand how deep and in which directions, loads are transmitted/deflected from the skin surface to/from the underlying layers in response to contact interaction with an external object.

4. Constitutive models of the skin

Here we present what are considered state-of-the-art mechanical constitutive models of the skin. The focus is on non-linear elasticity and viscoelasticity theories. In the **Supplementary Material section**, plastic effects [80], softening and damage [81], recent coupled thermomechanical [82] as well as mechanobiological models for growth [64] will be presented. Other types of constitutive laws such as chemo-mechanobiological models of wound healing [12, 83-85] are beyond the scope of the present review.

4.1 Basic continuum mechanics for anisotropic hyperelastic solids

Non-linear continuum mechanics provides a flexible mathematical framework to model a wide range of constitutive behaviours [86, 87] from non-linear elasticity and finite strain plasticity to thermoelasticity and biological growth.

Accounting for finite deformations is essential for many applications in skin biophysics, and it is therefore sensible to develop constitutive equations *a priori* valid for finite kinematics. To this end, in this section, essential definitions of kinematic and kinetic quantities are provided, and, without loss of generality, particularised for Cartesian coordinate systems. Because of the popularity of their use in the constitutive modelling of biological tissues [9], particularly those featuring anisotropic mechanical properties, tensor invariants and structural tensors are also introduced. Invariant formulations typically postulate the existence of a strain energy function depending on a set of tensorial invariants of a given deformation or strain measure [87-90]. Introducing a dependency of the strain energy to tensor agencies characterising local microstructural features (e.g. local collagen fibre bundle orientation) is a very efficient way to incorporate microstructural information within a macroscopic continuum constitutive formulation. This class of material models corresponds to that of the microstructurally-based models defined in the previous section. In order to ensure a direct physical interpretation of constitutive parameters it is judicious to select a set of tensor invariants that characterise particular deformation modes the tissue is known to be subjected to and that also can be physically measured [91, 92]. For collagenous tissues, a standard assumption is to consider the tissue as a *continuum* composite material made of one or several families of (oriented) collagen fibres embedded in a highly compliant isotropic solid matrix composed mainly of proteoglycans. A preferred fibre alignment is defined by the introduction of a so-called *structural* or *structure tensor* which appears as an argument of the strain energy function [88, 90]. These notions are detailed in the next sections.

4.1.1 Kinematics of a continuum and deformation invariants

A key basic kinematic entity in continuum mechanics is represented by the deformation gradient $\mathbf{F}$ defined as:

$$\mathbf{F}(\mathbf{X}) := \frac{\partial \varphi(\mathbf{X})}{\partial \mathbf{X}} = \sum_{i,I=1}^{3} \frac{\partial \varphi_i}{\partial \mathrm{X}_I} \mathbf{e}_\mathbf{i} \otimes \mathbf{E}_\mathbf{I} \tag{1}$$

$\mathbf{X}$ is the position of a material point in the *Lagrangian*—or *reference*—configuration while $\mathbf{x} = \varphi(\mathbf{X})$ is its material placement in the *Eulerian*—or *current*— configuration. $\{\mathbf{E}_I\}_{I=1,2,3}$ and $\{\mathbf{e}_i\}_{i=1,2,3}$ are fixed orthonormal bases in the *Lagrangian* and *Eulerian* configurations respectively. ".", ":", $\otimes$ and "T" respectively denote the scalar product of second-order tensors, double-contraction tensor product, tensor outer product and transpose operators. $\mathbf{F}$ maps infinitesimal line vectors from the material to spatial configuration while $\mathrm{cofactor}(\mathbf{F}) = J\,\mathbf{F}^{-\mathrm{T}}$ and $J = \mathrm{determinant}(\mathbf{F})$ respectively maps oriented infinitesimal surface and volume. The right (material) and left (spatial) Cauchy-Green deformation tensors are respectively defined as $\mathbf{C} = \mathbf{F}^{\mathrm{T}}.\mathbf{F}$ and $\mathbf{b} = \mathbf{F}.\mathbf{F}^{\mathrm{T}}$. Because these two tensors only contain information about change of length, and therefore exclude local material rotations, they are appropriate to define valid constitutive equations that satisfy the Principle of Material Frame Indifference [87]. From the deformation tensor $\mathbf{C}$, one can define the Green-Lagrange strain tensor $\mathbf{E} = (\mathbf{C} - \mathbf{I})/2$ where $\mathbf{I}$ is the second-order identity tensor. The classical three principal deformation invariants of $\mathbf{C}$ which define the isotropic (or non-directional) response of a given material are defined as follows [86]:

$$I_1 = \mathrm{trace}\left(\mathbf{C}\right) = \mathbf{C} : \mathbf{I}; \quad I_2 = \frac{1}{2}[I_1 - \mathbf{C}^2 : \mathbf{I}]; \quad I_3 = \mathrm{determinant}\left(\mathbf{C}\right) \tag{2}$$

To characterise a general orthotropic symmetry one can introduce three unit vectors $\boldsymbol{n}_0^i$. associated respectively with the principal material directions i in the reference configuration. Because these material directions are *signed* directional properties one introduces the concept of structural tensors $\mathfrak{B}_0^i$ [87-90] which are even functions of these unit vectors:

$$\mathfrak{B}_0^i = \boldsymbol{n}_0^i \otimes \boldsymbol{n}_0^i \{i = 1,2,3\} (\text{no summation on } i) \tag{3}$$

The spatial counterparts of these structural tensors are defined as:

$$\mathfrak{B}_t^i = \frac{1}{\lambda_i^2} \mathbf{F}.\mathfrak{B}_0^i.\mathbf{F}^{\mathrm{T}} = \frac{1}{\lambda_i^2} \mathbf{F}.(\boldsymbol{n}_0^i \otimes \boldsymbol{n}_0^i).\mathbf{F}^{\mathrm{T}} = \boldsymbol{n}_t^i \otimes \boldsymbol{n}_t^i \ \{i = 1,2,3\} (\text{no summation on } i) \tag{4}$$

where $\boldsymbol{n}_t^i \ \{i = 1,2,3\}$ are the unit vectors in the spatial configuration and $\lambda_i \ \{i = 1,2,3\}$ are the stretches along these directions.

For material *isotropy* all material directions are equivalent so that:

$$\mathfrak{B}_0^1 = \mathfrak{B}_0^2 = \mathfrak{B}_0^3 = \boldsymbol{n}_0^1 \otimes \boldsymbol{n}_0^1 = \boldsymbol{n}_0^2 \otimes \boldsymbol{n}_0^2 = \boldsymbol{n}_0^3 \otimes \boldsymbol{n}_0^3 = \mathbf{1} \otimes \mathbf{1} \tag{5}$$

For *transverse isotropy*, if the preferred material direction is given by $\boldsymbol{n}_0^3$:

$$\mathfrak{B}_0^3 = \boldsymbol{n}_0^3 \otimes \boldsymbol{n}_0^3, \quad \mathfrak{B}_0^1 = \mathfrak{B}_0^2 = \frac{1}{2}(\mathbf{I} - \mathfrak{B}_0^3) \tag{6}$$

For *orthotropic symmetry* the preferred material directions are orthogonal to each other.
In the context of soft tissue mechanics, depending on the spatial scale of investigation, a single unit vector $\boldsymbol{n}_0^i$ can represent the local orientation of a single collagen microfibril or fibril, that of a single fibre bundle or that of a family of fibres. This gives rise to a *transverse isotropy* symmetry if one assumes that these fibres are embedded in an isotropic matrix. Two additional tensorial invariants characteristic of transverse isotropy symmetry can be defined [87, 88, 90]:

$$I_4^i = \mathbf{C} : \mathfrak{B}_0^i = \lambda_i^2, \quad I_5^i = \mathbf{C}^2 : \mathfrak{B}_0^i \tag{7}$$

I_4^i is a very convenient invariant with a direct physical interpretation as it is the square of the stretch along the corresponding fibre direction. It is worth pointing that **C** and **b** have the same invariants.

4.1.2 Constitutive equations for invariant-based hyperelasticity

As a general procedure to formulate constitutive equations for hyperelastic materials, one can postulate the existence of a strain energy density ψ, *isotropic* function of its deformation or strain invariant arguments. Stress and elasticity tensors are obtained by respectively first and second order differentiation [87]. Hyperelastic formulations can serve as a basis for inelastic formulations such as finite strain plasticity, finite strain viscoelasticity and growth, or any combination of these constitutive behaviours.
The Lagrangian second Piola-Kirchhoff stress tensor, **S**, is readily obtained by differentiation of the strain energy density function with respect to the right Cauchy-Green deformation tensor whilst applying the chain rule of differentiation for the n deformation invariants I_i:

$$\mathbf{S} = 2 \sum_{i=1}^{n\,\text{invariants}} \left(\frac{\partial \psi}{\partial I_i} \frac{\partial I_i}{\partial \mathbf{C}} \right) \tag{8}$$

The Cauchy stress tensor, often referred as *true* stress tensor, is obtained by push-forward operation of the second Piola-Kirchhoff stress tensor **S** from the reference to the current configuration [87]:

$$\boldsymbol{\sigma} = \frac{1}{J}(\varphi_* \mathbf{S}) = \frac{1}{J}\mathbf{F}.\mathbf{S}.\mathbf{F}^{\mathrm{T}} = \frac{2}{J}\mathbf{F}.\left(\frac{\partial \psi}{\partial \mathbf{C}}\right).\mathbf{F}^{\mathrm{T}} = \frac{2}{J}\sum_{i=1}^{n\,\text{invariants}} \left(\frac{\partial \psi}{\partial I_i}\mathbf{F}.\frac{\partial I_i}{\partial \mathbf{C}}.\mathbf{F}^{\mathrm{T}} \right) \tag{9}$$

while, the (volume ratio)-weighted Cauchy stress is the Kirchhoff stress tensor:

$$\boldsymbol{\tau} = J\boldsymbol{\sigma} = 2\frac{\partial \psi}{\partial \mathbf{b}}.\mathbf{b} = 2\sum_{i=1}^{n\,\text{invariants}} \left(\frac{\partial \psi}{\partial I_i}\frac{\partial I_i}{\partial \mathbf{b}} \right).\mathbf{b} \tag{10}$$

Remarks about the associated material and spatial elasticity tensors in the context of finite element procedures are provided in **section 1.1** of the **Supplementary Material**. The particular form of the tangent stiffness required for the implementation of constitutive models in the commercial software package Abaqus/Implicit (Simulia, Dassault Systèmes, Providence, RI, USA) is also derived.

4.2 Non-linear elastic models of the skin

In this section, a selection of some of the seminal and/or current state-of-the-art non-linear elastic models of skin are presented. As mentioned earlier in this review, the anisotropic mechanical properties of the skin are critical for most applications, so the focus of this review is therefore on constitutive models capturing these characteristics.

4.2.1 Lanir's model

A very significant microstructurally-based continuum model of skin was first proposed by Lanir [93] who assumed that skin was a continuum composite made of an isotropic ground substance matrix in which oriented collagen and elastin fibres were embedded. These fibres obeyed an angular distribution $\mathcal{R}_k(\theta)$ (see section **section 1.2** of the **Supplementary Material**). The total strain energy function of the material is defined as:

$$\psi = (1-\mathcal{V}_c-\mathcal{V}_e)\frac{\mu}{2}(I_1-3)+\sum_k \mathcal{V}_k \sum_\theta \mathcal{R}_k(\theta)\frac{K_k}{2}\left(\lambda-1\right)^2 \tag{11}$$

μ is a shear modulus defining a neo-Hookean hyperelastic potential for the matrix, $\mathcal{V}_k$, K_k and $\mathcal{R}_k$ are respectively the volume fraction, fibre stiffness and fibre orientation probability density function of each fibrous phase k (collagen: $k=c$ and elastin: $k=e$).

Collagen and elastin fibres are assumed to be linear elastic and unable to sustain compression along their axis:

$$\begin{aligned} f_k\left(\lambda\right) &= K_k\left(\lambda-1\right), && \lambda \geq 1 \\ f_k\left(\lambda\right) &= 0, && \text{otherwise} \end{aligned} \tag{12}$$

In Lanir's model, collagen fibres are assumed to be undulated and can only resist loads when fully straightened. The degree of crimp of collagen fibres oriented in the direction θ is not uniform and follows a Gaussian distribution $D(x)$, where x is the stretch required to straighten an uncrimped fibre. The Cauchy stress in skin is given as:

$$\boldsymbol{\sigma} = \frac{1}{J}\sum_k \mathcal{V}_k \int_0^\pi \left[\mathcal{R}_k(\theta) f_k^*(\lambda)\mathbf{F}\frac{\partial \lambda}{\partial \mathbf{E}}\mathbf{F}^{\mathrm{T}}\right] d\theta - p\mathbf{1} \tag{13}$$

$f_k^*(\lambda)$ is the force per unit undeformed cross sectional area of an individual fibre at stretch λ and p is a hydrostatic pressure that represents the mechanical contribution of the isotropic matrix. For collagen fibres $f_k^*(\lambda)$ is expressed as follows:

$$f_{k=c}^*\left(\lambda\right) = f_c^*\left(\lambda\right) = \int_1^\lambda D\left(x\right) f_c\left(\frac{\lambda}{x}\right) dx \tag{14}$$

As elastin fibres are assumed to be undulation-free, $f_e^*\left(\lambda\right) = f_e\left(\lambda\right)$.

Although Lanir [93] did not identify its model with experimental data, Meijer *et al.* [94] exploited it by characterising in-plane mechanical properties of human forearm skin using an hybrid numerical-experimental approach. Collagen fibre stiffness and mean undulation were estimated from the physical tests while the other constitutive parameters were extracted from the literature. Very low values of collagen fibre stiffness ranging from 51 to 86 MPa were determined from the identification procedure. As an explanation, the partial mechanical recruitment of fibres for the specific limited strain range applied during the physical test was invoked. Lanir's model was used as a constitutive framework for an *in vitro* porcine skin model in a study by Jor *et al.* [95]. Constitutive parameters were determined through numerical optimisation, and, as it is often the case in identification procedures, multiple comparable solutions were obtained. The mean orientation of collagen fibres was determined to lay within the 2-13 degrees range which is consistent with observations. Young's modulus ranges for the ground substance matrix and collagen fibres were respectively 5-12 kPa and 48-366 MPa. Fixing structural parameters that can be experimentally measured (e.g. fibre splay distribution) is a way to accelerate numerical identification and eliminate feasible but unrealistic solutions, thus reducing the issue of non-unicity in parameter sets.

Remark: fibre dispersion can be accounted for by means of two main modelling approaches [96]. The first one, termed the "*angular integration approach*" is due to Lanir [93] while the second approach, known as the "*generalised structure tensor*" approach is due to Gasser *et al.* [97]. For a more detailed discussion of these topics and a new approximation of the π-periodic von Mises distribution see **section 1.2** of the **Supplementary Material**.

4.2.2 Models based on Bischoff-Arruda-Grosh's formulation

This class of models is based on the notion of entropic elasticity and the micromechanics of macromolecule mechanical networks [98]. These concepts are briefly reviewed in **section 1.4** of the **Supplementary Material**. Bischoff *et al.* [99] extended the eight-chain model of Arruda and Boyce [98] developed for polymer elasticity to orthotropy by considering distinct values $\mathrm{a}=\|\mathbf{a}\|$, $\mathrm{b}=\|\mathbf{b}\|$ and $\mathrm{c}=\|\mathbf{c}\|$ for the three characteristic dimensions of the original cuboid microscopic unit cell defined by Arruda and Boyce (see **Figure 8** of the **Supplementary Material**). Earlier, Bischoff *et al.* [100] had demonstrated that, despite being mechanically isotropic, the Arruda-Boyce model could reproduce load-induced anisotropy. However, the model could not capture the mechanical response of rabbit skin under biaxial extension [54]. Bischoff-Arruda-Grosh (BAG)'s strain energy function per unit volume is decomposed into chain and bulk energies:

$$\psi = \psi_{\text{chain}} + \psi_{\text{bulk}} \tag{15}$$

$$\psi_{\text{chain}} = \psi_0 + \frac{n\,\mathfrak{K}\,\theta}{4}\left\{ N\sum_{i=1}^{4}\left[\frac{\overline{r}_i}{N}\beta_i + \ln\left(\frac{\beta_i}{\sinh\beta_i}\right)\right] - \frac{\mathcal{L}^{-1}\left(1/\sqrt{N}\right)}{\sqrt{N}}\ln\left(\lambda_{\mathbf{a}}^{a^2}\lambda_{\mathbf{b}}^{b^2}\lambda_{\mathbf{c}}^{c^2}\right)\right\} \tag{16}$$

where ψ_0 a reference energy of the chain in the reference configuration, calculated so that the reference state is stress free, n is the volumetric chain density, $\overline{r}_i = r_i / d$ is the end-to-end length of deformed chain normalised by the chain link length d, $\sqrt{N}$ is the length of each *undeformed* chain:

$$N = \frac{1}{4}\left(a^2 + b^2 + c^2\right) \tag{17}$$

λ_{i} are the stretches along the principal material axes (**a**, **b**, **c**) defined as:

$$\lambda_{\mathrm{i}} = \sqrt{\mathbf{C}:(\mathbf{i}\otimes\mathbf{i})}, \qquad (\mathbf{i}=\mathbf{a},\mathbf{b}\,\text{or}\,\mathbf{c}) \tag{18}$$

$$\beta_i = \mathcal{L}^{-1}\left(\frac{\overline{r}_i}{N}\right) \tag{19}$$

Finally, the bulk energy is defined as:

$$\psi_{\text{bulk}} = \frac{\kappa}{\alpha^2}\left\{\cosh\left[\alpha(J-1)\right]-1\right\} \tag{20}$$

where κ is the bulk modulus and α, a parameter that controls the shape of the pressure-J curve. Bischoff *et al.* [99] calibrated their constitutive model using data from biaxial testing on rabbit skin [54] and obtained an excellent fit with only seven parameters. The parameters were $n=3.75.10^{22}\,[\mathrm{m}^{-3}]$, $N=1.25$, $\kappa=50[\mathrm{kPa}]$, $\alpha=1$ and $\{a,b,c\}=\{1.37,1.015,1.447\}$.

Flynn *et al.* developed a series of skin models based on BAG's formulation to investigate the wrinkling behaviour of skin [101], scar tissue contraction [102] and wrinkling/ageing of the skin [103]. Kuhl *et al.* [104] particularised BAG'smodel to the case of transverse isotropy by setting two of the unit cell dimensions equal and fitted their model to the ubiquitous rabbit skin data from Lanir and Fung [54] but the fit was not as good as that provided by the original BAG's model.

4.2.3 Model based on Limbert-Middleton's/ Itskov-Aksel's formulation

A polyconvex anisotropic strain energy function for soft tissues was developed by Limbert and Middleton [105] and independently formulated by Itskov *et al.* [106] shortly after. The constitutive framework was based on the generalised structural tensor invariant formulation proposed by Itskov and Aksel [107]. Rabbit skin biaxial tensile test data from Lanir and Fung [54] were used by Limbert and Middleton to identify sets of constitutive parameters. It was shown that a 3-term series formulation was sufficient to obtain a very good fit between the experimental measurements and the predictions of the model. The starting point of the formulation which features novel invariants (compared to those described in **section 4.1.1**) is the definition of a generalised structural tensor (indexed by k) as the weighted sum of three-mutually orthogonal structural tensors [106]:

$$\mathfrak{B}^i_{0[k]} = \sum_{i=1}^{3} w_k^i \mathfrak{B}_0^i = w_k^1\mathfrak{B}_0^1 + w_k^2\mathfrak{B}_0^2 + w_k^3\mathfrak{B}_0^3, \quad \left\{k=1,2,\ldots,n\right\} \tag{21}$$

where $\omega_k^i\,(i=1,2,3;\ k=1,2,...,n)$ are non-negative scalars dependent on the principal directions. The generaliszed structural tensors must satisfy the normalisation condition so that:

$$trace\left(\mathfrak{B}^i_{0[k]}\right)=1 \quad if \quad \sum_{i=1}^{3}\omega_k^i=1 \tag{22}$$

Itskov and Aksel [107] proposed the following two sets of invariants to describe the generalised orthotropic behaviour of hyperelastic materials:

$$I_{[k]}=\sum_{i=1}^{3}\omega_k^i\left(\mathfrak{B}^i_{0[k]}:\mathbf{C}\right) \tag{23}$$

$$J_{[k]}=I_3\left[\omega_k^1\mathrm{trace}\left(\mathbf{C}^{-1}\mathfrak{B}^1_{0[k]}\right)+\omega_k^2\mathrm{trace}\left(\mathbf{C}^{-1}\mathfrak{B}^2_{0[k]}\right)+\omega_k^3\mathrm{trace}\left(\mathbf{C}^{-1}\mathfrak{B}^3_{0[k]}\right)\right] \tag{24}$$

The original strain energy function proposed by Itskov and Aksel [107] was designed to model the mechanics of transversely isotropic calendered rubber sheets at high strains which it did very well:

$$\psi=\frac{1}{4}\sum_{k=1}^{n}\mu_k\left[\frac{1}{\alpha_k}\left(I_{[k]}^{\alpha_k}-1\right)+\frac{1}{\beta_k}\left(J_{[k]}^{\beta_k}-1\right)+\frac{1}{\chi_k}\left(I_3^{-\chi_k}-1\right)\right] \tag{25}$$

This function was subsequently modified by Limbert and Middleton [105] to capture the typical exponential behaviour of the toe region of the stress-strain curve of biological soft tissues:

$$\psi=\frac{1}{4}\sum_{k=1}^{n}\mu_k\left[\frac{1}{\alpha_k}(e^{\left(I_{[k]}-1\right)^{\alpha_k}}-1)+\frac{1}{\beta_k}\left(J_{[k]}^{\beta_k}-1\right)+\frac{1}{\chi_k}\left(I_3^{-\chi_k}-1\right)\right] \tag{26}$$

For both strain energy functions ψ, the polyconvexity condition is fulfilled if the material coefficients $\mu_k,\alpha_k.\beta_k$ and χ_k satisfy the following inequalities:

$$\mu_k\geq 0,\qquad \alpha_k\geq 1,\qquad \beta_k\geq 1,\qquad \chi_k\geq -\frac{1}{2}\qquad \left\{k=1,2,...,n\right\} \tag{27}$$

Although the function developed by Limbert and Middleton was able to fit very well the data from Lanir and Fung [54] it featured twelve parameters with no direct physical interpretation which, depending on the intended application, might be a limiting factor.

4.2.4 Models based on Gasser-Ogden-Holzapfel's anisotropic hyperelastic formulation

Gasser-Ogden-Holzapfel (GOH)'s constitutive formulation [97] was designed to capture the orthotropic hyperelastic behaviour of arterial tissues whilst accounting for fibre splay around two main directions corresponding to each collagen fibre families, characteristic of arterial microstructure. It is an extension of the original model developed by Gasser and his colleagues [108] and is based on the introduction of a new structural tensor $\mathbf{H}_i$ accounting for fibre dispersion of fibre family i:

$$\mathbf{H}_i=\kappa_i\mathbf{1}+(1-3\kappa_i)\boldsymbol{n}_0^i\otimes\boldsymbol{n}_0^i=\kappa_i\mathbf{1}+(1-3\kappa_i)\mathfrak{B}^i_0 \tag{28}$$

where κ_i is a measure of fibre dispersion. The deceptively simple form for $\mathbf{H}_i$ was derived by introducing a statistical distribution which was integrated analytically. One can observe that $\mathbf{H}_i$ is a simple weighting of isotropy and transverse isotropy. When $\kappa_i=0$, $\mathbf{H}_i$ collapses to the classical structure tensor $\mathfrak{B}^i_0$ that corresponds to perfect alignment of fibres without dispersion. If κ_i reaches its maximum value $\kappa_i=1/3$, isotropic symmetry is recovered. The structural tensor is assumed to be only defined when fibres exhibit tension ($\mathbf{H}_i:\mathbf{C}-1>0$) The strain energy function of GOH's model was defined as

$$\psi=\frac{\mu}{2}(I_1-3)+\sum_{i=1}^{2}\frac{k_{i1}}{k_{ki2}}\left\{\exp\left\{k_{ki2}\left[\mathbf{H}_i:\mathbf{C}-1\right]^2\right\}-1\right\} \tag{29}$$

where μ,k_{i1},k_{ki2} are material parameters. μ is a shear modulus defining a neo-Hookean hyperelastic potential whilst k_{i1} and k_{ki2} are respectively a stress-like and unitless scaling parameters.

The GOH model was used in the context of skin mechanics by Ní Annaidh *et al.* [34] who conducted a series of physical uniaxial tensile tests to failure using digital image correlation (DIC) to measure stress-strain characteristics and mean collagen fibre distribution [41]. The physical characterisation was conducted on cadaveric human skin specimens at various body locations and along several orientations (defined with respect to Langer lines).

GOH's model was fitted to the experimental tensile stress-strain curves and implemented into the finite element environment of Abaqus (Simulia, Dassault Systèmes, Providence, RI, USA). The physical experiments were replicated by means of finite element analysis and demonstrated very good performance of the numerical model.

Combining 3D DIC and bulge tests, Tonge *et al.* [50] determined in-plane anisotropic mechanical properties of post-mortem human skin using cyclic full-field measurements. Two main directions of anisotropy were considered and a series of full skin samples (located on the back torso) obtained from six male and female donors (43, 44, 59, 61, 62 and 83 years-old) were used. The effect of preconditioning and humidity of the sample on the stress-strain response was investigated and was shown to be negligible. Age of the donors had a significant effect on the stiffness and directional properties of the skin. Specimens for older donors exhibited a stiffer and more isotropic response compared to those of younger donors. The authors also found that the bulge test method was limited by its inability to accurately determine stress and material parameters due to significant bending effects. In a companion paper, Tonge et al [109] analysed the results of their bulge tests [50] using an analytical method based on thin shell theory which considered the effects of bending stiffness of the skin. The method accounts for through-the-thickness linear strain gradients. These authors fitted the shell version of GOH's model featuring a fully-integrated fibre distribution to their experimental data. Two cases were considered for the GOH model—2D and 3D fibre distributions—whilst the fully-integrated fibre model was restricted to 2D planar fibre orientation. It was found that both the 2D and 3D GOH model were unable to capture the anisotropic mechanics of skin from bulge tests unlike the 2D fully-integrated fibre model which was shown to capture it very well. Tonge *et al.* [109] attributed the differences between their results and those of Ní Annaidh *et al.* [34, 41] mainly to the younger age of their donors, lower strain level considered in their tests and their assumption about fibre orientation. Tonge *et al.* [109] considered only one fibre family aligned with the principal stretch direction while Ní Annaidh *et al.* [34, 41] assumed that skin was made of two fibre families symmetric about the loading axis. In the context of surgical simulation procedures, the GOH model was used by Buganza-Tepole *et al.* [63] to model the mechanics of skin. In that study, computed stress profiles in skin flap were used as a surrogate measure of likelihood of tissue necrosis, following reconstructive surgery.

4.2.5 Models based on Flynn-Rubin-Nielsen's formulation

To address the issue of computationally expensive integration methods required for microstructural models of soft tissues featuring statistical distributions of material or structural characteristics (e.g. integration of fibre splay angular distribution over the unit sphere, distribution of engaged fibres) Flynn *et al.* [110] proposed a new model termed "*discrete fibre icosahedral structural model*". The model relies on the use of a *discrete* rather than *continuous* fibre orientation distribution kernel which allows closed-form solutions for strain energy and stress. Six discrete directions are considered: they are oriented parallel to the lines connecting opposing vertices of a regular icosahedron. Six unit vectors $\boldsymbol{n}_0^i\{i=1,\ldots,6\}$ corresponding to distinct fibre bundles are thus defined (see details in **section 1.5** of the **Supplementary Material**). Flynn *et al.* [110] introduced a strain energy function per unit mass of the collection of six fibre bundles which features separate contributions for collagen and elastin fibres:

$$\psi = \sum_{i=1}^{6} w_i \left[\psi_c(\lambda_i) + \psi_e(\lambda_i)\right] + U(J) \tag{30}$$

with

$$\psi_e(\lambda_i) = \frac{1}{\rho_0}\sum_{i=1}^{6} w_i \frac{E_e}{4}\left\langle \lambda_i^2 - 1 \right\rangle \tag{31}$$

where w_i are positive weights, associated with each of the six structural tensors, that balance the respective structural contributions of each fibre direction and ρ_0 is the mass density in the reference configuration. $\langle\ \rangle$ are the Macaulay Brackets defined as follows: $\langle x \rangle = 1/2\left(x + |x|\right)$. Because collagen fibres are typically crimped in the macroscopic stress-free reference configuration [93, 110], it is sensible to introduce a so-called *undulation parameter* $x \geq 1$, which is the value of stretch at which a fibre starts to bear tension:

$$\int_1^{\infty} D(x)\,dx \tag{32}$$

This means that the fraction of fibres that are fully taut (i.e. straight) at a stretch λ is given by the following integral, where D is an undulation probability distribution:

$$\int_1^{\lambda} D\left(x\right)dx \tag{33}$$

The stiffness of any of the six collagen bundles is:

$$\frac{d}{d\lambda}\left(\frac{\lambda\rho_0}{J}\frac{d\psi_c(\lambda)}{d\lambda}\right) = E_c\int_1^{\lambda} D\left(x\right)dx \tag{34}$$

Assuming that all the collagen fibres are slack and are stress-free for stretch lower or equal to unity, and further assuming that deformations are isochoric:

$$\frac{d\psi_c(\lambda)}{d\lambda} = \frac{1}{\lambda\rho_0}\int_1^{\lambda}\left[E_c\int_1^{\lambda} D\left(x\right)dx\right]dy \tag{35}$$

Flynn *et al.* [110] considered two undulation probability distributions: step and triangle distributions. They offer the advantage of being simple enough so that a closed-form analytical expression can be obtained for ψ_c. The example of a using unit step distribution is provided in **section 1.5** of the **Supplementary Material**. This strain energy function was used by Flynn *et al.* [110] to model the biaxial tensile response of rabbit skin [54] (8.7% error) and uniaxial response of porcine skin [111] (7.6% error). The constitutive model was later extended by Flynn and Rubin [112] to address shortcomings linked to the relation between fibre weight and anisotropic response, namely, the fact that for equal weights w_i the mechanical response is not necessarily isotropic. These authors introduced a generalised strain invariant γ:

$$\gamma = \left(\mathbf{C} + \mathbf{C}^{-1}\right).\sum_{i=1}^{6} w_i \mathfrak{B}_0^i - 2 \tag{36}$$

where w_i are positive weights, associated with each of the six structural tensors $\mathfrak{B}_0^i = \boldsymbol{n}_0^i \otimes \boldsymbol{n}_0^i$, that balance the respective structural contributions of each fibre direction.
Unlike for the earliest model of Flynn *et al.* [110], here, equal weights can only lead to isotropy of mechanical properties. Finally, Flynn and Rubin [112] proposed the following strain energy density:

$$\psi = \frac{\sigma_0}{2\rho_0}\left[\gamma + \sum_{m=1}^{M}\frac{\gamma_m}{m}\left(\frac{\gamma}{\gamma_m}\right)\right] \tag{37}$$

where ρ_0 is the mass density in the reference configuration, σ_0 is a stress-like material parameter, γ_m are dimensionless positive material parameters and M is the order of the polynomial expansion. Using the same experimental data as in their 2011 paper [54, 111], Flynn and Rubin [112] identified constitutive parameters of their new strain energy function (equation (37)). The fit was not as good as in their previous study [110] as the fitting errors for rabbit and pig skin data were respectively 12 and 17%. However, in that case, the weights were a pure measure of anisotropy.

4.2.6 Model based on Limbert's formulation

Most of the microstructurally-based constitutive models of soft tissues assume an additive decomposition of the strain energy function into decoupled matrix and fibre elastic potentials. This means that fibre-fibre and matrix-fibre interactions are not *explicitly* captured in the constitutive formulation. The network models based on BAG's formulation captures only *implicitly* and *globally* these interactions. To address this first shortcoming, Limbert [113] developed a novel invariant-based multi-scale constitutive framework to characterise the transversely isotropic and orthotropic elastic responses of biological soft tissues. The constitutive equations were particularised to model skin. The model was not only capable to accurately reproduce the experimental multi-axial behaviour of rabbit skin, as in [114] but could also *a posteriori* predict stiffness values of individual tropocollagen molecules in agreement with physical and molecular-dynamics-based computational experiments [113]. Another key motivational aspect of the formulation is that the constitutive parameters can be directly extracted from physical measurements by segregating the orthogonal deformation modes of its constituents. Another desirable feature of the constitutive equations is that the response is based on physical geometrical/structural parameters that can be measured experimentally or determined *ab initio* from molecular dynamic simulations.

Limbert's formulation is based on the constitutive framework of Lu and Zhang [115] for transversely isotropic materials which make use of four invariants that characterise decoupled deformations modes solely related to purely volumetric (J) , deviatoric stretch in the fibre direction $(\overline{\lambda})$, cross-fibre shear (α_1^i) and fibre-to-fibre/matrix-to-fibre shear (α_2^i) stress responses. Orthotropic symmetry is accounted for by introducing a second family of fibres. The index $i=1,2$ identifies each fibre family:

$$J=\sqrt{I_3};\qquad \overline{\lambda}_i=I_3^{-\frac{1}{6}}\sqrt{I_4^i};\qquad \alpha_1^i=\frac{I_1I_4^i-I_5^i}{\sqrt{I_3I_4^i}};\qquad \alpha_2^i=\frac{I_5^i}{\left(I_4^i\right)^2} \tag{38}$$

Limbert proposed the following strain energy function:

$$\psi=\psi^v(J)+\sum_{i=1}^{2}\left[\psi_i^{\overline{\lambda}}(\overline{\lambda}_i)+\hat{\psi}_i^1(\alpha_1^i)+\tilde{\psi}_i^2(\alpha_2^i,\overline{\lambda}_i)\right] \tag{39}$$

ψ^v, $\psi_i^{\overline{\lambda}}$, $\hat{\psi}_i^1$ and $\tilde{\psi}_i^2$ are respectively the volumetric, deviatoric fibre, cross-fibre shear and fibre-to-fibre/fibre-to-matrix shear energies. The functional forms of the energies and the constitutive parameters are detailed below.

$$\hat{\psi}_i^1(\alpha_1^i)=\frac{1}{2}\mu_1^i\left(\alpha_1^i-2\right);\qquad \tilde{\psi}_i^2(\alpha_2^i,\overline{\lambda}_i)=\frac{1}{2}\mu_2^i\left(\alpha_2^i-1\right)^2\underbrace{\frac{1}{1+a_i\,\mathrm{e}^{-b_i(\overline{\lambda}_i-\overline{\lambda}_i^c)}}}_{\text{Sigmoid coupling function}} \tag{40}$$

A notable feature of this constitutive approach is that collagen fibres and matrix are allowed to interact via explicit decoupled shear interactions whilst collagen fibres behave like a worm-like chain model [104, 116].

$$\psi_i^{\overline{\lambda}}(\overline{\lambda}_i)=\begin{cases}\aleph_i\mu_0^i(\overline{\lambda}_i^{\,2}+\dfrac{2}{\overline{\lambda}_i}-3)+\xi_0^i\aleph_i\ln(\overline{\lambda}_i^{\,r_{0i}^2}) & \text{if } \overline{\lambda}_i\le 1\\ \aleph_i\mathfrak{K}\theta\dfrac{L_i}{4L_p^i}\left(2\dfrac{\overline{\lambda}_i^{\,2}r_{0\beta}^2}{L_i^2}+\left(1-\dfrac{\overline{\lambda}_i r_{0i}}{L_i}\right)^{-1}-\dfrac{\overline{\lambda}_i r_{0i}}{L_i}\right)+\xi_0^i\aleph_i\ln(\overline{\lambda}_i^{\,r_{0\beta}^2}) & \text{if } \overline{\lambda}_i>1\end{cases} \tag{41}$$

The constitutive model resulted in a set of twenty three constitutive parameters $\mathbf{p}=\mathbf{p}^1\cup\mathbf{p}^2=\{\mathfrak{K},\theta,\kappa,\mu_0^i,\mu_1^i,\mu_2^i,\aleph_i,L_i,L_p^i,r_i,a_i,b_i,\overline{\lambda}_i^c\}_{i=1,2}$. Moreover, all the constitutive parameters of this multiscale formulation have a direct physical interpretation. Limbert [113] determined the parameter set $\mathbf{p}^2$ using a numerical global optimisation algorithm while the parameter set $\mathbf{p}^1$ was assumed *a priori* based on existing data [104] and data obtained via visual inspection of the biaxial stress-strain curves [114]. The physical meaning of these parameters is provided in **Table 1** of **section 1.6** of the **Supplementary Material**. Although the model slightly under-predicts the response of rabbit skin along the head-tail direction at low stretch (<1.35), an excellent fit was obtained (**Figure 9**). Limbert implemented the non-linear constitutive model as tri-linear hexahedral finite element using an enhanced strain formulation [117] which has been proven to be superior to a standard displacement-based formulation, particularly for shear-dominated problems and nearly incompressible materials. Moreover, analytically-exact direct sensitivity analyses subroutines were also implemented to assess the sensitivity of the shear response of the model to its constitutive parameters during a simulated indentation test [113]. From the persistence lengths of tropocollagen molecules determined from the optimisation procedure (22 and 65 nm for fibre families 1 and 2) Limbert [113] calculated equivalent Young's moduli of respectively 293 and 865 MPa. These values lie within one order of magnitude less of what has been determined experimentally and obtained through computational modeling studies (see for example Gautieri *et al.* [118]). However, using the same equation used by Limbert to calculate Young's modulus, Sun *et al.* [119] estimated Young's modulus of collagen molecules to range between 350 MPa and 12 GPa.

4.2.7 Models based on Weiss's transversely isotropic hyperelastic formulation

Groves *et al.* [120] used Weiss's model [121] to model the anisotropic mechanics of skin by identifying constitutive parameters from a series of uniaxial tensile tests. The original model proposed by Weiss *et al.* [121] was formulated to capture the transversely isotropic hyperelastic response of ligaments of the knee joint but without including fibre dispersion which is not significant in these soft tissues.

The strain energy function used by Groves *et al.* [120] was defined as the sum of a Veronda-Westmann (VW) potential ψ^{VW} [56] and a piece-wise anisotropic fibre function ψ_i^{fibre} [121], to model the isotropic and anisotropic responses respectively:

$$\psi(I_1, I_2, I_4^1, I_4^2, I_4^3) = \psi^{VW}(I_1, I_2) + \sum_{i=1}^{3} \psi_i^{fibre}(I_4^i = \lambda^i) \tag{42}$$

where:

$$\psi^{VW} = c_1 \left\{ \exp\left[c_2(I_1 - 3)\right] - 1 \right\} - \frac{c_1 c_2}{2}(I_2 - 3) \tag{43}$$

c_1 is a shear-like modulus while c_2 is a dimensionless parameter that scales the response connected to the second invariant.

and

$$\frac{\partial \psi_i^{fibre}(\lambda^i)}{\partial \lambda^i} = \frac{1}{\lambda^i} \begin{cases} 0 & if\ \lambda^i \le 1 \\ c_3 \left\{ \exp\left[c_4(\lambda^i - 1)\right] - 1 \right\} & if\ 1 < \lambda^i < \overline{\lambda}^i \\ c_5 \lambda^i + c_6 & if\ \lambda^i \ge \overline{\lambda}^i \end{cases} \tag{44}$$

$\overline{\lambda}^i = \sqrt{\overline{I}_4^i}$ represents the stretch at which the (collagen) fibres are assumed to be fully taut. c_3 is an elastic modulus-like parameter scaling the exponential response, c_4 controls the rate of un-crimping of the fibres, c_5 is the elastic modulus of the taut fibre while c_6 is a correcting factor to ensure continuity of the stiffness response at $\lambda^i = \overline{\lambda}^i$.

In their experimental procedure, Groves *et al.* [120] used eight human discoid skin samples from two female donors (aged 56 and 68) following mastectomy and fourteen post-mortem murine skin samples obtained from eight mice (aged 18-24 months). For each sample, tensile tests were simultaneously conducted along three axis (0, 45 and 90 degrees). Using an inverse analysis based on finite element simulations of the testing procedures constitutive parameters were determined. For each sample, three sets of four parameters ($c_3, c_4, \sqrt{\overline{I}_4^i}$ and an additional parameter characterising the deviation from the assumed fibre orientation) for each fibre energy function were obtained in addition to the two parameters of the VW function. Although Groves *et al.* [120] demonstrated a good fit between their three-fibre family model and their experimental data, they also acknowledged the limitations of using a Simplex optimization algorithm for their inverse analysis which could only capture *local* minima of their cost function.

4.3 Nonlinear viscoelastic models of the skin

The skin exhibits a wide range of viscoelastic effects including stress relaxation, creep, rate-dependency of stress and hysteresis [8]. A large number of researchers have characterised the viscoelastic properties of skin under various testing conditions [55, 122-129]. Observed macroscopic viscoelastic effects can be attributed to two main mechanisms that operate in concert. Viscoelasticity of the skin can originate from the intrinsic viscoelastic characteristics of its nano- and microstructural constitutents (e.g. proteoglycans, elastic fibres) and also from the time-dependent rearrangement of its microstructure under macroscopic loads which takes a finite amount of time to occur (flow of interstitial fluid across the porous structures, progressive sliding of collagen fibrils past each other). Proteoglycan macromolecules such as decorin bound on the collagen fibrils and play an important role in these interactions which are mediated by the side chains of glycosaminoglycans. Because the forces acting between fibrils are of a non-covalent nature, these links can break and reconnect [55, 130, 131]. One should also note that there are other complex physics phenomena at play. For example, the thermal motion of ions, including Na+ and K+, displacing toward the negatively charged ends of glycosaminoglycans of fibril-associated proteoglycans, induce an attractive force between two collagen fibrils.

To date, there are only very few nonlinear viscoelastic anisotropic constitutive models of skin, see [55, 132-135] and references therein. This is partly due to the considerable challenges of experimentally characterising the behavior of skin, particularly *in vivo*, and the success of simpler theories such as quasi-linear viscoelasticity (QLV) [8, 136].

The literature on general viscoelastic constitutive models is rich and, here, only a brief account of the most common approaches to model biological soft tissues (following the classification of Ehret [137]) is reported. More recent and state-of-the-art nonlinear viscoelastic models of skin are presented.

4.3.1 Quasi-linear viscoelasticity and its derivatives

The application of QLV theory to soft tissue mechanics has been particularly popularised by the work of Fung and co-workers [8, 136]. The idea behind QLV is to assume that the time-dependent stress response $\sigma(t)$ following uniaxial loading can be expressed as a convolution integral of the form:

$$\sigma(t) = \int_{-\infty}^{t} G(t-\tau)\frac{\partial \sigma_e(\tau)}{\partial t} d\tau \tag{45}$$

where σ_e is the instantaneous elastic stress and G the reduced relaxation function. This function controls how the current stress response is modulated by past loading history.

The notion of quasi-linearity stems from the linear relation of the integrand terms and the analogy with rate equations of linear viscoelasticity. The uniaxial relationship can be extended to a full 3D representation by introducing second-order and fourth order tensors describing respectively the stress and reduced relaxation function [8]. This represents a flexible framework where anisotropic properties, and decoupling between deviatoric and volumetric responses can be captured by appropriate constitutive equations.

Bischoff [138] applied QLV at the collagen fibre level to model porcine skin by developing an anisotropic microstructurally-motivated constitutive model which also includes fibre dispersion. A notable feature of the model is the ability to capture a fibre-level viscoelastic orthotropic response with only seven parameters. However, the authors recognised the need for additional experiments to fully characterise the mechanical response as numerical identification procedures are plagued by non-unicity of constitutive parameters. Additional characterisation tests would likely lead to convergence toward a single set of optimal parameters.

4.3.2 Explicitly rate-dependent models

By design, these types of model—also called viscoelastic models of the *differential* type—capture strain-rate sensitivity and *short-term* viscous effects following application of load [139]. They are based on *differential* rather than *integral* equations like for QLV, and are therefore inappropriate to capture long-term memory viscoelastic effects such as relaxation. Long-term memory effects encompass the whole deformation history of the material. The so-called *principle of fading memory* [140] states that deformations that occurred in the recent time history have greater influence on the actual stresses than those which occurred in a more distant past history.

Explicitly rate-dependent models of soft tissues are particularly well suited to high strain rate situations such as those occurring during vehicle accidents, sport activities, impact and blast [139, 141-144]. These models generally postulate the existence of a viscous potential ψ^v from which the viscous dissipative effects (denoted by scalar $\mathcal{D}$) arise by differentiation with respect to the rate of the Cauchy-Green deformation tensor $\dot{\mathbf{C}} = \partial \mathbf{C} / \partial t$:

$$\mathcal{D} = \frac{\partial \psi^v}{\partial \dot{\mathbf{C}}} : \dot{\mathbf{C}} \tag{46}$$

The total second Piola-Kirchhoff stress tensor which include purely elastic effects through a potential ψ^e, and purely viscous effects through ψ^v, is obtained by differentiation of the total potential ψ assuming that $\dot{\mathbf{C}}$ is a parameter or internal variable:

$$\mathbf{S} = 2\left(\frac{\partial \psi^e}{\partial \mathbf{C}} + \frac{\partial \psi^v}{\partial \dot{\mathbf{C}}}\right) \tag{47}$$

The framework proposed by Pioletti *et al.* [139] for modelling the rate-dependent isotropic viscohyperelastic behavior of ligaments and tendons was later extended by Limbert and Middleton [142] to transverse isotropy using tensor formalism. This model was subsequently combined with damage equations to model the failure of human skin in response to puncturing biting loads [141].

4.3.3 Internal variables based on deformation/strain decomposition

Unidimensional (small-strain) rheological models based on combinations of spring and dashpot elements are efficient means to conceptualise particular viscoelastic behaviours [87]. The arrangement of a dashpot and a spring in series constitutes a Maxwell element with elastic modulus E and viscosity η and The total strain ε in the element can be decomposed into elastic and inelastic strains as $\varepsilon = \varepsilon_e + \varepsilon_i$ and the total strain rate is:

$$\frac{\partial \varepsilon}{\partial t} = \frac{1}{E}\frac{\sigma}{\eta} + \frac{\partial \sigma}{\partial t} \tag{48}$$

A very simple approach to account for the viscoelastic properties of skin would be to assume that it is a generalised standard viscoelastic solid made of n Maxwell elements so that it can be described by a strain energy function of the form $\psi = \mathcal{P}(t)\psi^{\infty}$ where ψ^{∞} is the time-independent or instantaneous strain energy which is convolved with a time-dependent kernel represented by a n-terms Prony series $\mathcal{P}$ defined through characteristic times and moduli. τ_i and c_i as:

$$\mathcal{P}(t) = 1 + \sum_{i=1}^{n} c_i \left[1 - \exp\left(-\frac{t}{\tau_i}\right)\right] \tag{49}$$

Borrowing the concept of linear strain decomposition and applying it to the 3D finite strain regime, it is possible to establish a multiplicative decomposition of the deformation gradient into an elastic and inelastic parts as $\mathbf{F} = \mathbf{F}^e.\mathbf{F}^i$ [145, 146]. From this definition one can define the fictitious *elastic* and *inelastic* right Cauchy-Green deformation tensors as:

$$\mathbf{C}^e = \mathbf{F}^{e\,\mathrm{T}}.\mathbf{F}^e; \qquad \mathbf{C}^i = \mathbf{F}^{i\,\mathrm{T}}.\mathbf{F}^i \tag{50}$$

One can then postulate the existence of a free energy $\psi(\mathbf{C}^e, \mathbf{C}^i)$ decomposed into *equilibrium* and *non-equilibrium terms* where $\mathbf{C}^i$ is treated as an internal variable [145]:

$$\psi(\mathbf{C}) = \psi(\mathbf{C}^e, \mathbf{C}^i) = \psi^{equilibrium}(\mathbf{C}^e) + \psi^{n.equilibrium}(\mathbf{C}^i) \tag{51}$$

Naturally, one can generalise this concept to n Maxwell elements so that one introduces n internal (tensor) variables $\mathbf{C}_k^i$, arguments of n non-equilibrium potentials $\psi_k^{n.equilibrium}$:

$$\psi(\mathbf{C}, \mathbf{C}_k^i) = \psi^{equilibrium}(\mathbf{C}) + \sum_{k=1}^{n} \psi_k^{n.equilibrium}(\mathbf{C}_k^i) \tag{52}$$

The second Piola-Kirchhoff stress is then obtained as the sum of equilibrium and non-equilibrium terms as:

$$\mathbf{S} = \mathbf{S}^{equilibrium} + \sum_{k=1}^{n} \mathbf{S}_k^{n.equilibrium} = 2\left[\frac{\partial \psi^{equilibrium}(\mathbf{C}^e)}{\partial \mathbf{C}^e} + \sum_{k=1}^{n} \frac{\psi_k^{n.equilibrium}(\mathbf{C}_k^i)}{\partial \mathbf{C}_k^i}\right] \tag{53}$$

A notable feature of the present formulation is that non-equilibrium or viscous deformations are not restricted to the small strain regime unlike the vast majority of viscoelastic models of biological soft tissues found in the literature.

Bischoff *et al.* [132] combined this type of formulation with their previous orthotropic eight-chain model [99] to model the viscoelastic behavior of soft tissues. The model was fitted to the experimental data on rabbit skin [54]. Vassoler *et al.* [147] recently proposed a variational framework making use of the multiplicative decomposition of the deformation gradient into elastic and inelastic parts to represent the mechanics of fibre-reinforced biological composites and this would be appropriate for skin.

Limbert (private communication) extended his decoupled invariant orthotropic hyperelastic model to finite strain viscoelasticity following a similar approach to that described in this section. The particular approach for anisotropic viscoelastic effects follows the tensor formalism of Nguyen et al. [148] and Nedjar [149] who introduced viscosity tensors. An essential feature of the model is that the matrix and the fibre phase are treated separately, each featuring their own deformation gradient. The non-linear creep and/or relaxation response is based on the multiplicative viscoelastic split of the deformation gradient combined with the assumption of the existence of viscoelastic potentials for each phase. The deformation gradient and its multiplicative decomposition apply to all the continua (matrix and fibre phase) linking them implicitly. Separate flow rules are specified for the matrix and fibre families.

The flow rules of the fibre families are combined to provide an anisotropic flow rule of the fibre phase. Details of the constitutive formulation and finite element implementation of the present constitutive model for the dermis can be found in Nguyen et al.'s paper [148]. One should point out that, besides the *matrix* phase, the multiplicative decomposition of the deformation gradient applies to the *fibre phase*, not to the individual families of fibres (two, in our case).

$$\mathbf{F} = \mathbf{F}^{e}_{matrix\,(k)}\mathbf{F}^{v}_{matrix\,(k)} = \mathbf{F}^{e}_{fibre\,(p)}\mathbf{F}^{v}_{fibre\,(p)} \tag{54}$$

The elastic right Cauchy-Green deformation tensors associated with the matrix and fibre phases are defined as:

$$\mathbf{C}^{e}_{matrix} = (\mathbf{F}^{v}_{matrix})^{-\mathrm{T}}(\mathbf{F}^{T}\mathbf{F})(\mathbf{F}^{v}_{matrix})^{-1} \tag{55}$$

and

$$\mathbf{C}^{e}_{fibre} = (\mathbf{F}^{v}_{fibre})^{-\mathrm{T}}(\mathbf{F}^{T}\mathbf{F})(\mathbf{F}^{v}_{fibre})^{-1} \tag{56}$$

The general formulation of the free energy density can be expressed as the sum of equilibrium and non-equilibrium energies depending on the total and viscous deformation tensors and the fibre orientation vectors (defined by $\boldsymbol{n}_0$ and $\boldsymbol{m}_0$ If one considers two family of collagen fibres):

$$\psi(\mathbf{C},\mathbf{C}^{v}_{matrix},\mathbf{C}^{v}_{fibre},\boldsymbol{n}_0,\boldsymbol{m}_0) = \underbrace{\psi^{\infty}(\mathbf{C},\boldsymbol{n}_0,\boldsymbol{m}_0)}_{\text{equilibrium part}} + \underbrace{\psi^{v}(\mathbf{C}^{e}_{matrix},\mathbf{C}^{e}_{fibre},\boldsymbol{n}_0,\boldsymbol{m}_0)}_{\text{non-equilibrium part}} \tag{57}$$

where

$$\psi^{\infty}(\mathbf{C},\boldsymbol{n}_0,\boldsymbol{m}_0) = \psi^{\infty}_{M}(I_1,I_2,I_3) + \psi^{\infty}_{F}(I_4,I_5,I_6,I_7) \tag{58}$$

$$\psi^{v}(\mathbf{C}^{e}_{matrix},\mathbf{C}^{e}_{fibre},\boldsymbol{n}_0,\boldsymbol{m}_0) = \mathcal{W}^{v}_{M}(I^{e}_{1(\mathrm{M})},I^{e}_{2(\mathrm{M})},I^{e}_{3(\mathrm{M})}) + \mathcal{W}^{v}_{F}(I^{e}_{4(F)},I^{e}_{5(F)},I^{e}_{6(F)},I^{e}_{7(F)}) \tag{59}$$

with

$$I_4 = \mathbf{C}:(\boldsymbol{n}_0\otimes\boldsymbol{n}_0);\ I_5 = \mathbf{C}^2:(\boldsymbol{n}_0\otimes\boldsymbol{n}_0);\ I_6 = \mathbf{C}:(\boldsymbol{m}_0\otimes\boldsymbol{m}_0);\ I_7 = \mathbf{C}^2:(\boldsymbol{m}_0\otimes\boldsymbol{m}_0) \tag{60},$$

$$I^{e}_{1(k)} = \mathbf{C}^{e}_{(k)}:\mathbf{I};\ I^{e}_{2(k)} = \frac{1}{2}\Big(\mathbf{C}^{e\ 2}_{(k)}:\mathbf{I} - I^{e}_{1(k)}\Big);\quad I^{e}_{3(k)} = \mathrm{determinant}(\mathbf{C}^{e}_{(k)}) \tag{61}$$

$$I^{e}_{4(k)} = \mathbf{C}^{e}_{(k)}:(\boldsymbol{n}_0\otimes\boldsymbol{n}_0);\ I^{e}_{5(k)} = \mathbf{C}^{e\ 2}_{(k)}:(\boldsymbol{n}_0\otimes\boldsymbol{n}_0);\ I^{e}_{6(k)} = \mathbf{C}^{e}_{(k)}:(\boldsymbol{m}_0\otimes\boldsymbol{m}_0);\ I^{e}_{7(k)} = \mathbf{C}^{e}_{(k)} \tag{62}$$

where

$$k = matrix \text{ or } fibre \tag{63}$$

Finally, the specific form of the free energy using the decoupled invariants introduced in **section 4.2.6** is defined as follows:

$$\psi(\mathbf{C},\mathbf{C}^{v}_{matrix},\mathbf{C}^{v}_{fibre},\boldsymbol{n}_0,\boldsymbol{m}_0) = \underbrace{\psi^{\infty}_{M}(J) + \sum_{\beta=1}^{2}\Big[\psi^{\infty}_{\beta}(\overline{\lambda}_{\beta},\alpha^{\beta}_{1},\alpha^{\beta}_{2})\Big]}_{equilibrium\ part} + \underbrace{\Phi^{v}_{M}(J^{e}) + \sum_{\beta=1}^{2}\Big[\Phi^{v}_{\beta}(\overline{\lambda}^{e}_{\beta},\alpha^{\beta}_{1e},\alpha^{\beta}_{2e})\Big]}_{non-equilibrium\ part} \tag{64}$$

where invariants with superscript/subscript "e" refer to those associated with the *elastic* right Cauchy-Green deformation tensor $\mathbf{C}^{e}$. The equilibrium part of the free energy is identical to the total elastic energy defined in equation (39) . The reduced dissipation inequality is:

$$\underbrace{-2\frac{\partial\psi^{v}_{M}}{\partial\mathbf{C}^{v}_{matrix}}}_{\mathbf{S}^{v}_{M}} : \frac{1}{2}\dot{\mathbf{C}}^{v}_{matrix}\ \underbrace{-2\frac{\partial\psi^{v}_{F}}{\partial\mathbf{C}^{v}_{fibre}}}_{\mathbf{S}^{v}_{F}} : \frac{1}{2}\dot{\mathbf{C}}^{v}_{fibre} \geq 0 \tag{65}$$

where $\mathbf{S}^{v}_{M}$ and $\mathbf{S}^{v}_{F}$ are the stresses driving the viscous relaxation of the matrix and fibre phases. To satisfy the positive dissipation criterion for the matrix/fibre phase, the following evolution equations are proposed [145, 148]:

$$\frac{1}{2}\dot{\mathbf{C}}^{v}_{matrix} = \mathbb{V}^{-1}_{M}:\mathbf{S}^{v}_{M} \qquad \text{and} \qquad \frac{1}{2}\dot{\mathbf{C}}^{v}_{matrix} = \mathbb{V}^{-1}_{M}:\mathbf{S}^{v}_{M} \tag{66}$$

where $\mathbb{V}^{-1}_{M}$ and $\mathbb{V}^{-1}_{F}$ are the inverse of positive definite fourth-order isotropic/anisotropic viscosity tensors. These are defined in **section 1.7** of the **Supplementary Material**, together with particular non-equilibrium potentials for anisotropic viscoelasticity.

Flynn and Rubin [150] extended the original Flynn-Rubin's [112] and Flynn-Rubin-Nielsen's [110] formulations to phenomenologically model dissipative effects in soft tissues. They followed the theoretical and numerical approach of Hollenstein *et al.* [151] which can capture both rate-independent and rate-dependent anelastic response including stress relaxation effects. The model was applied to stress relaxation data of rabbit skin [54] with various degrees of success depending on the magnitude of stretch [150].

4.3.4 Internal variables based on stress decomposition

Another popular approach for describing the viscous non-linear elasticity of biological soft tissues is to considers a set of non-measurable (i.e. internal variable) strain-like internal variables $\mathbf{E}_k$ in the reference configuration, the free energy of a viscoelastic material can be defined as follows [87]:

$$\psi(\mathbf{C},\mathbf{E}_k) = \psi^{equilibrium}(\mathbf{C}) + \sum_{k=1}^{n} \psi_k^{n.equilibrium}(\mathbf{C},\mathbf{E}_k) \tag{67}$$

where, in analogy with equation (52), the free energy (and stress) can be split into equilibrium and non-equilibrium contributions associated respectively with elastic and viscous deformation mechanisms:

$$\mathbf{S} = \mathbf{S}^{equilibrium} + \sum_{k=1}^{n} \mathbf{Q}_k^{n.equilibrium} \tag{68}$$

The over-stress $\mathbf{Q}_k^{n.equilibrium}$ are work-conjugate to $\mathbf{E}_k$. Drawing a parallel with rheological elements of linear viscoelasticity, and instead of formulating evolution equations for the strain-like variables $\mathbf{E}_k$, one can formulate rate equations in terms of the stress-like internal variables $\mathbf{Q}_k^{n.equilibrium}$. These equations can be solved by means of convolution integrals [145, 152]. Using a multi-modal Maxwell element rheological analogy, this type of formulation was applied by Holzapfel and Gasser [152] to model the viscoelastic orthotropic behavior of arteries. Peña *et al.* [153, 154] developed a similar approach to model the ligaments of the knee but conceptually used a combination of Kelvin-Voigt elements. Ehret *et al.* [155] proposed a microstructurally-motivated finite strain viscoelastic model for soft tissues which is very relevant for skin mechanics. Gasser and Forsell [156] developed a finite strain viscoelastic framework using an elastic and Maxwell body configurations which respectively correspond to an elastic and viscous phase. The model was motivated by the desire to gain an insight into the passive mechanics of the myocardium tissue during pacing lead perforation. The non-equilibrium energy in equation (67) could have been equivalently defined in terms of internal stress-like variables $\mathbf{Q}_k^{n.equilibrium}$ as proposed by Simo [157]. Only in special cases, the approach based on the multiplicative decomposition of the deformation gradient is consistent with the one based on convolution integrals [157].

5. Application – Skin wrinkles

Over the course of a life time, human skin undergoes a series of chemo-mechano-biological alterations (i.e. intrinsic ageing) which occur in combination with the effects of external environmental factors such as solar radiations or chemical pollution (i.e. extrinsic ageing). These microstructural and material biophysical changes typically translate into the formation of wrinkles which become more pronounced as intrinsic and extrinsic ageing progress [158]. Skin wrinkles have been the subject of much attention because of their societal importance in relation to age and beauty but also, in the case of expression wrinkles, because of their role in conveying emotions, and thus, as a vehicle for communication. Besides these important aspects of human life, unveiling the underlying mechanical principles that condition the morphologies and patterns of wrinkles are essential in evaluating, and ultimately, predicting, how an aged skin interacts with its environment. Many products that interact with, support or protect human skin actually cause discomfort for the user and even irritation or damage to the skin. Examples include incontinence products, medical device and sport equipment. Through adhesive and deformation-induced friction, skin wrinkles play a central role in these contact interactions, [21, 68, 159] and any alteration of the skin surface (e.g. wrinkles) is likely to modulate these effects. Moreover, the growing market of stretchable and wearable epidermal electronics [160] put wrinkles in the spotlight as these systems, do not only interact with the skin and its wrinkles, but are also often multi-layer systems themselves which are prone to wrinkling behaviour [161].

5.1 Basic classification of skin wrinkles

Here, one should provide a slightly more nuanced definition of skin wrinkles. *Skin wrinkles* (or skin folds) [162] are generally associated with ageing and manifest as amplification of the natural skin microrelief (see **section 1.7** and **Figure 10** in the **Supplementary Material section**) which is believed to be the results of material and structural alterations of the skin internal structure [158] in combination with changes in the mechanical environment of the body (e.g. relaxation of tension lines and resorption of hypodermal tissue).

Expression (or temporary) wrinkles (also called *expression lines*) are associated with skin and facial movement. They can originate from facial muscular activation (i.e. smiling) or by simple mechanical actions on the skin surface such as twisting, shear or compression. *Gravitational folds* on the face arise from the combined effect of constant gravitational loads applied to a microstructurally ageing-altered epidermis, dermis and hypodermis.

5.2 A brief summary of the physics of wrinkles

Wrinkling, ubiquitous in Nature, is a multiscale spatial phenomenon which can span over eight orders of magnitude [163]. From a physical point of view, wrinkles are the result of a complex interplay between material and structural properties, boundary and loading conditions, the exact nature of which remains to be elucidated [164], particularly for non-linear materials assembled into geometrically-complex structures such as the skin. Although the study of surface instabilities dates back to the seminal work of Biot [165, 166], Cerda and Mahadevan revisited the Föppl–von Kármán equations for thin elastic plates using asymptotic and scaling arguments and established a simple theory of wrinkling, valid far from the onset of surface instability. They showed that the wavelength of wrinkles λ is proportional to $K^{-0.25}$ and A where K is an equivalent stiffness arising from an "elastic substrate" effect and A is the amplitude of wrinkles. Wrinkles can be induced by a variety of ways including residual strains in bi-layer structures [167], differential growth in multi-layer biological structures [168] (see **Figure 1,** the convoluted geometry of the basement membrane separating the viable epidermis from the papillary dermis can be explained by differential growth), compressive and tensile [169] loads combined with geometric constraints (i.e. inextensibility, geometrical coupling with a thicker foundation) in very thin structures (i.e. membranes and shells) or any rebalancing of material and structural properties in these single or multi-layer systems. A simple conceptual model to explain the formation of wrinkles consists of a bi-layer plate structure featuring a thin and stiff layer laying on a much thicker and softer foundation [164]. Upon in-plane compression of both layers, due to its higher bending stiffness, the top (thin) layer will favour large wavelength bending deformations while the bottom (soft) layer will penalise these wavelengths and rather promote smaller wavelengths. As a result of this energy-minimising structural response to competition between bending energies of the top and bottom layers, intermediate wavelengths, and so, length scales, will emerge under the form of wrinkles. If compression continues after the formation of wrinkles, the latter will evolve into folds and, finally, creases when self-contact of the surface occurs. Since the paper of Cerda and Mahadevan [164] a large body of work on surface instabilities has been being produced, particularly in the physics community, as understanding and harnessing surface instabilities opens up a broad range of industrial applications from nano-metrology to programmable surfaces, whereby generation of self-organised wrinkling patterns can be controlled by judicious structural/material arrangements and tuned localised loading conditions [163, 170]. Holland *et al.* [171] recently provided an in-depth analysis of instabilities of soft films on compliant substrates and showed the high sensitivity of these soft bi-layer systems to stiffness ratio, boundary conditions and modes of compression. They also introduced novel metrics, the *effective strain*, *effective stiffness* and *effective wavelength* and recommend their standardised use in the analysis of instabilities.

In the last decade, there has also been a growing interest in studying surface instabilities (e.g. wrinkles, folds and creases) in biological systems as they play a central role in many physiological functions and processes including morphogenesis/growth of normal and cancerous tissues as well as ageing [26, 168, 172-177]. Of particular relevance to skin and ageing, skin wrinkles constitute a rich test-bed for many theories of surface instability phenomena. However, the majority of resulting mathematical models are often restricted to idealised geometries (e.g. perfectly flat structures, i.e. plates), simplified boundary and loading conditions or simplistic constitutive models.

5.3 Analytical models of skin wrinkles

Because the skin can sustain finite deformations and strains *in vivo*, it is sensible to model it using appropriate corresponding theories. Although precluding material anisotropic effects, a neo-Hookean constitutive formulation is probably the simplest form of materially-stable hyperelasticity valid for finite kinematics. In the physics of wrinkling, the ratio of stiffness and that of thickness between the different layers making up a structure are central in conditioning the onset of wrinkle formation as well as wrinkle characteristics [164, 167].

The *stratum corneum* is the skin layer most sensitive to external environmental conditions (see **sections 2.1** and **2.2**) and its Young's modulus can span several orders of magnitude as a result of alterations in relative humidity [25]. Considering the skin as an assembly of a thin layer of thickness h (i.e. the *stratum corneum*) bonded to an underlying infinitely deep half-space, both made of a neo-Hookean material with distinct mechanical properties (shear moduli μ_f and μ_s for, respectively the thin film and thick substrate) is a reasonable assumption to study the characteristics of wrinkles as a function of layer stiffness ratio. Cao and Hutchinson [167] proposed such a model which was based on an extension of Biot's exact finite strain bifurcation analysis to bi-layer systems. Assuming isochoric behaviour and application of plane strain compression to both layers, the compression bifurcation strain is:

$$\varepsilon_0 = \frac{1}{4}\sqrt[3]{\left(\frac{3\mu_s}{\mu_f}\right)^2} \tag{69}$$

They showed that, for both layers in a stress-free reference state, the compressive bifurcation strain at the onset of wrinkling matches very well that determined by Allen [178] who considered the film to be linear elastic provided the modulus ratio μ_f / μ_s is large enough (>10). The critical wave number is then determined as:

$$k_0 = \frac{1}{h}\sqrt[3]{\frac{3\mu_s}{\mu_f}} \tag{70}$$

leading to a wrinkle wave length λ_0:

$$\lambda_0 = \frac{2\pi}{k_0} = 2\pi h \sqrt[3]{\frac{\mu_f}{3\mu_s}} \tag{71}$$

When the material properties of both layers are identical $(\mu_f / \mu_s = 1)$, $\varepsilon_0 = 0.456$ which is the solution established by Biot [165] for a homogeneous neo-Hookean half-space. However, based on another study [179], Cao and Hutchinson recognise that, given the high sensitivity of wrinkling to imperfections, the likelihood of the film reaching a strain value $\varepsilon_0 = 0.456$ before onset of wrinkling is very low.

Lejeune *et al.* [180] recently developed a comprehensive quad-layer model to shed light on observed geometric instabilities in thin film-substrate systems, thereby accounting for interfacial layers absent from theoretical bi-layer models which do not account from material or structural imperfections from manufacturing processes. Their modelling framework would be applicable to skin provided strains are small and materials could be considered as isotropic linear elastic. Motivated by epidermal electronics applications, Lejeune *et al.* [161] later generalised their previous approach by extending it with an arbitrary number of layers featuring arbitrary thicknesses and by using an algorithmic approach which was validated by testing it against finite element computations. Through analytical and numerical calculations, Goriely *et al.* [177] studied the role of structural (e.g. thin or thick shell assumption) and constitutive parameters (e.g. type of hyperelastic constitutive formulation) on compression- and extension-induced structural instabilities in elastomers and in biological soft tissues. For certain cases, the typical strain-hardening behaviour of soft tissues was found not to be a stabilising factor delaying the onset of instabilities. Besides, for a compressed half-space, a soft tissue material is more stable than an elastomeric material while an opposite behaviour is observed when considering a compressed spherical thick shell. Dervaux and Ben Amar [168] proposed a mechanobiological model of constrained growth in bi-layered structures that could explain the wrinkled nature of the basement membrane separating the viable epidermis from the papillary dermis. However, they recognised that the Föppl–von Kármán approximation for the thin top layer is violated when the stiffness of the two layers are of the same order of magnitude.

Ciarletta *et al.* [181] developed an analytical model of shear-induced wrinkling instabilities in skin by assuming the skin to be a mono-layer neo-Hookean solid endowed with a surface energy and subjected to a residual stretch corresponding to a cleavage line (i.e. Langer line). By conducting a perturbation analysis these authors corroborated experimental observations showing that shearing the skin surface along cleavage lines requires a greater magnitude of shear than shearing along the direction of compression. It was also demonstrated that surface energy delays the onset of instability. The model was then extended to transverse isotropy by introducing a single family of fibres (i.e. collagen and elastin) and studied using a Stroh formalism. The mathematical analysis showed that the shear threshold at which surface instabilities occur is lower in the presence of fibres, and further decreases as the apparent stiffness of fibres increase (like what is often reported in the context of ageing). Motivated by metrology applications, Gower [182] later devised an analytical framework to study wrinkles in soft fibre-reinforced solids in order to establish a link between wrinkle characteristics and material constitutive parameters. He considered a transversely isotropic hyperelastic formulation featuring two distinct invariants, one for representing fibre extension and the other to represent fibre compression. The model showed how the angle between the fibres and the surface wrinkle orientation indicates the mechanical status of fibres: fibres resisting only extension, only compression, or a combination of both. Moreover, at the onset of surface wrinkling, and for the constitutive parameters considered, this angle was shown to be discrete by taking only 3 or 4 possible values. Against experimental evidence and physical intuition, Carfagna *et al.* [183] demonstrated that oblique wrinkles (*i.e.* not aligned with a principal direction of deformation) can arise in soft isotropic solids. Understanding the mechanics of wrinkle formation is an essential step toward the development of applications aiming at reducing or removing wrinkles [184] by straightening of wrinkles [185]. For example, Yu *et al.* [184] recently developed a wearable and physico-chemically tuneable polysiloxane-based material that can be topically applied to the skin surface. After curing, the cross-linked polymer layer bonded to the skin effectively straightens wrinkles. Beyond cosmetics, applications of this technology extend to restoration of the skin barrier function, pharmaceutical delivery and wound dressings.

5.4 Computational models of skin wrinkles

Although analytical models of skin wrinkles can be extremely insightful in unravelling physical mechanisms that explain experimental observations, they quickly become too restrictive if research objectives are to investigate naturally complex biological structures, non-uniform loading conditions or to account for more sophisticated non-linear materials. In these cases, numerical techniques such as the ubiquitous finite element method are the only way forward.

Flynn and McCormack [101] developed an experimentally-based computational model of compression-induced macroscopic skin wrinkles. The model provided a valuable insight into the influence of the number of layers and pre-stress on wrinkle formation. In the *in vitro* and *in silico* experiments it was observed that the depth of wrinkles significantly increases under 20-30% strain. This model was subsequently used to simulate ageing effects on compressive wrinkle formation but still did not take into account real skin microrelief [103]. Based on the modelling framework of their multi-stage buckling theory which suggested that wrinkle morphology suddenly changes from *stratum corneum* wrinkling to epidermis wrinkling leading respectively to shallow fine furrows and deep coarse wrinkles, Kuwazuru *et al.* [186] devised an experimental apparatus to address this question. It was demonstrated that the skin wrinkling rate experiences a step increase at the age of 33 translating into a sudden change in the morphology of skin wrinkles. What these authors called "buckling mode switch" is the result of what had already been explained by Cerda and Mahadevan [164], namely the competition between bending energies of individual layers which favour particular wave lengths during wrinkle formation. Any change in the ratio of bending energies (through changes in layer thickness and/or material properties) affect the morphology of wrinkles. Recently, Shiihara *et al.* [187] conducted a series of finite element analyses to study the effect of skin microrelief on large wrinkles. Their simplified two-dimensional (2D) analyses were based on non-anatomical skin microrelief and dynamic implicit-based buckling-post-buckling procedures [188]. Shiihara *et al.* [187] suggested that fine microrelief at the surface inhibit large wrinkles (i.e. deeper than 0.35 mm). Until the recent work of Limbert and Kuhl [189], no physics-based study had examined the role of (anatomically-realistic) skin microrelief on the characteristics of surface micro-wrinkles.

Using an anatomically-based bi-layer finite element model featuring neo-Hookean materials, these authors highlighted the critical role of layer stiffness ratio on wrinkle characteristics and surface strains in simulated in-plane compression (**Figure 4**, see also **section 1.13** of the **Supplementary Material**). As predicted by theoretical and computational models of growth-induced surface instabilities of flat bi-layer systems [190], period-doubling effects were also observed in the finite element analyses. The highly non-linear nature of surface instabilities make their numerical realisation very challenging, and standard Newton-Raphson incremental solving procedures might be insufficient [188], thus requiring better path-following procedures such as arc-length methods [189, 191] and/or dynamic regularisation techniques [189]. Cubic finite element shape functions continuous across element boundaries are desirable to capture steep curvature gradients such as those occurring in surface instabilities. Isogeometric finite element formulations [192-194] are therefore superior to those based on Lagrange polynomial interpolation. Identifying critical conditions that trigger surface instabilities is also a challenging endeavour but progress in this area is steadily moving forward [195].

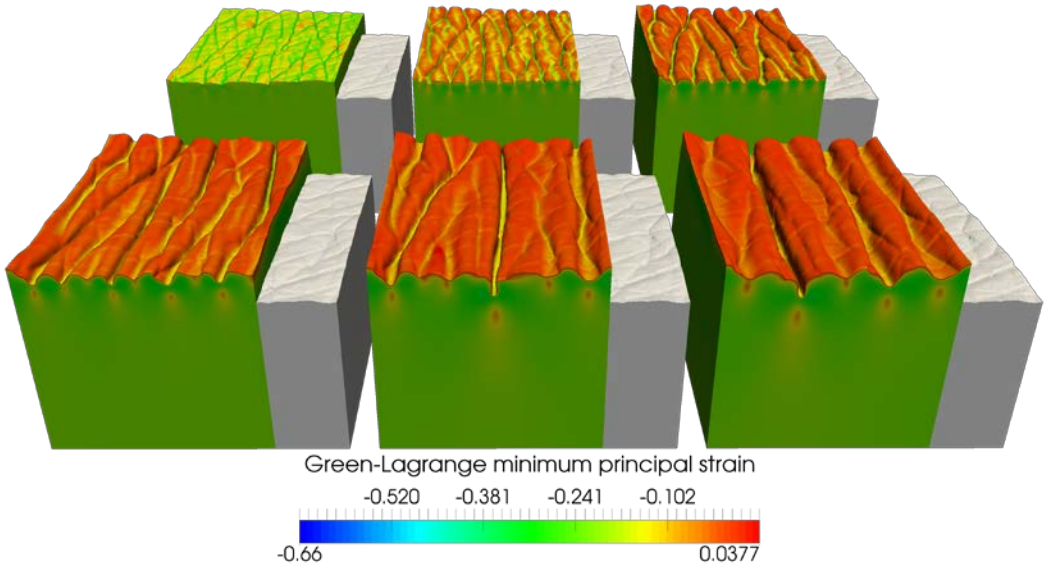

Figure 4. Colour plots of minimum principal strains after 25% uniform in-plane compression as a function of the stiffness ratio $\alpha = E_{stratum\,corneum} / E_{substrate}$. The undeformed skin geometry is plotted in white to highlight the significant surface topography alterations arising from wrinkling instabilities which strongly depend on α. Adapted from Limbert and Kuhl [189].

6. Perspective and conclusion

From this review which offered a relatively large and eclectic selection of constitutive models of the skin, it is clear that these models have now reached a high level of sophistication, and can capture a wide range of relevant biophysical features. Nevertheless, as pointed out by Jor *et al.* [6] in their review paper on the computational and experimental characterisation of skin, a significant limiting factor in the development and adoption of advanced constitutive theories is the scarcity and *relevance* of captured experimental data. There are several fundamental aspects, or more precisely, reasons, and questions associated with this observation:

1. Large intra- and inter-individual variability of biophysical properties;
2. The *in vivo* and *ex vivo* biophysical environments of the skin are fundamentally different;
3. Extreme sensitivity of the skin to environmental conditions;
4. How to best integrate multi-modality and multiscale imaging, characterisation and modelling techniques?

Intra-individually, the skin is a complex heterogeneous adaptive structure which varies according to body location, health status and history, diet, age, lifestyle, *external* environmental conditions (e.g. temperature, humidity, pollution level, water quality, sun exposure, contact with external surfaces) and *internal* environmental conditions (e.g. hormones, pregnancy, water and glucose levels, tension lines).

Besides intra-individual variability, there is a strong biophysical variability, particularly that associated with sex and ethnicity. There are therefore formidable challenges in *representatively* characterising the skin ultrastructure as well as its biophysical properties. Should we describe the skin as an individual-specific system, or rather, as a statistical system describing particular populations? Or, even more daringly, as a combination of both? This issue is, of course, not unique to the skin, but pervasive throughout many complex biological systems. Data mining and machine learning techniques [196] are likely to play an increasing role in the future to make sense of large and complex heterogeneous data sets, whether they originate from physical or computer experiments, expert knowledge (e.g. anatomists, clinicians, nurses, vets) or from any other means (e.g. patient's observations, shamanic knowledge).
Perhaps, another related buzz word of modern times to throw in here, is *artificial intelligence* (AI)! AI is simply the processing ability of a (non-human) computer to solve problems without having been taught how. Only when the techniques discussed above will have assisted us in establishing a more fundamental and mechanistic understanding of the multi-factorial nature of skin biophysics, will we be able to seamlessly integrate these huge data sets into, first, *descriptive*, and then, *predictive*, mathematical and computational models. Multi-variate and multiscale data-based and/or physics-based statistical models of the skin built from the results of machine learning (i.e. meta-models) could then replace computationally expensive physics-based finite element models, and be used to predict a variety of scenarios and outcomes. For example, one could ask: What should be the optimum stiffness/thickness of a silicon layer on a seating surface so that pressure on the skin does not reach a critically-damaging threshold? How would this change if relative humidity increases by 30%? And if the patient is between 50 and 65 years of age instead of 25? Of course, it depends! And it depends on a lot of factors. The answers to these questions are likely to be statistical distributions rather than single deterministic values. Perhaps, in the same way that statistical information is currently being integrated into constitutive models (e.g. fibre dispersion, degree of crimping of collagen fibres), additional stochastic elements could be added into constitutive equations effectively developing what could be termed *stochastic partial differential equations* [197]. This would be another approach to encompass variability, directly into the constitutive equations, rather than at the input data level when conducting probabilistic simulations.
The reliance of structural and structurally-based phenomenological models on accurate descriptions of the skin ultrastructure and the associated mechanical properties of its sub-components, means that imaging and characterisation techniques needs to span multiple spatial and temporal scales if one wants to capture more reliably the complex biophysics of the skin. Additionally, and as a corollary to that, multiscale modelling techniques needs to be developed in concert with these physical experimental protocols. Computational multiscale methods combining atomistic, molecular and continuum techniques are likely to play an increasingly important role in the modeling of skin biophysics in the forthcoming decades [57, 198, 199]. Moreover, integration of imaging and physical testing (i.e. *in situ* imaging) [200] is a very promising approach that should be followed, as much can be learnt about microstructural mechanisms under real loading conditions. For a detailed discussion of challenges/opportunities of tissue structure imaging and mechanical characterisation, see the review by Jor *et al.* [6]. These authors also discuss the critically important point concerning the differences between *in vivo* and *ex vivo* testing of skin. They rightly point out that, to better translate research into the clinical setting, major attention should be directed toward the development of *in vivo* quantitative characterisation techniques. The advent of cheap, powerful personal and cloud computing is rapidly transforming the face of research in the life sciences. In the very near future, on-demand physics-based computing accessible from any personal electronic device such as tablets and smart phones, and from any location on the planet, is likely to become an everyday commodity, like electricity. It is anticipated that patients will be able to collect *in vivo* data, process and transmit it so that health practitioners will be able to use these tools, remotely, or in clinics, to assist their decision process while engineers and scientists will continue to embrace, develop and push forward this trend. In the meantime, biophysical modellers are likely to keep busy!

Data accessibility not applicable
Competing interests none
Authors' contributions not applicable

Acknowledgements / Funding statement
The idea of this article arose following many fruitful discussions with Prof. Michel Destrade (NUI Galway, Ireland), Prof. T. Christian Gasser (KTH Stockholm, Sweden) and Dr. Artur L. Gower (University of Manchester, UK) initiated during the EPSRC-sponsored workshop "Constitutive behaviour of soft tissues: connecting experimental and modelling perspectives", August 31–September 2, 2016, University of Manchester organised by Prof. William Parnell and Dr. Tom Shearer (University of Manchester, UK). GL would like to thank them for their invitation to participate to the workshop. Finally, GL would also like to gratefully acknowledge the financial support he has received over the last few years from the Royal Society, The Royal Academy of Engineering, The British High Commission in South Africa, EPSRC, Procter & Gamble, L'Oréal and the US Air Force.

Ethics statement not applicable

7. References

[1] Burns, T., Breathnach, S., Cox, N. & Griffiths, C. 2004 *Rook's Textbook of Dermatology*. 7th edition ed. Oxford, Blackwell Science.
[2] Silver, F.H., Siperko, L.M. & Seehra, G.P. 2003 Mechanobiology of force transduction in dermal tissue. *Skin Res Technol* **9**, 3-23.
[3] Jablonski, N.G. 2006 *Skin: a natural history*. Berkeley and Los Angeles, California, University of California Press; 266 p.
[4] Belytschko, T., Liu, W.K. & Moran, B. 2000 *Nonlinear Finite Elements for Continua and Structures*. Oxford, Wiley.
[5] Forrester, A.I.J. 2010 Black-box calibration for complex systems simulation. *Philos T R Soc A* **368**, 3567-3579.
[6] Jor, J.W.Y., Parker, M.D., Taberner, A.J., Nash, M.P. & Nielsen, P.M.F. 2013 Computational and experimental characterization of skin mechanics: identifying current challenges and future directions. *Wiley Interdisciplinary Reviews: Systems Biology and Medicine* **5**, 539-556.
[7] Li, W. 2015 Modelling methods for In Vitro biomechanical properties of the skin: A review. *Biomedical Engineering Letters* **5**, 241-250.
[8] Fung, Y.C. 1981 *Biomechanics: mechanical properties of living tissues*. New York, Springer-Verlag.
[9] Humphrey, J.D. 2003 Continuum biomechanics of soft biological tissues. *P Roy Soc A-Math Phys* **459**, 3-46.
[10] Lanir, Y. 2016 Multi-scale structural modeling of soft tissues mechanics and mechanobiology. *J Elast*, 1-42.
[11] Shimizu, H. 2007 *Shimizu's Textbook of Dermatology*, Hokkaido University Press - Nakayama Shoten Publishers; 564 p.
[12] Buganza Tepole, A. & Kuhl, E. 2014 Computational modeling of chemo-bio-mechanical coupling: a systems-biology approach toward wound healing. *Comput Meth Biomech Biomed Eng*, 1-18.
[13] Kvistedal, Y.A. & Nielsen, P.M.F. 2009 Estimating material parameters of human skin in vivo. *Biomech Model Mechanobiol* **8**, 1-8.
[14] Lanir, Y. 1987 Skin mechanics. In *Handbook of Bioengineering* (eds. R. Skalak & S. Chien). New York, McGraw-Hill.
[15] Vierkötter, A. & Krutmann, J. 2012 Environmental influences on skin aging and ethnic-specific manifestations. *Dermato-endocrinology* **4**, 227-231.
[16] Silver, F.H., Freeman, J.W. & DeVore, D. 2001 Viscoelastic properties of human skin and processed dermis. *Skin Res Technol* **7**, 18-23.
[17] Limbert, G. 2014 Chapter 4: State-of-the-art constitutive models of skin biomechanics. In *Computational Biophysics of the Skin* (ed. B. Querleux), pp. 95-131. Singapore, Pan Stanford Publishing Pte. Ltd.
[18] Marieb, E.N. & Hoehn, K. 2010 *Human Anatomy & Physiology*. 8th edition ed. San Francisco, USA, Pearson International Edition; 1114 p.

[19] Chan, L.S. 1997 Human skin basement membrane in health and autoimmune diseases. *Frontiers in Bioscience* **2**, 343-352.
[20] Leyva-Mendivil, M.F., Page, A., Bressloff, N.W. & Limbert, G. 2015 A mechanistic insight into the mechanical role of the stratum corneum during stretching and compression of the skin. *J Mech Behav Biomed Mater* **49**, 197-219.
[21] Leyva-Mendivil, M.F., Lengiewicz, J., Page, A., Bressloff, N.W. & Limbert, G. 2017 Skin microstructure is a key contributor to its friction behaviour. *Trib Lett* **65**, 12.
[22] Dandekar, K., Raju, B.I. & Srinivasan, M.A. 2003 3-D finite-element models of human and monkey fingertips to investigate the mechanics of tactile sense. *J Biomech Eng* **125**, 682-691.
[23] Xu, F. & Lu, T. 2011 *Introduction to Skin Biothermomechanics and Thermal Pain*. Heidelberg Dordrecht London New York, Springer; 414 p.
[24] Biniek, K., Levi, K. & Dauskardt, R.H. 2012 Solar UV radiation reduces the barrier function of human skin. *PNAS* **109**, 17111-17116.
[25] Wu, K.S., van Osdol, W.W. & Dauskardt, R.H. 2006 Mechanical properties of human stratum corneum: effects of temperature, hydration, and chemical treatment. *Biomaterials* **27**, 785-795.
[26] Ciarletta, P. & Ben Amar, M. 2012 Papillary networks in the dermal-epidermal junction of skin: A biomechanical model. *Mech Res Commun* **42**, 68-76.
[27] Burgeson, R.E. & Christiano, A.M. 1997 The dermal-epidermal junction. *Current Opinion in Cell Biology* **9**, 651-658.
[28] Ribeiro, J.F., dos Anjos, E.H.M., Mello, M.L.S. & de Campos Vidal, B. 2013 Skin collagen fiber molecular order: a pattern of distributional fiber orientation as assessed by optical anisotropy and image analysis. *Plos One* **8**, e54724.
[29] Gosline, J., Lillie, M., Carrington, E., Guerette, P., Ortlepp, C. & Savage, K. 2002 Elastic proteins: biological roles and mechanical properties. *Philosophical Transactions of the Royal Society of London. Series B: Biological Sciences* **357**, 121-132.
[30] Sherratt, M.J. 2013 Age-Related Tissue Stiffening: Cause and Effect. *Advances in Wound Care* **2**, 11-17.
[31] Langer, K. 1861 Zur Anatomie und Physiologie der Haut. Über die Spaltbarkeit der Cutis. *Sitzungsbericht der Mathematisch-naturwissenschaftlichen Classe der Wiener Kaiserlichen Academie der Wissenschaften Abt* **44**.
[32] Langer, K. 1978 On the anatomy and physiology of the skin: I. The cleavability of the cutis. *British Journal of Plastic Surgery* **31**, 3-8.
[33] Langer, K. 1978 On the anatomy and physiology of the skin: II. Skin Tension (With 1 Figure). *British Journal of Plastic Surgery* **31**, 93-106.
[34] Ní Annaidh, A., Bruyère, K., Destrade, M., Gilchrist, M.D. & Otténio, M. 2011 Characterization of the anisotropic mechanical properties of excised human skin. *J Mech Behav Biomed Mater* **5**, 139-148.
[35] Alexander, H. & Cook, T.H. 1977 Accounting for natural tension in the mechanical testing of human skin. *J Invest Dermatol* **69**, 310-314.
[36] Flynn, C., Taberner, A.J., Nielsen, P.M.F. & Fels, S. 2013 Simulating the three-dimensional deformation of in vivo facial skin. *J Mech Behav Biomed Mater* **28**, 484-494.
[37] Flynn, C., Stavness, I., Lloyd, J. & Fels, S. 2013 A finite element model of the face including an orthotropic skin model under in vivo tension. *Computer Methods in Biomechanics & Biomedical Engineering*.
[38] Deroy, C., Destrade, M., Mc Alinden, A. & Ní Annaidh, A. 2016 Non-invasive evaluation of skin tension lines with elastic waves. *Skin Res Technol*.
[39] Rosado, C., Antunes, F., Barbosa, R., Fernando, R., Estudante, M., Silva, H.N. & Rodrigues, L.M. 2016 About the in vivo quantitation of skin anisotropy. *Skin Res Technol*, http://dx.doi.org/10.1111/srt.12353.
[40] Wan Abas, W.A.B. 1994 Biaxial tension test of human skin in vivo. *Biomed Mater Eng* **4**, 473-486.
[41] Ní Annaidh, A., Bruyère, K., Destrade, M., Gilchrist, M.D., Maurini, C., Otténio, M. & Saccomandi, G. 2012 Automated estimation of collagen fibre dispersion in the dermis and its contribution to the anisotropic behaviour of skin. *Ann Biomed Eng* **40**, 1666-1678.
[42] Ottenio, M., Tran, D., Annaidh, A.N., Gilchrist, M.D. & Bruyère, K. 2015 Strain rate and anisotropy effects on the tensile failure characteristics of human skin. *J Mech Behav Biomed Mater* **41**, 241-250.
[43] Kvistedal, Y.A. & Nielsen, P.M.F. 2004 Investigating stress-strain properties of in-vivo human skin using multiaxial loading experiments and finite element modeling. *Proceedings of the 26th Annual International Conference of the IEEE Engineering in Medicine and Biology Society, Vols 1-7* **26**, 5096-5099.
[44] Batisse, D., Bazin, R., Baldeweck, T., Querleux, B. & Lévêque, J.L. 2002 Influence of age on the wrinkling capacities of skin. *Skin Res Technol* **8**, 148-154.

[45] Delalleau, A., Josse, G., Lagarde, J.M., Zahouani, H. & Bergheau, J.M. 2006 Characterization of the mechanical properties of skin by inverse analysis combined with the indentation test. *J Biomech* **39**, 1603-1610.
[46] Diridollou, S., Patat, F., Gens, F., Vaillant, L., Black, D., Lagarde, J.M., Gall, Y. & Berson, M. 2000 In vivo model of the mechanical properties of the human skin under suction. *Skin Res Technol* **6**, 214-221.
[47] Dobrev, H.q. 2000 Use of Cutometer to assess epidermal hydration. *Skin Res Technol* **6**, 239-244.
[48] Hendriks, F.M., Brokken, D., van Eemeren, J., Oomens, C.W.J., Baaijens, F.P.T. & Horsten, J. 2003 A numerical-experimental method to characterize the non-linear mechanical behaviour of human skin. *Skin Res Technol* **9**, 274-283.
[49] Weickenmeier, J., Jabareen, M. & Mazza, E. 2015 Suction based mechanical characterization of superficial facial soft tissues. *J Biomech* **48**, 4279-4286.
[50] Tonge, T.K., Atlan, L.S., Voo, L.M. & Nguyen, T.D. 2013 Full-field bulge test for planar anisotropic tissues: Part I – Experimental methods applied to human skin tissue. *Acta Biomater* **9**, 5913-5925.
[51] Geerligs, M., Oomens, C.W.J., Ackermans, P.A.J., Baaijens, F.P.T. & Peters, G.W.M. 2011 Linear shear response of the upper skin layers. *Biorheology* **In press**.
[52] Geerligs, M., van Breemen, L.C.A., Peters, G.W.M., Ackermans, P.A.J., Baaijens, F.P.T. & Oomens, C.W.J. 2011 In vitro indentation to determine the mechanical properties of epidermis. *J Biomech* **44**, 1176-1181.
[53] Lamers, E., van Kempen, T.H.S., Baaijens, F.P.T., Peters, G.W.M. & Oomens, C.W.J. 2013 Large amplitude oscillatory shear properties of human skin. *J Mech Behav Biomed Mater* **28**, 462-470.
[54] Lanir, Y. & Fung, Y.C. 1974 Two-Dimensional Mechanical Properties of Rabbit Skin—II: Experimental Results. *J Biomech* **7**, 171-182.
[55] Wong, W.L.E., Joyce, T.J. & Goh, K.L. 2016 Resolving the viscoelasticity and anisotropy dependence of the mechanical properties of skin from a porcine model. *Biomech Model Mechanobiol* **15**, 433-446.
[56] Veronda, D.R. & Westmann, R. 1970 Mechanical characterization of skin - finite deformations. *J Biomech* **3**, 111-124.
[57] Marino, M. 2016 Molecular and intermolecular effects in collagen fibril mechanics: a multiscale analytical model compared with atomistic and experimental studies. *Biomech Model Mechanobiol* **15**, 133-154.
[58] Spencer, A.J.M. 1984 Constitutive Theory for Strongly Anisotropic Solids. In *Continuum Theory of the Mechanics of Fibre-Reinforced Composites* (ed. A.J.M. Spencer), pp. 1-32. Vienna, Springer Vienna.
[59] Šolinc, U. & Korelc, J. 2015 A simple way to improved formulation of FE^2 analysis. *Comput. Mech.* **56**, 905-915.
[60] Saeb, S., Steinmann, P. & Javili, A. 2016 Aspects of computational homogenization at finite deformations: a unifying review from Reuss' to Voigt's bound. *Appl Mech Rev* **68**, 050801-050801-050833.
[61] Buganza Tepole, A., Gart, M., Gosain, A.K. & Kuhl, E. 2014 Characterization of living skin using multi-view stereo and isogeometric analysis. *Acta Biomater* **10**, 4822-4831.
[62] Buganza Tepole, A., Gosain, A.K. & Kuhl, E. 2012 Stretching skin: The physiological limit and beyond. *Int. J. Non-Linear Mech.* **47**, 938-949.
[63] Buganza Tepole, A., Gosain, A.K. & Kuhl, E. 2014 Computational modeling of skin: Using stress profiles as predictor for tissue necrosis in reconstructive surgery. *Comput. Struct.* **143**, 32-39.
[64] Buganza Tepole, A., Ploch, C.J., Wong, J., Gosain, A.K. & Kuhl, E. 2011 Growing skin: A computational model for skin expansion in reconstructive surgery. *J Mech Phys Solids* **59**, 2177-2190.
[65] Zöllner, A., Buganza Tepole, A., Gosain, A.K. & Kuhl, E. 2012 Growing skin: tissue expansion in pediatric forehead reconstruction. *Biomech Model Mechanobiol* **11**, 855-867.
[66] Zöllner, A.M., Buganza Tepole, A. & Kuhl, E. 2012 On the biomechanics and mechanobiology of growing skin. *J Theor Biol* **297**, 166-175.
[67] Zöllner, A.M., Holland, M.A., Honda, K.S., Gosain, A.K. & Kuhl, E. 2013 Growth on demand: Reviewing the mechanobiology of stretched skin. *J Mech Behav Biomed Mater* **28**, 495-509.
[68] Leyva-Mendivil, M.F., Lengiewicz, J., Page, A., Bressloff, N.W. & Limbert, G. 2017 Implications of multi-asperity contact for shear stress distribution in the viable epidermis – An image-based finite element study. *Biotribology*, in press.
[69] Young, P.G., Beresford-West, T.B.H., Coward, S.R.L., Notarberardino, B., Walker, B. & Abdul-Aziz, A. 2008 An efficient approach to converting three-dimensional image data into highly accurate computational models. *Philos T R Soc A* **366**, 3155-3173.
[70] Limbert, G., van Lierde, C., Muraru, O.L., Walboomers, X.F., Frank, M., Hansson, S., Middleton, J. & Jaecques, S. 2010 Trabecular bone strains around a dental implant and associated micromotions--a micro-CT-based three-dimensional finite element study. *J Biomech* **43**, 1251-1261.

[71] Linder-Ganz, E., Shabshin, N., Itzchak, Y. & Gefen, A. 2007 Assessment of mechanical conditions in sub-dermal tissues during sitting: A combined experimental-MRI and finite element approach. *J Biomech* **40**, 1443-1454.
[72] Limbert, G., Bryan, R., Cotton, R., Young, P., Hall-Stoodley, L., Kathju, S. & Stoodley, P. 2013 On the mechanics of bacterial biofilms on non-dissolvable surgical sutures: A laser scanning confocal microscopy-based finite element study. *Acta Biomater* **9**, 6641-6652.
[73] Gerhardt, L.C., Strässle, V., Lenz, a., Spencer, N.D. & Derler, S. 2008 Influence of epidermal hydration on the friction of human skin against textiles. *Journal of the Royal Society, Interface / the Royal Society* **5**, 1317-1328.
[74] Adams, M.J., Briscoe, B.J. & Johnson, S.A. 2007 Friction and lubrication of human skin. *Trib Lett* **26**, 239-253.
[75] Derler, S., Gerhardt, L.C., Lenz, a., Bertaux, E. & Hadad, M. 2009 Friction of human skin against smooth and rough glass as a function of the contact pressure. *Tribology International* **42**, 1565-1574.
[76] Kwiatkowska, M., Franklin, S.E., Hendriks, C.P. & Kwiatkowski, K. 2009 Friction and deformation behaviour of human skin. *Wear* **267**, 1264-1273.
[77] Wolfram, L.J. 1983 Friction of Skin. *Journal of the Society of Cosmetic Chemists* **34**, 465-476.
[78] Stupkiewicz, S., Lewandowski, M.J. & Lengiewicz, J. 2014 Micromechanical analysis of friction anisotropy in rough elastic contacts. *Int J Solids Struct* **51**, 3931-3943.
[79] Goldstein, B. & Sanders, J. 1998 Skin Response to Repetitive Mechanical Stress : a New Experimental Model in Pig. *Arch. Phys. Med. Rehabil.* **79**, 265-272.
[80] Weickenmeier, J. & Jabareen, M. 2014 Elastic–viscoplastic modeling of soft biological tissues using a mixed finite element formulation based on the relative deformation gradient. *Int J Numer Meth Bio* **30**, 1238-1262.
[81] Li, W. & Luo, X.Y. 2016 An invariant-based damage model for human and animal skins. *Ann Biomed Eng* **44**, 3109-3122.
[82] McBride, A., Bargmann, S., Pond, D. & Limbert, G. 2016 Thermoelastic modelling of the skin at finite deformations. *Journal of Thermal Biology* **62**, 201-209.
[83] Vermolen, F.J., Gefen, A. & Dunlop, J.W.C. 2012 In Vitro "Wound" Healing: Experimentally Based Phenomenological Modeling. *Advanced Engineering Materials* **14**, B76-B88.
[84] Sherratt, J.A. & Dallon, J.C. 2002 Theoretical models of wound healing: past successes and future challenges. *Cr Biol* **325**, 557-564.
[85] Buganza Tepole, A. 2017 Computational systems mechanobiology of wound healing. *Comput Meth Appl Mech Eng* **314**, 46-70.
[86] Marsden, J.E. & Hughes, T.J.R. 1994 *Mathematical Foundations of Elasticity*. New-York, Dover; 556 p.
[87] Holzapfel, G.A. 2000 *Nonlinear Solid Mechanics. A Continuum Approach for Engineering*. Chichester, UK, John Wiley & Sons; 470 p.
[88] Boehler. 1978 Lois de comportement anisotrope des milieux continus. *Journal de Mécanique* **17**, 153-190.
[89] Limbert, G. & Taylor, M. 2002 On the constitutive modeling of biological soft connective tissues. A general theoretical framework and tensors of elasticity for strongly anisotropic fiber-reinforced composites at finite strain. *Int J Solids Struct* **39**, 2343-2358.
[90] Spencer, A.J.M. 1992 *Continuum theory of the mechanics of fibre-reinforced composites*. New York, Springer-Verlag.
[91] Criscione, J.C., Humphrey, J.D., Douglas, A.S. & Hunter, W.C. 2000 An invariant basis for natural strain which yields orthogonal stress response terms in isotropic hyperelasticity. *J Mech Phys Solids* **48**, 2445-2465.
[92] Criscione, J.C., Douglas, A.S. & Hunter, W.C. 2001 Physically based strain invariant set for materials exhibiting transversely isotropic behavior. *J Mech Phys Solids* **49**, 871-897.
[93] Lanir, Y. 1983 Constitutive equations for fibrous connective tissues. *J Biomech* **16**, 1-22.
[94] Meijer, R., Douven, L.F.A. & Oomens, C.W.J. 1999 Characterisation of Anisotropic and Non-linear Behaviour of Human Skin In Vivo. *Comput Meth Biomech Biomed Eng* **2**, 13-27.
[95] Jor, J.W.Y., Nash, M.P., Nielsen, P.M.F. & Hunter, P.J. 2011 Estimating material parameters of a structurally based constitutive relation for skin mechanics. *Biomech Model Mechanobiol* **10**, 767-778.
[96] Holzapfel, G.A. & Ogden, R.W. 2016 On fiber dispersion models: exclusion of compressed fibers and spurious model comparisons. *J Elast*, 1-20.
[97] Gasser, T.C., Ogden, R.W. & Holzapfel, G.A. 2006 Hyperelastic modelling of arterial layers with distributed collagen fibre orientations. *J Roy Soc Inter* **3**, 15-35.
[98] Arruda, E.M. & Boyce, M.C. 1993 A three-dimensional constitutive model for the large stretch behavior of rubber elastic-materials. *J Mech Phys Solids* **41**, 389-412.

[99] Bischoff, J.E., Arruda, E.A. & Grosh, K. 2002 A microstructurally based orthotropic hyperelastic constitutive law. *J Appl Mech* **69**, 570-579.
[100] Bischoff, J.E., Arruda, E.M. & Grosh, K. 2000 Finite element modeling of human skin using an isotropic, nonlinear elastic constitutive model. *J Biomech* **33**, 645-652.
[101] Flynn, C. & McCormack, B.A.O. 2008 Finite element modelling of forearm skin wrinkling. *Skin Res Technol* **14**, 261-269.
[102] Flynn, C. & McCormack, B.A.O. 2008 A simplified model of scar contraction. *J Biomech* **41**, 1582-1589.
[103] Flynn, C.O. & McCormack, B.A.O. 2010 Simulating the wrinkling and aging of skin with a multi-layer finite element model. *J Biomech* **43**, 442-448.
[104] Kuhl, E., Garikipati, K., Arruda, E. & Grosh, K. 2005 Remodeling of biological tissue: Mechanically induced reorientation of a transversely isotropic chain network. *J Mech Phys Solids* **53**, 1552-1573.
[105] Limbert, G. & Middleton, J. 2005 A polyconvex anisotropic strain energy function. Application to soft tissue mechanics. In *ASME Summer Bioengineering Conference* (Vail, CO, USA.
[106] Itskov, M., Ehret, A.E. & Mavrilas, D. 2006 A polyconvex anisotropic strain-energy function for soft collagenous tissues. *Biomech Model Mechanobiol* **5**, 17-26.
[107] Itskov, M. & Aksel, N. 2004 A class of orthotropic and transversely isotropic hyperelastic constitutive models based on a polyconvex strain energy function. *Int J Solids Struct* **41**, 3833-3848.
[108] Holzapfel, G.A., Gasser, T.C. & Ogden, R.W. 2000 A new constitutive framework for arterial wall mechanics and a comparative study of material models. *J Elast* **61**, 1-48.
[109] Tonge, T.K., Voo, L.M. & Nguyen, T.D. 2013 Full-field bulge test for planar anisotropic tissues: Part II – A thin shell method for determining material parameters and comparison of two distributed fiber modeling approaches. *Acta Biomater* **9**, 5926-5942.
[110] Flynn, C., Rubin, M.B. & Nielsen, P. 2011 A model for the anisotropic response of fibrous soft tissues using six discrete fibre bundles. *Int J Numer Meth Bio* **27**, 1793-1811.
[111] Ankersen, J., Birkbeck, A.E., Thomson, R.D. & Vanezis, P. 1999 Puncture resistance and tensile strength of skin simulants. *Proceedings of the Institution of Mechanical Engineers Part H-Journal of Engineering in Medicine* **213**, 493-501.
[112] Flynn, C. & Rubin, M.B. 2012 An anisotropic discrete fibre model based on a generalised strain invariant with application to soft biological tissues. *Int. J. Eng. Sci.* **60**, 66-76.
[113] Limbert, G. 2011 A mesostructurally-based anisotropic continuum model for biological soft tissues--Decoupled invariant formulation. *J Mech Behav Biomed Mater* **4**, 1637-1657.
[114] Bischoff, J.E., Arruda, E.M. & Grosh, K. 2002 Finite element simulations of orthotropic hyperelasticity. *Finite Elem. Anal. Des.* **38**, 983-998.
[115] Lu, J. & Zhang, L. 2005 Physically motivated invariant formulation for transversely isotropic hyperelasticity. *Int J Solids Struct* **42**, 6015-6031.
[116] Kratky, O. & Porod, G. 1949 Röntgenuntersuchungen gelöster Fadenmoleküle. *Rec Trav Chim Pays-Bas Belg* **68**, 1106-1122.
[117] Korelc, J., Šolinc, U. & Wriggers, P. 2010 An improved EAS brick element for finite deformation. *Comput. Mech.* **46**, 641-659.
[118] Gautieri, A., Vesentini, S., Redaelli, A. & Buehler, M.J. 2011 Hierarchical structure and nanomechanics of collagen microfibrils from the atomic scale up. *Nano Lett* **11**, 757-766.
[119] Sun, Y.L., Luo, Z.P., Fertala, A. & An, K.N. 2002 Direct quantification of the flexibility of type I collagen monomer. *Biomech Biophys Res Commun* **295**, 382-386.
[120] Groves, R.B., Coulman, S.A., Birchall, J.C. & Evans, S.L. 2013 An anisotropic, hyperelastic model for skin: Experimental measurements, finite element modelling and identification of parameters for human and murine skin. *J Mech Behav Biomed Mater* **18**, 167-180.
[121] Weiss, J.A., Maker, B.N. & Govindjee, S. 1996 Finite element implementation of incompressible transversely isotropic hyperelasticity. *Comput Meth Appl Mech Eng* **135**, 107-128.
[122] Barbenel, J.C. & Evans, J.H. 1973 The time-dependent mechanical properties of skin. *J Invest Dermatol* **69**, 165-172.
[123] Pereira, J.M., Mansour, J.M. & Davis, B.R. 1990 Analysis of Shear-Wave Propagation in Skin - Application to an Experimental Procedure. *J Biomech* **23**, 745-751.
[124] Pereira, J.M., Mansour, J.M. & Davis, B.R. 1991 Dynamic Measurement of the Viscoelastic Properties of Skin. *J Biomech* **24**, 157-162.
[125] Lanir, Y. 1979 The rheological behavior of the skin: experimental results and a structural model. *Biorheology* **16**, 191-202.

[126] Wu, J.Z., Cutlip, R.G., Welcome, D. & Dong, R.G. 2006 Estimation of the viscous properties of skin and subcutaneous tissue in uniaxial stress relaxation tests. *Bio-Med. Mater. Eng.* **16**, 53-66.
[127] Khatyr, F., Imberdis, C., Vescovo, P., Varchon, D. & Lagarde, J.M. 2004 Model of the viscoelastic behaviour of skin in vivo and study of anisotropy. *Skin Res Technol* **10**, 96-103.
[128] Boyer, G., Laquieze, L., Le Bot, A., Laquieze, S. & Zahouani, H. 2009 Dynamic indentation on human skin in vivo: ageing effects. *Skin Res Technol* **15**, 55-67.
[129] Boyer, G., Zahouani, H., Le, B.A. & Laquieze, L. 2007 In vivo characterization of viscoelastic properties of human skin using dynamic micro-indentation. *2007 Annual International Conference of the Ieee Engineering in Medicine and Biology Society, Vols 1-16*, 4584-4587.
[130] Goh, K.L., Listrat, A. & Béchet, D. 2014 Hierarchical Mechanics of Connective Tissues: Integrating Insights from Nano to Macroscopic Studies. *Journal of Biomedical Nanotechnology* **10**, 2464-2507.
[131] Redaelli, A., Vesentini, S., Soncini, M., Vena, P., Mantero, S. & Montevecchi, F.M. 2003 Possible role of decorin glycosaminoglycans in fibril to fibril force transfer in relative mature tendons—a computational study from molecular to microstructural level. *J Biomech* **36**, 1555-1569.
[132] Bischoff, J.E., Arruda, E.M. & Grosh, K. 2004 A rheological network model for the continuum anisotropic and viscoelastic behavior of soft tissue. *Biomech Model Mechanobiol* **3**, 56-65.
[133] Kearney, S.P., Khan, A., Dai, Z. & Royston, T.J. 2015 Dynamic viscoelastic models of human skin using optical elastography. *Physics in Medicine and Biology* **60**, 6975-6990.
[134] Lokshin, O. & Lanir, Y. 2009 Viscoelasticity and preconditioning of rat skin under uniaxial stretch: microstructural constitutive characterization. *J Biomech Eng* **131**, 031009-031010.
[135] Lokshin, O. & Lanir, Y. 2009 Micro and macro rheology of planar tissues. *Biomaterials* **30**, 3118-3127.
[136] Fung, Y.C. 1973 Biorheology of soft tissues. *Biorheology* **10**, 139-155.
[137] Ehret, A. 2011 Generalised concepts for constitutive modelling of soft biological tissues. *PhD Thesis RWTH Aachen University*, 1-230.
[138] Bischoff, J. 2006 Reduced Parameter Formulation for Incorporating Fiber Level Viscoelasticity into Tissue Level Biomechanical Models. *Ann Biomed Eng* **34**, 1164-1172.
[139] Pioletti, D.P., Rakotomanana, L.R., Benvenuti, J.F. & Leyvraz, P.F. 1998 Viscoelastic constitutive law in large deformations: application to human knee ligaments and tendons. *J Biomech* **31**, 753-757.
[140] Coleman, B.D. & Noll, W. 1961 Foundations of linear viscoelasticity. *Review of modern physics* **3**, 239-249.
[141] Limbert, G. 2004 Development of an advanced computational model for the simulation of damage to human skin. (pp. 1-95. Cardiff, Welsh Development Agency (Technology and Innovation Division) - FIRST Numerics Ltd.
[142] Limbert, G. & Middleton, J. 2004 A transversely isotropic viscohyperelastic material: application to the modelling of biological soft connective tissues. *Int J Solids Struct* **41**, 4237-4260.
[143] Limbert, G. & Middleton, J. 2005 An anisotropic viscohyperelastic constitutive model of the posterior cruciate ligament suitable for high loading-rate situations. In *IUTAM Symposium on Impact Biomechanics: from Fundamental Insights to Applications* (pp. pp. 1-8. Dublin, Ireland.
[144] Limbert, G. & Middleton, J. 2006 A constitutive model of the posterior cruciate ligament. *Med Eng Phys* **28**, 99-113.
[145] Reese, S. & Govindjee, S. 1998 A theory of finite viscoelasticity and numerical aspects. *Int J Solids Struct* **35**, 3455-3482.
[146] Lubarda, V.A. 2004 Constitutive theories based on the multiplicative decomposition of deformation gradient: thermoelasticity, elastoplasticity and biomechanics. *Applied Mechanics Review* **57**, 95-108.
[147] Vassoler, J.M., Reips, L. & Fancello, E.A. 2012 A variational framework for fiber-reinforced viscoelastic soft tissues. *Int J Numer Meth Eng* **89**, 1691-1706.
[148] Nguyen, T.D., Jones, R.E. & Boyce, B.L. 2007 Modeling the anisotropic finite-deformation viscoelastic behavior of soft fiber-reinforced composites. *Int J Solids Struct* **44**, 8366-8389.
[149] Nedjar, B. 2007 An anisotropic viscoelastic fibre–matrix model at finite strains: Continuum formulation and computational aspects. *Comput Meth Appl Mech Eng* **196**, 1745-1756.
[150] Flynn, C. & Rubin, M.B. 2014 An anisotropic discrete fiber model with dissipation for soft biological tissues. *Mech. Mater.* **68**, 217-227.
[151] Hollenstein, M., Jabareen, M. & Rubin, M.B. 2013 Modeling a smooth elastic–inelastic transition with a strongly objective numerical integrator needing no iteration. *Comput. Mech.* **52**, 649-667.
[152] Holzapfel, G.A. & Gasser, T.C. 2001 A viscoelastic model for fiber-reinforced composites at finite strains: Continuum basis, computational aspects and applications. *Comput Meth Appl Mech Eng* **190**, 4379-4403.
[153] Pena, E., Calvo, B., Martinez, M.A. & Doblare, M. 2007 An anisotropic visco-hyperelastic model for ligaments at finite strains. Formulation and computational aspects. *Int J Solids Struct* **44**, 760-778.

[154] Pena, E., Calvo, B., Martinez, M.A. & Doblare, M. 2008 On finite-strain damage of viscoelastic-fibred materials. Application to soft biological tissues. *Int J Numer Meth Eng* **74**, 1198-1218.
[155] Ehret, A.E., Itskov, M. & Weinhold, G.W. 2009 A micromechanically motivated model for the viscoelastic behaviour of soft biological tissues at large strains. *Nuovo Cimento C* **32**, 73-80.
[156] Gasser, T.C. & Forsell, C. 2011 The numerical implementation of invariant-based viscoelastic formulations at finite strains. An anisotropic model for the passive myocardium. *Comput Meth Appl Mech Eng* **200**, 3637-3645.
[157] Simo, J.C. 1987 On a fully three-dimensional finite-strain viscoelastic damage model: formulation and computational aspects. *Comput Meth Appl Mech Eng* **60**, 153-173.
[158] Kligman, A.M., Zheng, P. & Lavker, R.M. 1985 The anatomy and pathogenesis of wrinkles. *Br J Derm* **113**, 37-42.
[159] Veijgen, N.K., Masen, M.A. & van der Heide, E. 2013 Variables influencing the frictional behaviour of in vivo human skin. *J Mech Behav Biomed Mater* **28**, 448-461.
[160] Wang, S., Li, M., Wu, J., Kim, D.-H., Lu, N., Su, Y., Kang, Z., Huang, Y. & Rogers, J.A. 2012 Mechanics of Epidermal Electronics. *J Appl Mech* **79**, 031022-031022.
[161] Lejeune, E., Javili, A. & Linder, C. 2016 An algorithmic approach to multi-layer wrinkling. *Extreme Mechanics Letters*.
[162] Piérard, G.E., Uhoda, I. & Piérard-Franchimont, C. 2004 From skin microrelief to wrinkles. An area ripe for investigation. *J Cosm Derm* **2**, 21-28.
[163] Genzer, J. & Groenewold, J. 2006 Soft matter with hard skin: From skin wrinkles to templating and material characterization. *Soft Matter* **2**, 310-323.
[164] Cerda, E. & Mahadevan, L. 2003 Geometry and physics of wrinkling. *Phys. Rev. Lett.* **90**, 074302-074301:074302-074304.
[165] Biot, M.A. 1963 Surface instability of rubber in compression. *Applied Scientific Research, Section A* **12**, 168-182.
[166] Biot, M.A. 1963 Incremental elastic coefficients of an isotropic medium in finite strain. *Applied Scientific Research, Section A* **12**, 151-167.
[167] Cao, Y. & Hutchinson, J.W. 2012 Wrinkling phenomena in neo-Hookean film/substrate bilayers. *J Appl Mech* **79**, 031019-031019.
[168] Dervaux, J. & Ben Amar, M. 2010 Localized growth of layered tissues. *IMA J Appl Math* **75**, 571-580.
[169] Taylor, M., Bertoldi, K. & Steigmann, D.J. 2014 Spatial resolution of wrinkle patterns in thin elastic sheets at finite strain. *J Mech Phys Solids* **62**, 163-180.
[170] Efimenko, K., Rackaitis, M., Manias, E., Vaziri, A., Mahadevan, L. & Genzer, J. 2005 Nested self-similar wrinkling patterns in skins. *Nat Mater* **4**, 293-297.
[171] Holland, M.A., Li, B., Feng, X.Q. & Kuhl, E. 2017 Instabilities of soft films on compliant substrates. *J Mech Phys Solids* **98**, 350-365.
[172] Ben Amar, M. & Goriely, A. 2005 Growth and instability in elastic tissues. *J Mech Phys Solids* **53**, 2284-2319.
[173] Ben Amar, M.B.A., M., Chatelain, C. & Ciarletta, P. 2011 Contour Instabilities in Early Tumor Growth Models. *Phys. Rev. Lett.* **106**.
[174] Dervaux, J. & Ben Amar, M. 2008 Morphogenesis of growing soft tissues. *Phys. Rev. Lett.* **101**, -.
[175] Dervaux, J., Ciarletta, P. & Ben Amar, M. 2009 Morphogenesis of thin hyperelastic plates: A constitutive theory of biological growth in the Föppl-von Kármán limit. *J Mech Phys Solids* **57**, 458-471.
[176] Goriely, A. & Ben Amar, M. 2005 Differential growth and instability in elastic shells. *Phys. Rev. Lett.* **94**, -.
[177] Goriely, A., Destrade, M. & Ben Amar, M. 2006 Instabilities in elastomers and in soft tissues. *Q J Mech Appl Math* **59**, 615-630.
[178] Allen, H.G. 1969 Chapter 8 - Wrinkling and other forms of local instability. In *Analysis and Design of Sandwich Panels* (pp. 156-189. New York, Pergamon.
[179] Cao, Y. & Hutchinson, J.W. 2011 From wrinkles to creases in elastomers: the instability and imperfection-sensitivity of wrinkling. *P Roy Soc A-Math Phys*, doi:10.1098/rspa.2011.0384.
[180] Lejeune, E., Javili, A. & Linder, C. 2016 Understanding geometric instabilities in thin films via a multi-layer model. *Soft Matter* **12**, 806-816.
[181] Ciarletta, P., Destrade, M. & Gower, A.L. 2013 Shear instability in skin tissue. *The Quarterly Journal of Mechanics and Applied Mathematics*, hbt007.
[182] Gower, A.L. 2015 Connecting the material parameters of soft fibre-reinforced solids with the formation of surface wrinkles. *Journal of Engineering Mathematics* **95**, 217-229.

[183] Carfagna, M., Destrade, M., Gower, A. & Grillo, A. 2017 Oblique wrinkles. *Philosophical Transactions of the Royal Society of London Part A*.
[184] Yu, B., Kang, S.-Y., Akthakul, A., Ramadurai, N., Pilkenton, M., Patel, A., Nashat, A., Anderson, D.G., Sakamoto, F.H., Gilchrest, B.A., et al. 2016 An elastic second skin. *Nat Mater* **15**, 911-918.
[185] Destrade, M., Ogden, R.W., Sgura, I. & Vergori, L. 2014 Straightening wrinkles. *J Mech Phys Solids* **65**, 1-11.
[186] Kuwazuru, O., Miyamoto, K., Yoshikawa, N. & Imayama, S. 2012 Skin wrinkling morphology changes suddenly in the early 30s. *Skin Res Technol* **18**, 495-503.
[187] Shiihara, Y., Sato, M., Hara, Y., Iwai, I. & Yoshikawa, N. 2014 Microrelief suppresses large wrinkling appearance: an in silico study. *Skin Res Technol* **0**, 1-8.
[188] Wong, Y.W. & Pellegrino, S. 2006 Wrinkled membranes Part III: Numerical Simulations. *Journal of Mechanics of Materials and Structures* **1**, 61-93.
[189] Limbert, G. & Kuhl, E. 2017 On skin microrelief and the emergence of expression micro-wrinkles. *Soft Matter*, submitted.
[190] Budday, S., Kuhl, E. & Hutchinson, J.W. 2015 Period-doubling and period-tripling in growing bilayered systems. *Philosophical magazine (Abingdon, England)* **95**, 3208-3224.
[191] de Souza Neto, E.A. & Feng, Y.T. 1999 On the determination of the path direction for arc-length methods in the presence of bifurcations and `snap-backs'. *Comput Meth Appl Mech Eng* **179**, 81-89.
[192] Dortdivanlioglu, B., Javili, A. & Linder, C. 2016 Computational aspects of morphological instabilities using isogeometric analysis. *Comput Meth Appl Mech Eng* **316**, 261-279.
[193] Chen, L., Nguyen-Thanh, N., Nguyen-Xuan, H., Rabczuk, T., Bordas, S.P.A. & Limbert, G. 2014 Explicit finite deformation analysis of isogeometric membranes. *Comput Meth Appl Mech Eng* **277**, 104-130.
[194] Buganza Tepole, A., Kabaria, H., Bletzinger, K.-U. & Kuhl, E. 2015 Isogeometric Kirchhoff–Love shell formulations for biological membranes. *Comput Meth Appl Mech Eng* **293**, 328-347.
[195] Javili, A., Steinmann, P. & Kuhl, E. 2014 A novel strategy to identify the critical conditions for growth-induced instabilities. *J Mech Behav Biomed Mater* **29**, 20-32.
[196] Barber, D. 2012 *Bayesian reasoning and machine learning*. Cambridge, Cambridge University Press; 697 p.
[197] Liu, W. & Röckner, M. 2015 *Stochastic Partial Differential Equations: An Introduction*. First edition ed, Springer; 272 p.
[198] Buehler, M.J. 2006 Large-scale hierarchical molecular modeling of nanostructured biological materials. *J Comput Theor Nanos* **3**, 603-623.
[199] Rim, J.E., Pinsky, P.M. & van Osdol, W.W. 2009 Multiscale modeling framework of transdermal drug delivery. *Ann Biomed Eng* **37**, 1217-1229.
[200] Bancelin, S., Lynch, B., Bonod-Bidaud, C., Ducourthial, G., Psilodimitrakopoulos, S., Dokládal, P., Allain, J.-M., Schanne-Klein, M.-C. & Ruggiero, F. 2015 Ex vivo multiscale quantitation of skin biomechanics in wild-type and genetically-modified mice using multiphoton microscopy. *Sci Rep-Uk* **5**, 17635.

1. SUPPLEMENTARY MATERIAL

1.1 Remark about elasticity tensors in the context of finite element numerical procedures

Elasticity tensors that characterise the stiffness of a hyperelastic material can be defined in the Lagrangian and Eulerian configurations, respectively as:

$$\mathbb{C}^{\mathbf{E}} = 2\frac{\partial \mathbf{S}}{\partial \mathbf{C}} = 4\frac{\partial^2 \psi}{\partial \mathbf{C} \otimes \partial \mathbf{C}} = \frac{\partial^2 \psi}{\partial \mathbf{E} \otimes \partial \mathbf{E}} \tag{1}$$

and $$\mathbb{c}^{\mathbf{d}} = 4\left(\mathbf{F} \otimes \mathbf{F}^{\mathrm{T}}\right) : \frac{\partial^2 \psi}{\partial \mathbf{C} \otimes \partial \mathbf{C}} : \left(\mathbf{F}^{\mathrm{T}} \otimes \mathbf{F}\right) = \left(\mathbf{F} \otimes \mathbf{F}^{\mathrm{T}}\right) : \frac{\partial^2 \psi}{\partial \mathbf{E} \otimes \partial \mathbf{E}} : \left(\mathbf{F}^{\mathrm{T}} \otimes \mathbf{F}\right) = 4\mathbf{b} : \frac{\partial^2 \psi}{\partial \mathbf{b} \otimes \partial \mathbf{b}} : \mathbf{b} \tag{2}$$

The material, so, objective, rate of the second Piola-Kirchhoff stress tensor is expressed as:

$$\dot{\mathbf{S}} = \frac{1}{2}\mathbb{C}^{\mathbf{E}} : \dot{\mathbf{C}} = \mathbb{C}^{\mathbf{E}} : \dot{\mathbf{E}} \tag{3}$$

These elasticity tensors are generally not constant and depend on deformation [1]. They are essential in the implementation of constitutive models into non-linear implicit-based finite element codes as they are used to calculate the numerical tangent stiffness, and therefore, condition the rate of convergence of the system of non-linear algebraic equations [2]. However, an aspect which is often overlooked and/or misunderstood, is that to benefit from the theoretical quadratic rate of convergence of non-linear finite element solvers of the Newton-Raphson type, it is essential to calculate the *consistently linearised* tangent modulus, consistent with the work-conjugate strain rate-stress pair, chosen in combination with the appropriate *objective stress rate*. In the finite element software package Abaqus/Implicit (Simulia, Dassault Systèmes, Providence, RI, USA), widely used in research and development across academia, government and industry, the use of the UMAT subroutine allows the user to code displacement-based constitutive models of arbitrary complexity. In that case, explicit expression of the components of the true stress (i.e. Cauchy stress) and consistent elasticity tensors corresponding to the incremental solving procedure must be provided. As an Eulerian code, and for continuum elements, Abaqus/Implicit requires the explicit definition of the tangent tensor, $\mathbb{T}^{\text{ABAQUS}}$, consistent with a Zaremba-Jaumann objective rate of Kirchhoff stress and spatial strain rate so that:

$$\overset{\nabla \text{ZJ}}{\boldsymbol{\tau}} = \mathbb{T}^{\text{ABAQUS}} : \mathbf{d} \tag{4}$$

The spatial strain rate $\mathbf{d}$ is defined as:

$$\mathbf{d} = \frac{1}{2}\left(\dot{\mathbf{F}}.\mathbf{F}^{-1} + \mathbf{F}^{-\mathrm{T}}.\dot{\mathbf{F}}^{\mathrm{T}}\right) = \frac{1}{2}\left(\mathbf{l} + \mathbf{l}^{\mathrm{T}}\right) \tag{5}$$

where $\mathbf{l}$ is the spatial velocity gradient while the objective Zaremba-Jaumann rate of Kirchhoff stress is defined as [1]:

$$\overset{\nabla \text{ZJ}}{\boldsymbol{\tau}} = \dot{\boldsymbol{\tau}} - \mathbf{w}.\boldsymbol{\tau} + \boldsymbol{\tau}.\mathbf{w} \tag{6}$$

The rate of spin $\mathbf{w}$ is introduced as:

$$\mathbf{w} = \mathbf{l} - \mathbf{d} - = \frac{1}{2}\left(\dot{\mathbf{F}}.\mathbf{F}^{-1} - \mathbf{F}^{-\mathrm{T}}.\dot{\mathbf{F}}^{\mathrm{T}}\right) = \frac{1}{2}\left(\mathbf{l} - \mathbf{l}^{\mathrm{T}}\right) \tag{7}$$

In order to derive $\mathbb{T}^{\text{ABAQUS}}$, one needs to derive the tangent tensor consistent with the Lie derivative of the Kirchhoff stress tensor which is also known as the Oldroyd objective rate of this tensor. It is obtained by pulling back the *spatial* strain rate to the *material* configuration so that the resulting stress rate is calculated in that configuration, and then pushed back to the spatial configuration:

$$\overset{\nabla \text{Oldroyd}}{\boldsymbol{\tau}} = \dot{\boldsymbol{\tau}} - \mathbf{l}.\boldsymbol{\tau} + \boldsymbol{\tau}.\mathbf{l}^{\mathrm{T}} = \mathbf{F}.\left[\mathbb{C}^{\mathbf{E}} : \left(\mathbf{F}^{\mathrm{T}}.\mathbf{d}.\mathbf{F}\right)\right].\mathbf{F}^{\mathrm{T}} = \mathbb{c}^{\mathbf{d}} : \mathbf{d} = \mathbb{c}^{\mathbf{d}} : \mathbf{l} \tag{8}$$

Although the final explicit form of $\mathbb{T}^{\text{ABAQUS}}$ has been previously reported in the literature [3], the detailed intermediary derivation steps were not provided, and, for sake of completeness, are given below.

Equation (8) leads to:

$$\dot{\boldsymbol{\tau}} = \mathbb{c}^{\mathbf{d}} : \mathbf{l} + \mathbf{l}.\boldsymbol{\tau} - \boldsymbol{\tau}.\mathbf{l}^{\mathrm{T}} = \mathbb{c}^{\mathbf{d}} : \mathbf{l} + \mathbf{I} \,\bar{\otimes}\, \boldsymbol{\tau} : \mathbf{l} + \boldsymbol{\tau} \,\underline{\otimes}\, \mathbf{I} : \mathbf{l} = \left(\mathbb{c}^{\mathbf{d}} + \mathbf{I} \,\bar{\otimes}\, \boldsymbol{\tau} + \boldsymbol{\tau} \,\underline{\otimes}\, \mathbf{I} \right) : \mathbf{l} \tag{9}$$

where the non-standard tensor operators $\bar{\otimes}$ and $\underline{\otimes}$ are defined as [4]:

$$\left(\bullet \,\bar{\otimes}\, \circ \right)_{ijkl} = \bullet_{ik} \circ_{jl} \; ; \qquad \left(\bullet \,\underline{\otimes}\, \circ \right)_{ijkl} = \bullet_{il} \circ_{jk} \tag{10}$$

By injecting **Equation (9)** into **Equation (6)** one obtains the following formula for the Zaremba-Jaumann rate of Kirchhoff stress:

$$\overset{\nabla \mathrm{ZJ}}{\boldsymbol{\tau}} = \left(\mathbb{c}^{\mathbf{d}} + \mathbf{I} \,\bar{\otimes}\, \boldsymbol{\tau} + \boldsymbol{\tau} \,\underline{\otimes}\, \mathbf{I} \right) : \mathbf{l} - \mathbf{w}.\boldsymbol{\tau} + \boldsymbol{\tau}.\mathbf{w} = \left(\mathbb{c}^{\mathbf{d}} + \mathbf{I} \,\bar{\otimes}\, \boldsymbol{\tau} + \boldsymbol{\tau} \,\underline{\otimes}\, \mathbf{I} \right) : \mathbf{l} - \frac{1}{2}\left(\mathbf{l} - \mathbf{l}^{\mathrm{T}} \right).\boldsymbol{\tau} + \boldsymbol{\tau}.\frac{1}{2}\left(\mathbf{l} - \mathbf{l}^{\mathrm{T}} \right) \tag{11}$$

$$\overset{\nabla \mathrm{ZJ}}{\boldsymbol{\tau}} = \left(\mathbb{c}^{\mathbf{d}} + \mathbf{I} \,\bar{\otimes}\, \boldsymbol{\tau} + \boldsymbol{\tau} \,\underline{\otimes}\, \mathbf{I} \right) : \mathbf{l} - \frac{1}{2}\left(\mathbf{I} \,\bar{\otimes}\, \boldsymbol{\tau} : \mathbf{l} + \boldsymbol{\tau} \,\underline{\otimes}\, \mathbf{I} : \mathbf{l} \right) + \frac{1}{2}\left(\mathbf{l}^{\mathrm{T}}.\boldsymbol{\tau} + \boldsymbol{\tau}.\mathbf{l} \right) \tag{12}$$

$$\overset{\nabla \mathrm{ZJ}}{\boldsymbol{\tau}} = \left[\mathbb{c}^{\mathbf{d}} + \mathbf{I} \,\bar{\otimes}\, \boldsymbol{\tau} + \boldsymbol{\tau} \,\underline{\otimes}\, \mathbf{I} - \frac{1}{2}\left(\mathbf{I} \,\bar{\otimes}\, \boldsymbol{\tau} + \boldsymbol{\tau} \,\underline{\otimes}\, \mathbf{I} \right) + \frac{1}{2}\left(\mathbf{I} \,\underline{\otimes}\, \boldsymbol{\tau} + \boldsymbol{\tau} \,\bar{\otimes}\, \mathbf{I} \right) \right] : \mathbf{l} \tag{13}$$

After simplifications, one obtains:

$$\overset{\nabla \mathrm{ZJ}}{\boldsymbol{\tau}} = \left[\mathbb{c}^{\mathbf{d}} + \frac{1}{2}\left(\mathbf{I} \,\bar{\otimes}\, \boldsymbol{\tau} + \boldsymbol{\tau} \,\underline{\otimes}\, \mathbf{I} + \mathbf{I} \,\underline{\otimes}\, \boldsymbol{\tau} + \boldsymbol{\tau} \,\bar{\otimes}\, \mathbf{I} \right) \right] : \mathbf{l} \tag{14}$$

It follows that the correct tangent tensor to input into the Abaqus/Standard UMAT user subroutine is:

$$\mathbb{T}^{\mathrm{ABAQUS}} = \frac{1}{J}\left[\mathbb{c}^{\mathbf{d}} + \frac{1}{2}\left(\boldsymbol{\tau} \,\bar{\otimes}\, \mathbf{I} + \mathbf{I} \,\bar{\otimes}\, \boldsymbol{\tau} + \boldsymbol{\tau} \,\underline{\otimes}\, \mathbf{I} + \mathbf{I} \,\underline{\otimes}\, \boldsymbol{\tau} \right) \right] = \frac{1}{J}\mathbb{c}^{\mathbf{d}} + \frac{1}{2}\left(\boldsymbol{\sigma} \,\bar{\otimes}\, \mathbf{I} + \mathbf{I} \,\bar{\otimes}\, \boldsymbol{\sigma} + \boldsymbol{\sigma} \,\underline{\otimes}\, \mathbf{I} + \mathbf{I} \,\underline{\otimes}\, \boldsymbol{\sigma} \right) \tag{15}$$

This formula was provided by Zöllner *et al.* [3]. In indicial notation the tangent tensor can be expressed as:

$$\mathbb{T}^{\mathrm{ABAQUS}}_{ijkl} = \frac{1}{J}\mathbb{c}^{\mathbf{d}}_{ijkl} + \frac{1}{2}\left(\sigma_{ik}\delta_{jl} + \sigma_{jl}\delta_{ik} + \sigma_{il}\delta_{jk} + \sigma_{jk}\delta_{il} \right) \tag{16}$$

and

$$\mathbb{T}^{\mathrm{ABAQUS}}_{ijkl} = \frac{1}{J}F_{iA}F_{jB}F_{kC}F_{lD}\mathbb{C}^{\mathbf{E}}_{ABCD} + \frac{1}{2}\left(\sigma_{ik}\delta_{jl} + \sigma_{jl}\delta_{ik} + \sigma_{il}\delta_{jk} + \sigma_{jk}\delta_{il} \right) \tag{17}$$

1.2 Fibre dispersion models

It is clear that the complex microarchitecture of the collagen network in skin cannot be accurately captured by the strong assumption of *uniform* fibre alignment, even at a local level (see **Figure 1** of the main article). A better assumption, more in line with physical observations, is to assume that, at a local level, fibres are distributed around a main orientation, $\boldsymbol{n}_0$ with a certain probability to lay within a particular range of angular deviation from that main direction (**Figure 5**). This is embodied by the notion of *fibre dispersion* which can be accounted for by means of two main modelling approaches [5]. The first one, termed the "*angular integration approach*" is due to Lanir [6] while the second approach, known as the "*generalised structure tensor*" approach is due to Gasser *et al.* [7].

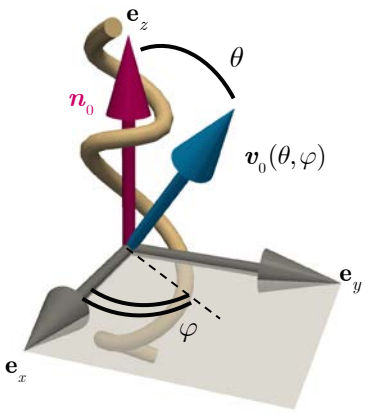

Figure 5. Schematic highlighting the Euler angles θ and φ defining the position of any vector (in that case, denoted by $\boldsymbol{v}_0$) in a three-dimensional Cartesian coordinate system defined by the unit vectors $\mathbf{e}_x$, $\mathbf{e}_y$ and $\mathbf{e}_z$. $\theta \in [0,\pi]$ and $\varphi \in [0,2\pi]$. The mean fibre direction $\boldsymbol{n}_0$ is indicated by the pink arrow aligned with the third Cartesian basis vector $\mathbf{e}_z$.

1.2.1 Angular integration approach

In this approach, also known as the *microsphere* approach, the strain energy function of a single fibre, $\psi_{fibre}(\lambda)$, is considered as a function of the fibre stretch λ. This strain energy is then integrated over the unit sphere $\mathbb{U}^2$ to represent the strain energy of a bundle of these fibres per unit reference volume, ψ_{bundle}. This could effectively be viewed as an homogenisation procedure where mesoscopic (or macroscopic) quantities are obtained by integration of fibre level microscopic quantities (e.g. strain energy of a single fibre $\psi_{fibre}(\lambda)$). It follows that:

$$\psi_{bundle} = n\int_{\mathbb{U}^2} \rho^{\boldsymbol{n}_0}(\boldsymbol{v}_0)\,\psi_{fibre}(\lambda)\,dA \tag{18}$$

where dA is the elemental solid angle, n is the number of fibres per unit reference volume, $\boldsymbol{v}_0$ is a unit vector bearing the direction of an arbitrary fibre, defined with respect to $\boldsymbol{n}_0$, a unit vector representing a mean direction around which fibre dispersion occurs, and $\rho^{\boldsymbol{n}_0}$ is the relative angular distribution of fibres around the mean direction which must satisfy the following normalisation condition [5]:

$$\frac{1}{4\pi}\int_{\mathbb{U}^2} \rho^{\boldsymbol{n}_0}(\boldsymbol{v}_0)dA = 1 \tag{19}$$

The homogenised second Piola-Kirchhoff stress tensor associated with a fibre bundle can then simply be defined as:

$$\mathbf{S}_{bundle} = 2\frac{\partial \psi_{bundle}}{\partial \mathbf{C}} = 2\,n\int_{\mathbb{U}^2} \rho^{\boldsymbol{n}_0}(\boldsymbol{v}_0)\frac{\partial \psi_{fibre}(\lambda)}{\partial \mathbf{C}}dA \tag{20}$$

Similarly, the associated Lagrangian elasticity tensor is:

$$\mathbb{C}^{\mathbf{E}}_{bundle} = 2\frac{\partial \mathbf{S}_{bundle}}{\partial \mathbf{C}} = 4\,n\int_{\mathbb{U}^2} \rho^{\boldsymbol{n}_0}(\boldsymbol{v}_0)\frac{\partial^2 \psi_{fibre}(\lambda)}{\partial \mathbf{C}\otimes\partial \mathbf{C}}dA \tag{21}$$

As pointed out by Holzapfel and Ogden [5], in **Equation (18)**, it is assumed that the elastic properties of all the fibres are defined by the same strain energy function ψ_{fibre}. This is was not the case in Lanir's study [6] where a probability distribution characterising the degree of fibre crimp, and therefore, the degree of mechanical activation, was considered, effectively leading to a modulation of ψ_{fibre} for each fibre.

1.2.2 Generalised structure tensor approach

In this ingenious approach, introduced by Gasser *et al.* [7], the idea is to use a homogenised structure tensor $\mathbf{H}$ which is obtained by integration of the structure tensor $\boldsymbol{v}_0 \otimes \boldsymbol{v}_0$ associated with an arbitrary fibre of direction $\boldsymbol{v}_0$, deviating from the mean fibre direction $\boldsymbol{n}_0$, over the unit sphere. This effectively amounts to defining a statistical strain-like invariant $(\mathbf{C} : \mathbf{H} - 1)$ (see **section 4.2.4** of the article). In that case, the strain energy of a bundle of fibres per unit reference volume ψ_{bundle} is defined as:

$$\psi_{bundle} = \psi_{bundle}(\mathbf{C}, \mathbf{H}) \tag{22}$$

where:

$$\mathbf{H} = \frac{1}{4\pi} \int_{\mathbb{U}^2} \rho^{\boldsymbol{n}_0}(\boldsymbol{v}_0)\, \boldsymbol{v}_0 \otimes \boldsymbol{v}_0 \, dA \tag{23}$$

with satisfaction of the normalisation condition (19) leading to $\mathbf{H} : \mathbf{I} = 1$.

Remark

Holzapfel and Ogden [5] recently discussed important theoretical aspects of the angular integration and generalised structure tensor approaches for fibre dispersion. They demonstrated the equivalence of these two formulations in terms of predictive power and therefore, implicitly recommend the latter approach because it has been proven very effective in describing experimental data for a broad range of biological fibrous tissues, is conceptually simple, much simpler to implement in a numerical context, and also, much less demanding with regards to computational power. Moreover, and of particular significance, these authors developed a formulation based on the generalised structure tensor approach which exclude *compressed* fibres within a dispersion group. By so doing, they proved that it is indeed possible, unlike what has previously been claimed in the literature.

1.3 A common angular distribution function: the π-periodic von Mises distribution function

In his seminal paper, Lanir [6] developed a microstructurally-based plane stress model of skin in which he introduced a planar fibre angular density distribution $\mathcal{R}_k(\theta)$ where $\mathcal{R}_k(\theta)\, d\theta$ is the fraction of all fibres of type k (collagen or elastin) oriented between θ and $(\theta + d\theta)$ in the reference configuration. In that case, θ represents the deviation from the mean fibre orientation $\boldsymbol{n}_0$. Lanir selected a circular normal distribution, also known as von Mises type distribution:

$$\mathcal{R}(\theta, \mu, \kappa) = \frac{\exp(\kappa\,[\cos(\theta) - \mu])}{2\pi I_0(\kappa)} \tag{24}$$

where $I_0(\kappa)$ is the modified Bessel function of order 0. Naturally, other forms of angular distribution functions are possible [7-9]. Fibre dispersion over the unit sphere is described by a spatial density function $\rho(\theta, \varphi)$ where θ and φ represent the Eulerian angles describing the direction of any material vector $\boldsymbol{v}_0$ [7] so that one can write $\rho(\theta, \varphi) = \rho(\boldsymbol{v}_0) = \rho[\boldsymbol{v}_0(\theta, \varphi)]$ (see **Figure 5**) where:

$$\boldsymbol{v}_0(\theta, \varphi) = (\sin\theta\cos\varphi)\,\mathbf{e}_x + (\sin\theta\sin\varphi)\,\mathbf{e}_y + (\cos\theta)\,\mathbf{e}_z \tag{25}$$

$dA = \sin\theta\, d\theta\, d\varphi$ represents the infinitesimal surface area of the unit sphere defined by the angular range $[(\theta, \theta + d\theta), (\varphi, \varphi + d\varphi)]$. Without loss of generality, if one assumes that any vector $\boldsymbol{v}_0(\theta, \varphi)$ is aligned with the base vector $\mathbf{e}_z$ rotational symmetry around $\mathbf{e}_z$ is obtained and the fibre density distribution becomes independent of φ so that $\rho = \rho(\theta) = \rho[\boldsymbol{v}_0(\theta)]$. The normalisation condition is then reduced to:

$$\int_0^{\pi} \rho[\boldsymbol{v}_0(\theta)]\, dA = 2 \tag{26}$$

The dispersion of collagen fibres around a preferred mean direction (transverse isotropy) can be accounted for by the use of a modified version of the standard π-periodic von Mises distribution function with dispersion parameter b [8, 10]:

$$\rho(\theta) = 4\sqrt{\frac{b}{2\pi}}\, \frac{\exp(b\,[\cos(2\theta) + 1])}{\operatorname{erfi}(\sqrt{2b})} \tag{27}$$

where erfi is the imaginary error function defined as:

$$\mathrm{erfi}(x) = -i\frac{2}{\sqrt{\pi}}\int_0^{ix} \mathrm{e}^{-t^2} dt \tag{28}$$

It can be shown [11] that the dispersion parameter κ of the structure tensor approach of Gasser *et al.* [7] can be expressed as:

$$\kappa = \frac{1}{2} + \frac{1}{8b} - \frac{1}{4}\sqrt{\frac{2}{\pi b}}\frac{\exp(2b)}{\mathrm{erfi}\left(\sqrt{2b}\right)} \tag{29}$$

Instead of using a MacLaurin series expansion to approximate the imaginary error function (which is often not standard in low-level programming languages), here, it is proposed to use a global Padé decomposition established by Winitzki [12]. This approximation offers the simultaneous advantages of low computing requirement and high accuracy:

$$\mathrm{erfi}(x) \simeq \frac{\mathrm{e}^{x^2}}{x\sqrt{\pi}}\frac{p_n(x)}{q_n(x)} \tag{30}$$

where

$$p_n(x) = \sum_{l=1}^{n} x^{2l} \sum_{k=1}^{l} \frac{(-1)^{k-1}}{2^{n-l}} \frac{(2n-2l+2k-1)!!}{(2k-1)!!} C_{l-k}^{n}, \tag{31}$$

$$q_n(x) = \sum_{k=0}^{n} \frac{(2k-1)!!}{2^k} C_k^n \, x^{2n-2k} \tag{32}$$

and

$$C_k^n = \frac{n!}{(n-k)!k!} \tag{33}$$

The relative error between erfi and its Padé approximant can be estimated [12]:

$$\left|\frac{p_n(x)}{q_n(x)} - \mathrm{erfi}(x)\right| < 2^{-n}\sqrt{\frac{n}{2}}\left|\mathrm{erfi}(x)\right| \tag{34}$$

In a numerical context, to prevent a singularity at the origin, a small numerical parameter ε can be introduced in the approximation (30) so that:

$$\mathrm{erfi}(x) \simeq \frac{\mathrm{e}^{x^2}}{(x+\varepsilon)\sqrt{\pi}}\frac{p_n(x)}{q_n(x)} \tag{35}$$

The very accurate 4-term Padé approximant of the imaginary error function erfi, $\mathrm{erfi}_4^{\mathrm{Padé}}$ is provided below:

$$\mathrm{erfi}_4^{\mathrm{Padé}}(x) = \frac{\mathrm{e}^{x^2}}{\sqrt{\pi}}\frac{f(x)}{g(x)} \tag{36}$$

$$f(x) = x\left(\begin{array}{l}\frac{654729075}{512} + \frac{126351225x^2}{256} + \frac{4999995x^4}{32} + \frac{637065x^6}{16} + \frac{134805x^8}{16} + \\ \frac{12255x^{10}}{8} + \frac{495x^{12}}{2} + 37x^{14} + \frac{11x^{16}}{2} + x^{18}\end{array}\right) \tag{37}$$

$$g(x) = \begin{array}{l}\frac{654729075}{1024} + \frac{172297125x^2}{256} + \frac{91216125x^4}{256} + \frac{2027025x^6}{16} + \frac{1091475x^8}{32} + \\ \frac{59535x^{10}}{8} + \frac{11025x^{12}}{8} + 225x^{14} + \frac{135x^{16}}{4} + 5x^{18} + x^{20}\end{array} \tag{38}$$

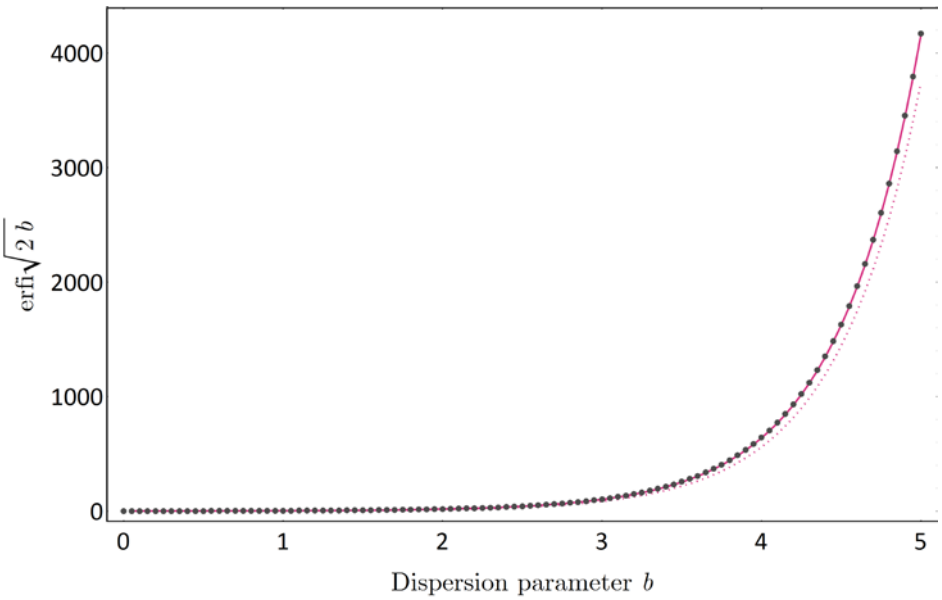

Figure 6. Comparison between $\mathrm{erfi}\sqrt{2b}$ (grey dots) and its approximation using 1 term (pink dotted line) and 4 terms (pink continuous line) in the Padé series. The 4-term series defined in **Equation (36)** shows an excellent agreement with the exact imaginary error function Erfi available in Mathematica® (Wolfram Research Inc., Champaign, IL, USA) to a nearly arbitrary order of precision.

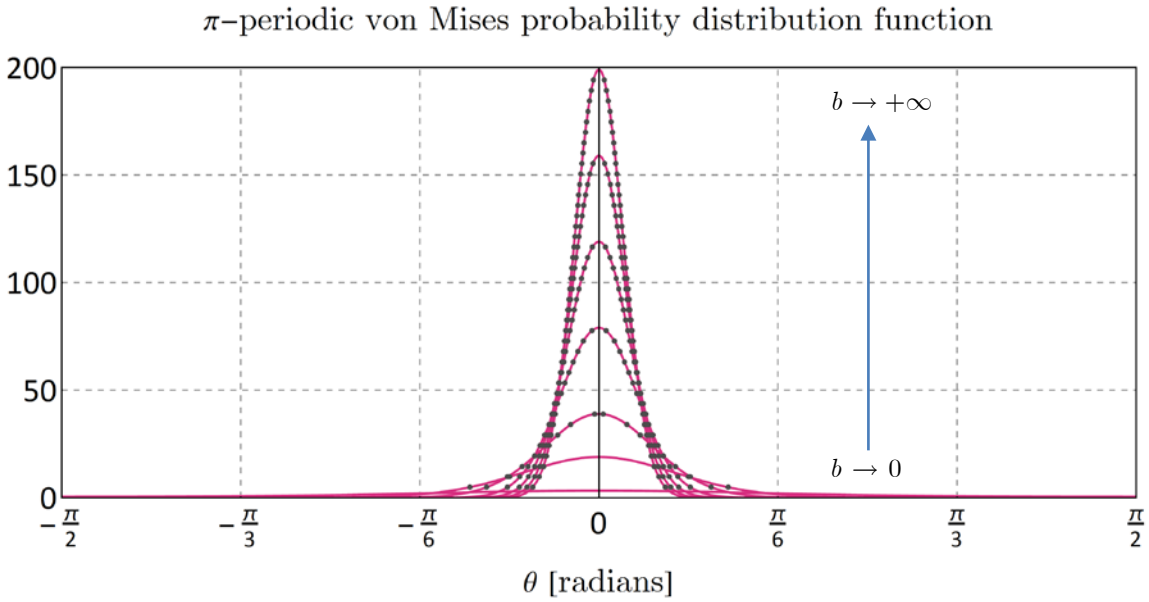

Figure 7. π -periodic von Mises angular distribution function calculated for the following dispersion parameter values: $b = \{1, 5, 10, 20, 30, 40, 50\}$. The continuous pink lines represent the distribution values calculated using the 4-term Padé approximant of $\mathrm{erfi}\sqrt{2b}$ defined by **Equation (36)** while the grey dots are corresponding discrete values calculated using the exact imaginary function Erfi available in Mathematica® (Wolfram Research Inc., Champaign, IL, USA).

1.4 Network models

Chain network models such as the Arruda-Boyce eight-chain model originates from concepts borrowed from statistical mechanics, namely, entropic elasticity of macromolecules [13]. In this theory, long molecular chains are assumed to rearrange their conformation under the influence of random thermal fluctuations so that their possible geometrical configurations can only be known in a statistical sense.
Polymer chains in rubber are typically described as *uncorrelated* [14] as their conformation is reminiscent of a random walk. The term *freely jointed* chains is also used. In contrast, biopolymer chains such as collagen assemblies feature smoothly varying curvature and are therefore considered *correlated*. These chains are best described using the concept of worm-like chains of Kratky and Porod [15]. In the context of soft tissue mechanics, several authors used this approach to describe the structure and mechanics of the basic building block of collagen assemblies, the tropocollagen molecule, the so-called collagen triple-helix [14, 16-21].
Both freely-jointed and worm-like entropic chains are assumed to be made of beads connected by N rigid links of equal length d, the so-called Kuhn length [22], so that the maximum length of a chain, the contour length, is $L = Nd$. The mechanics of macromolecular polymer structures is not only governed by the mechanical properties of individual chains but also by their electromagnetic and mechanical interactions which can take the form of covalent bonds, entanglement and physical cross-links. These combined effects give rise to strong network properties which can be implicitly captured by network models such as the eight-chain model of Arruda and Boyce [23]. The central idea behind these formulations is that there exists a representative nano-/microscopic unit cell able to capture network properties. The eight-chain model assumes that the unit cell is made of eight entropic chains of equal lengths connected from the centre of the cell to each of its corners (**Figure 8**), each equipped with their own strain energy ψ_{chain}. For uncorrelated and correlated chains one can consider respectively the freely jointed chain energy [**Equation (39)**] and the worm-like chain energy [**Equation (41)**] The unit cell is further assumed to feature a solid phase conferring isotropic bulk properties through the strain energy ψ_{bulk}.

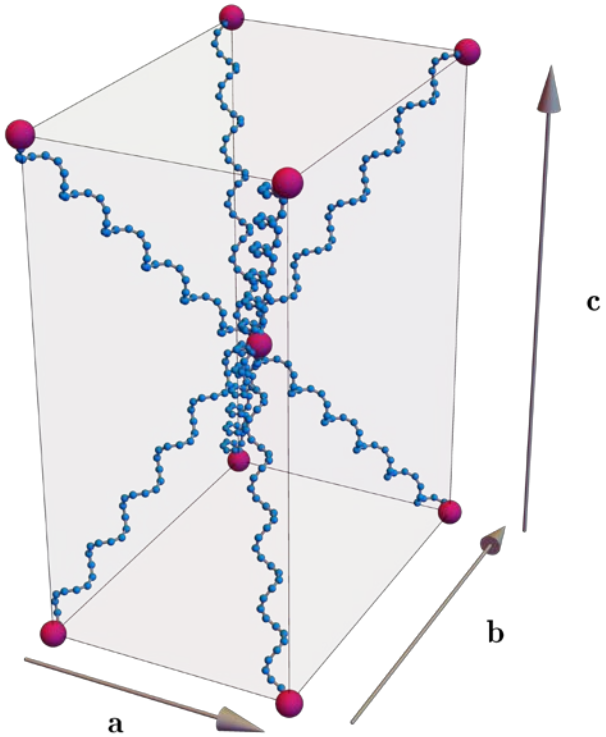

Figure 8. Schematic representation of the orthotropic eight chain network model of Bischoff *et al.* [16]. The light grey solid volume represents the bulk material admitting the strain energy function ψ_{bulk} while the eight single polymer chains are governed by the strain energy function ψ_{chain}. When $\|\mathbf{a}\| = \|\mathbf{b}\| = \|\mathbf{c}\|$ the Bischoff *et al.*'s model [16]degenerates to the Arruda-Boyce's model while the Kuhl *et al.*'s model [14] is recovered is two cell dimensions are identical (e.g. $\|\mathbf{a}\| = \|\mathbf{b}\|$).

1.4.1 The freely jointed chain model for uncorrelated chains

$$\psi_{\text{chain}} = \hat{\psi}^{FJC}_{Langevin}(r) = \hat{\psi}^{FJC}_0 + \mathfrak{K}\,\theta N\left\{\frac{r}{L}\mathcal{L}^{-1}(r) + \ln\left[\frac{\mathcal{L}^{-1}(r)}{\sinh(\mathcal{L}^{-1}(r))}\right]\right\} \tag{39}$$

where $\hat{\psi}^{FJC}_0$ is the ground state chain energy in the unperturbed state, r the current end-to-end distance of the chain and $\mathcal{L}^{-1}$ is the inverse of the Langevin function defined as $\mathcal{L}(x) = \coth(x) - 1/x$, $\mathfrak{K} = 1.3806503 \times 10^{-23}\left[\text{m}^2\text{kg s}^{-2}\text{K}^{-1}\right]$ is the Boltzmann constant and θ is the absolute temperature [K]. $\mathcal{L}^{-1}$ can be approximated using a Padé approximant [24] as:

$$\mathcal{L}^{-1}(x) \simeq \frac{3 - x^2}{1 - x^2}x \tag{40}$$

For a more in-depth analysis and alternative approximations of the inverse Langevin function, see recent papers by Nguessong *et al.* [25], Jedynak [26], Marchi and Arruda [27] and Darabi and Itskov [28].

1.4.2 The worm-like chain model for correlated chains

$$\psi_{\text{chain}} = \hat{\psi}^{WLC}(r) = \hat{\psi}^{WLC}_0 + \frac{\mathfrak{K}\,\theta L}{\Lambda}\left[2\frac{r^2}{L^2} + \frac{1}{\left(1 - \frac{r}{L}\right)} - \frac{r}{L}\right] \tag{41}$$

where L, Λ, r_0 and r are respectively the contour, persistence, initial end-to-end length and the current end-to-end length of the chain. Similarly to the freely jointed chain model, $\hat{\psi}^{WLC}_0$ is the chain energy in the unperturbed state.

1.5 Flynn-Rubin-Nielsen's formulation [29]

1.5.1 Discrete fibre vectors

The model developed by Flynn *et al.* [29] is based on a *discrete* rather than *continuous* fibre orientation distribution kernel which allows closed-form solutions for strain energy and stress. Six discrete directions are considered $\boldsymbol{n}^i_0\{i = 1,\ldots,6\}$: they are oriented parallel to the lines connecting opposing vertices of a regular icosahedron (i.e. a 20-faced polyhedron). These six directions, corresponding to distinct fibre bundles, are defined as:

$$\begin{aligned}
\boldsymbol{n}^1_0 &= \frac{2}{\sqrt{5}}\mathbf{e}_1 + \frac{1}{\sqrt{5}}\mathbf{e}_3; & \boldsymbol{n}^2_0 &= \frac{1}{2}\left(1 - \frac{1}{\sqrt{5}}\right)\mathbf{e}_1 + \sqrt{\frac{1}{2}\left(1 + \frac{1}{\sqrt{5}}\right)}\mathbf{e}_2 + \frac{1}{\sqrt{5}}\mathbf{e}_3 \\
\boldsymbol{n}^3_0 &= -\frac{1}{2}\left(1 + \frac{1}{\sqrt{5}}\right)\mathbf{e}_1 + \sqrt{\frac{1}{2}\left(1 - \frac{1}{\sqrt{5}}\right)}\mathbf{e}_2 + \frac{1}{\sqrt{5}}\mathbf{e}_3, & \boldsymbol{n}^4_0 &= -\frac{1}{2}\left(1 + \frac{1}{\sqrt{5}}\right)\mathbf{e}_1 - \sqrt{\frac{1}{2}\left(1 - \frac{1}{\sqrt{5}}\right)}\mathbf{e}_2 + \frac{1}{\sqrt{5}}\mathbf{e}_3 \\
\boldsymbol{n}^5_0 &= \frac{1}{2}\left(1 - \frac{1}{\sqrt{5}}\right)\mathbf{e}_1 - \sqrt{\frac{1}{2}\left(1 + \frac{1}{\sqrt{5}}\right)}\mathbf{e}_2 + \frac{1}{\sqrt{5}}\mathbf{e}_3, & \boldsymbol{n}^6_0 &= \mathbf{e}_3
\end{aligned} \tag{42}$$

From these six unit vectors, Flynn *et al.* [29] defined six structural tensors:

$$\mathfrak{B}^i_0 = \boldsymbol{n}^i_0 \otimes \boldsymbol{n}^i_0\{i = 1,\ldots,6\}(\text{no summation on } i), \quad \text{with } \sum_{i=1}^{6}\mathfrak{B}^i_0 = 2\mathbf{I} \tag{43}$$

1.5.2 A particular strain energy function for collagen fibre bundles assuming a unit step distribution

If one injects the definition of a unit step distribution function D:

$$D(x) = \begin{cases} 0, & x < x_1 \quad \text{or} \quad x > x_3 \\ \dfrac{1}{x_3 - x_1}, & \text{otherwise} \end{cases} \tag{44}$$

into **Equation (35)**, after simplification, one arrives to the following expression for the strain energy function of a single collagen fibre bundle:

$$\psi_c(\lambda)=\begin{cases}0, & \lambda < x_1 \\ \dfrac{E_c}{\rho_0}\dfrac{1}{4(x_3-x_1)}\left[(\lambda-x_1)(\lambda-3x_1)+2x_1^2\ln\left(\dfrac{\lambda}{x_1}\right)\right], & x_1 \le \lambda < x_3 \\ \dfrac{E_c}{\rho_0}\left\{\dfrac{1}{4(x_3-x_1)}\left[(x_3-x_1)(x_3-3x_1)+2x_1^2\ln\left(\dfrac{x_3}{x_1}\right)\right]+\left(\dfrac{x_3-x_1}{2}-x_3\right)\ln\left(\dfrac{\lambda}{x_3}\right)+\lambda-x_3\right\}, & x_3 < \lambda\end{cases} \tag{45}$$

1.6 Description of the constitutive parameters of Limbert's model [30]

Limbert's model [30] features a set of twenty three constitutive parameters $\mathbf{p} = \mathbf{p}^1 \cup \mathbf{p}^2 = \{\mathfrak{K}, \theta, \kappa, \mu_0^i, \mu_1^i, \mu_2^i, \aleph_i, L_i, L_p^i, r_i, a_i, b_i, \overline{\lambda}_i^c\}_{i=1,2}$ where:

$$\begin{aligned} \mathbf{p}^1 &= \left\{\mathfrak{K}, \theta, \kappa, \mu_0, a_{n_0}, b_{n_0}, a_{m_0}, b_{m_0}, \aleph_{n_0}, \aleph_{m_0}, \overline{\lambda}_{n_0}^c, \overline{\lambda}_{m_0}^c\right\}; \\ \mathbf{p}^2 &= \left\{\mu_1, \mu_2, L_{n_0}, L_p^{n_0}, r_{n_0}, \aleph_{m_0}, L_{m_0}, L_p^{m_0}, r_{m_0}\right\} \end{aligned} \tag{46}$$

Limbert [30] determined the parameter set $\mathbf{p}^2$ using a numerical global optimisation algorithm while the parameter set $\mathbf{p}^1$ was assumed *a priori* based on existing data [14] and data obtained via visual inspection of biaxial stress-strain curves for rabbit skin [31].

Table 1. Description of the constitutive parameters of decoupled-invariant orthotropic hyperelastic developed by Limbert [30] with assumed and numerically-optimised values obtained by identification with the rabbit skin data of Lanir and Fung [32].

	Measured or estimated constitutive parameters	
$\mathfrak{K}$	Boltzmann constant	$1.3806503.10^{-23}$ [J.K^{-1}]
θ	Absolute temperature	310 [K]
κ	Bulk modulus of the matrix	50 [kPa]
μ_0	Shear modulus of collagen fibres	0 [Pa]
a_{n_0}, a_{m_0}	First shape parameter for sigmoid coupling function (families 1 and 2)	50
b_{n_0}, b_{m_0}	Second shape parameter for sigmoid coupling function (families 1 and 2)	20
$\overline{\lambda}_{n_0}^c, \overline{\lambda}_{m_0}^c$	Critical stretch for sigmoid coupling function (families 1 and 2)	1.15 | 1.40
$\aleph_{n_0}, \aleph_{m_0}$	Density of collagen fibres (families 1 and 2)	7.10^{21} [m^{-3}]
	Constitutive parameters determined by numerical optimisation	
μ_1	Matrix shear modulus	150.123 [Pa]
μ_2	Maximum fibre-fibre/matrix-fibre shear modulus	9.981 [Pa]
L_{n_0}, L_{m_0}	Contour length of a tropocollagen molecule (families 1 and 2)	2.792
$L_p^{n_0}, L_p^{m_0}$	Persistence length of a tropocollagen molecule (families 1 and 2)	0.200 | 0.591
r_{n_0}, r_{m_0}	Initial length of a crimpled collagen molecule (families 1 and 2)	1.368 | 1.741

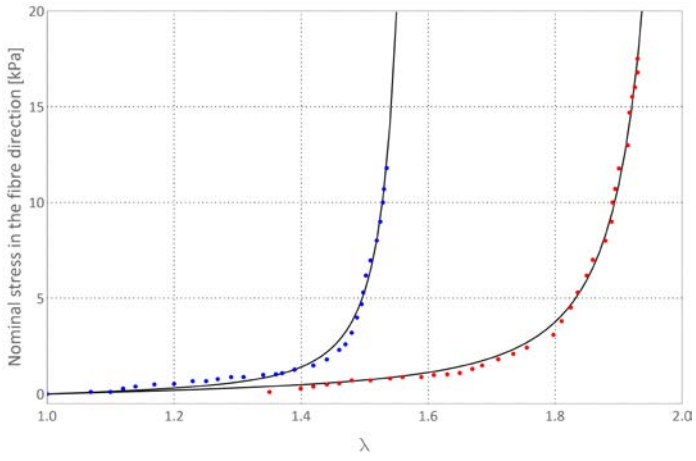

Figure 9. Experimental data from uniaxial tensile tests (stretch-nominal stress) on rabbit skin from Lanir and Fung [32] and the corresponding theoretical values (continuous lines) calculated after identification of the constitutive parameters of the decoupled invariant model developed by Limbert [30](Blue: head-to-tail fibre direction, $r^2 = 0.997$; Red: perpendicular to head-to-tail direction, $r^2 = 0.998$).

1.7 Finite strain viscoelasticity – Viscosity tensors

From the formulation established in **section 4.3.3**, the viscosity tensor for the matrix and fibre phases, denoted respectively as $\mathbb{V}_M$ and $\mathbb{V}_F$ are defined as:

$$\mathbb{V}_M^{-1} = \frac{1}{2\eta_{M_S}}\left(\mathbf{C}^v_{matrix} \odot \mathbf{C}^v_{matrix} - \frac{1}{3}\mathbf{C}^v_{matrix} \otimes \mathbf{C}^v_{matrix}\right) + \frac{1}{9\eta_{M_B}}\mathbf{C}^v_{matrix} \otimes \mathbf{C}^v_{matrix} \tag{47}$$

$$\mathbb{V}_F = \eta_{F_1}\frac{\boldsymbol{n}_0 \otimes \boldsymbol{n}_0}{\mathbf{C}^v_{fibre} : (\boldsymbol{n}_0 \otimes \boldsymbol{n}_0)} \otimes \frac{\boldsymbol{n}_0 \otimes \boldsymbol{n}_0}{\mathbf{C}^v_{fibre} : (\boldsymbol{n}_0 \otimes \boldsymbol{n}_0)} + \eta_{F_2}\frac{\boldsymbol{m}_0 \otimes \boldsymbol{m}_0}{\mathbf{C}^v_{fibre} : (\boldsymbol{m}_0 \otimes \boldsymbol{m}_0)} \otimes \frac{\boldsymbol{m}_0 \otimes \boldsymbol{m}_0}{\mathbf{C}^v_{fibre} : (\boldsymbol{m}_0 \otimes \boldsymbol{m}_0)} \tag{48}$$

where the non-standard tensor product $\odot$ is defined as:

$$(\bullet \odot \circ)_{ijkl} = (\bullet \,\overline{\otimes}\, \circ + \bullet \,\underline{\otimes}\, \circ)_{ijkl} = \frac{1}{2}(\bullet_{ik} \circ_{jl} + \bullet_{il} \circ_{jk}) \tag{49}$$

and η_{M_S} and η_{M_B} are the deviatoric and bulk viscosities of the matrix while η_{F_1} and η_{F_2} are the viscosities associated with the two families of fibres.

Particular non-equilibrium potentials for anisotropic viscoelasticity

The particular forms of the non-equilibrium viscous potentials are given as follows:

$$\Phi^v_M(J^e, \alpha^e_1) = \frac{1}{2}\kappa^v(J^e - 1)^2 + \frac{1}{2}\mu^v_M\left(\alpha^e_1 - 2\right) \tag{50}$$

$$\Phi^v_\beta(\bar{\lambda}^e_\beta) = \frac{1}{2}\mu^v_\beta\left(\bar{\lambda}^{e\,2}_\beta - 1\right)^2 \tag{51}$$

κ^v, μ^e_M, μ^v_1 and μ^v_2 are material parameters that define the properties of the elastic part of the non-equilibrium Maxwell component. This non-linear orthotropic viscohyperelastic constitutive model was implemented into a commercial finite element code and constitutive parameters were identified from proprietary experimental data.

1.8 Softening and damage

Preconditioning effects are often associated with viscoelasticity [33]. They are linked to short-term rearrangement of the tissue microstructure and, in some instances, permanent deformation and/or damage of the microstructure. Preconditioning of biological soft tissues before in vitro tensile tests is often recommended. On one hand, it is a way to re-load the tissue into a state closer to *in vivo* conditions, on the other hand, depending on the amount of pre-conditioning, this could lead to microstructural rearrangements going beyond what would be physiologically experienced by the tissue. Muñoz *et al.* [34] observed a typical softening effect—known as the Mullins effect in the context of filled rubber mechanics—during cyclic uniaxial testing of murine skin at large deformations. A similar effect was reported by Edsberg *et al.* [35] for human skin under cyclic pressures. Ehret and Itskov [36] developed a constitutive framework to capture the Mullins effects observed in biological soft tissues and fitted it to the experimental data of Muñoz *et al.* [34] demonstrating an excellent agreement.

Ehret *et al.* [37] later applied their constitutive model to porcine dermis and corroborated observations made by Muñoz *et al.*, namely the occurrence of significant residual deformations upon cycling loading. Recently, Li and Luo [38] proposed an invariant-based softening damage and failure constitutive model for human and animal skins. The 9-parameter model is based on a combination of the GOH model [7] and the energy-limiter approach of Volokh [39, 40]. The performance of the model was tested on a series of orthogonal uniaxial tensile tests on human, swine, bovine and rabbit skins and exhibited excellent results. The main drawback of the model is its conservative nature: upon unloading the material would fully recover its original shape and return to its virgin undamaged state, effectively healing. This shortcoming could easily be rectified [41].

Considering its soft interfacial and protective nature, it is reasonable to assume that, at an evolutionary level, the skin of mammals in general, and that of humans, in particular, must have evolved damage resistance strategies through optimisation of their ultrastructure.

Recently, Yang *et al.* [42] have discovered four microstructural mechanisms that explain the extreme tear resistance of rabbit skin by conducting a very comprehensive multi-modality study. This study combined physical tensile tests, scanning electron microscope, *in situ* synchrotron X-ray characterisation and constitutive modelling. The viscoelastic constitutive model used to represent the tensile response of skin is based on the mechanics of a wire made of circular segments and captures two hierarchical levels of the skin: nanometre level (collagen fibrils) and micrometer level (collagen fibres).

1.9 Plasticity

Mazza *et al.* [43, 44] developed a non-linear elasto-visco-plastic model to simulate ageing of the human face [43, 44]. It is based on the constitutive formulation of Rubin and Bodner [45] to model the dissipative response of soft tissues. In this study the dissipative effects were a combination of elastic and visco-plastic mechanisms. Rubin and Bodner [45] demonstrated the relevance of their model by capturing very well the cyclic dissipative response of superficial musculoaponeurotic system tissue. The constitutive equations were implemented as a user subroutine in the commercial finite element code Abaqus (Simulia, Dassault Systèmes, Providence, RI, USA) to simulate gravimetric descent of facial tissue [43]. Mazza *et al.* [43, 44] extended the model of Rubin and Bodner [45] by including an ageing parameter equipped with its own time evolution equation. This ageing-driven parameter was a modulator of tissue. A four-layer model of facial skin combined with a face-like geometrical base was developed and highlighted the great potential of this kind of computational models to study the effects of skin ageing on facial appearance. The Rubin and Bodner's constitutive model [45] was generalised by Weickenmeier and Jabareen [46] in terms of the viscoplasticity equations and hardening parameter whilst establishing a robust finite element framework featuring a strongly objective integration scheme. In this paper, this modelling framework was applied to identify the mechanical properties of facial skin by combining suction measurements obtained via a Cutometer® MPA 580 (Courage and Khazaka Electronic GmbH, Köln, Germany) and inverse finite element techniques. The procedure is described in more details in a subsequent paper by Weickenmeier *et al.* [47].

1.10 Growth

As any biological soft tissue, the skin undergoes growth and remodelling in physiological and abnormal conditions. This starts from morphogenesis of the embryo and continues through life as the skin ages and adapts in response to various types of physiological and abnormal physical stimulations. Examples include stretching of the skin during pregnancy and natural growth, healing and scarring in response to injury, tanning and extrinsic ageing in response to the photo-chemical effects of solar radiations, stiffening of the dermal collagen network as the result of glycation associated with diabetes.

In his seminal review paper, Taber [48] defined growth as the process of adding mass while remodelling "*involves changes in material properties*" and morphogenesis "*is the generation of animal form*". Epstein [49] recently refined these definitions by demonstrating that, given an arbitrary time-dependent constitutive law, one can establish a canonical decomposition into growth, remodelling, ageing and morphogenesis parts.

Motivated by surgical tissue expansion procedures [50], Socci *et al.* [51] developed an axisymmetric computational model of skin growth. The constitutive model was based on a multiplicative decomposition of the deformation gradient using three distinct configurations: (1) the stress-free configuration before growth; (2) the configuration at the end of the growth process, not necessarily geometrically compatible, as grown stress-free configuration; (3) the configuration of the grown body after restoring strain compatibility via elastic deformations and 4) the configuration of the grown body after subsequent application of external loads. The general point of departure of growth theories consists in multiplicatively splitting the deformation gradient $\mathbf{F} = \mathbf{F}^e.\mathbf{F}^g$ into a growth part (inelastic) $\mathbf{F}^g$ and an elastic deformation gradient $\mathbf{F}^e$ [52].

This effectively assumes that there exists an intermediate virtual configuration between the reference and current configurations in which individual *material particles* have their volume changed.

However, the growth (positive or negative) of each material particle renders them geometrically incompatible with their neighbours [48, 53]. The elastic deformations characterised by $\mathbf{F}^e$ bring back compatibility and, by so doing, introduce residual stress [54].

In the context of skin expansion procedures for reconstructive surgery, Tepole *et al.* [55] formulated a 3D constitutive model for skin growth embedded into a rigorous theoretical framework based on the thermodynamics of open systems [56]. The essence of this theory is encapsulated by the equivalence between the rate of variation of the material density ρ_0 and the mass in- and out-fluxes $\nabla_{\mathbf{X}}.\mathbf{R}$ and mass sources/sinks R_0 :

$$\frac{d\rho_0}{dt} = \nabla_{\mathbf{X}}.\mathbf{R} + R_0 \tag{52}$$

To replicate the clinically observed supra-physiological skin growth induced by balloon expansion, Tepole *et al.* [55] considered in-plane skin growth driven by a strain-based stimulus: growth occurs when a critical in-plane stretch is reached. The growth factor was described by a temporal evolution equation and the skin was modelled as a homogeneous neo-Hookean material. 3D tissue expansions were simulated by considering a series of expanders with different shapes and showed the promising potential of the computational model of skin growth. Tepole *et al.* [57] later extended this model by considering skin as an eight-chain transversely isotropic material [14]. Computational relaxation and creep tests were conducted to study the evolution of in-plane area stretch. Skin growth due to the application of circular-, square-, rectangular- and crescent-shape tissue expanders was also simulated and confirmed that such computational tools can assist clinicians in planning and providing quantitative insight into complex surgical procedures. Several iterations of the original Tepole *et al.*'s model [55] were made by the same group, mostly focusing on refining the computational procedures for simulating the inflation of the tissue expander [3, 58, 59]. Tepole *et al.* [60, 61] integrated *in vivo* experiments conducted on pig and isogeometric finite element techniques to calibrate and validate their computational growth simulations.

1.11 Thermomechanics

Thermomechanical phenomena are an essential aspect of skin physiology [62] through the natural functions of the skin such as thermo-regulation but also play a central role in traumatic injury scenarios such as multiple-degree burns induced by high temperature resulting from external heat sources (e.g. fire) or from friction interactions (e.g. deployment of airbag in automotive accidents can create severe burns of the upper body, particularly of the face, by heat-generating rubbing of the airbag membrane against the skin) [63]. The coupling between thermal effects and mechanical loads, and its subsequent effect on the biochemistry of the skin is particularly relevant to the formation of pressure ulcers (also known as pressure sores) and skin blisters [64, 65] where the notion of *skin microclimate* is key [66]. Skin microclimate is embodied by the intimate coupling of temperature and relative humidity at the surface of the skin which affects the microstructure and mechanical properties of the skin, and, can therefore lead to loss of skin mechanical integrity and barrier function. These few examples illustrate why it is relevant to develop advanced mechanistic constitutive models of the skin capable of replicating and predicting the potentially strong interplay between mechanics, thermodynamics and biochemistry.

The need to develop a fundamental understanding of how thermal exchanges across and at the surface of the skin operate is two-fold. At a fundamental level, it is first essential to unveil the complex physiology of skin in health, disease and ageing. From the knowledge bases previously established, one can seek to optimise the design and functionalities of devices intended to interact with the skin whilst ensuring protection of this vital organ. A discussion of these aspects and a review of state-of-the-art models up to 2011 are discussed in the excellent monograph by Xu and Lu [62].

The development of medical therapies involving thermal phenomena such as laser surgery, hyperthermia procedures for cancer treatment, infrared light therapy or cryotherapy has been responsible for driving research efforts toward the formulation of mathematical models of skin thermomechanics [62, 67]. Abnormal and potentially harmful thermomechanical loading of the skin can arise from diverse sources such as those discussed below. Associated with the ever-growing popular practice of skin tattooing as a decorative art form [68], is the subsequent need to have tattoos removed, typically after a few years [69].

Removal procedures are mainly based on the sublimation of ink pigment particles by generation of localised very high temperatures produced by Q-switched lasers [69, 70]. The wavelength of the laser source is tuned to match that of the absorption wave length of the specific colour of a given tattoo pigment. A laser pulse is then emitted for a duration shorter than the thermal relaxation time which represents the time required for a structure to cool down to half of its heating temperature.

However, the immediate and long-term thermal, photochemical and biological effects of such a destructive technique on a living tissue remain unclear. Severe side effects have been observed including dyspigmentation and textural changes because of the role of melanin which may have absorption wave lengths overlapping those of the targeted tattoo pigments. Other consequences of laser treatment include rupture of blood vessels, aerosolisation of tissue (i.e. generation of an instantaneous and localised plasma) and carcinogenicity. Another significant side effect of tattoos is the potential for patients undergoing MRI scanning procedures to sustain burn injuries [71, 72]. The presence of ferromagnetic metallic compounds in tattoo pigments, especially iron oxide, leads to electromagnetic interactions with the magnetic field produced by MRI machines. This effectively generates an electric induction current that heats the skin tissue from the inside. Recent armed conflicts in the Middle-East have highlighted the need to develop efficient soldier clothing and protection equipment that can be optimised to operate in extreme temperature environments [73]. This also apply to space exploration, and is also of particular relevance, considering alarming climate change facts and predictions [74]. Military and law-enforcement forces have also pioneered the use of directed-energy weapons (e.g. Active Denial System developed by the US Air Force Research Laboratory [75]) which rely on high-powered beam of high-frequency waves (95 GHz). Like a traditional microwave oven, these millimeter waves excite water and lipid molecules producing instant intense heat and pain in the skin [76]. As a complementary role to clinical and biological studies, modelling has the potential to shed light on complex multiphysics phenomena involving thermal transfer, operating in a highly compliant multiscale living structure. A brief review of state-of-the-art continuum models of skin thermomechanics post-2011 can be found in [67]. These authors developed the first finite deformation thermomechanical model of the skin that accounts for biological heat sources as proposed by Pennes [77]. Accounting for the finite deformations that the skin can sustain, within a thermomechanical fully coupled constitutive model, is essential for some applications: for example, deformations induced by the application of a thermal treatment device or by the growth of a cancerous tumour growth can be large. Moreover, even in physiological situations, the skin can sustain finite strains. McBride *et al.* [67] implemented their constitutive law into a finite element code and analysed a geometrically idealised four-layer finite element skin model. Although limited by the availability of dedicated experimental data in terms of thermomechanical and geometrical properties for each skin layer, the coupled-physics framework enjoys a sound thermodynamically consistent formulation that could be experimentally validated in the future.

1.12 Skin microrelief

Skin microrelief is made of a network of furrows and ridges—also called *sulcus cutis* or glyphic patterns—criss-crossing each other and thus delimiting polygonal plateaux with rectangular, square, trapezoidal and triangular shapes. These polygonal patterns—present at birth—lose their isotropic distribution with age and become more anisotropic by forming preferred structural orientations [78-80]. The characteristics of skin microrelief can be classified according to the orientation and depth of featured lines into primary, secondary, tertiary and quaternary lines [78, 79, 81-84].

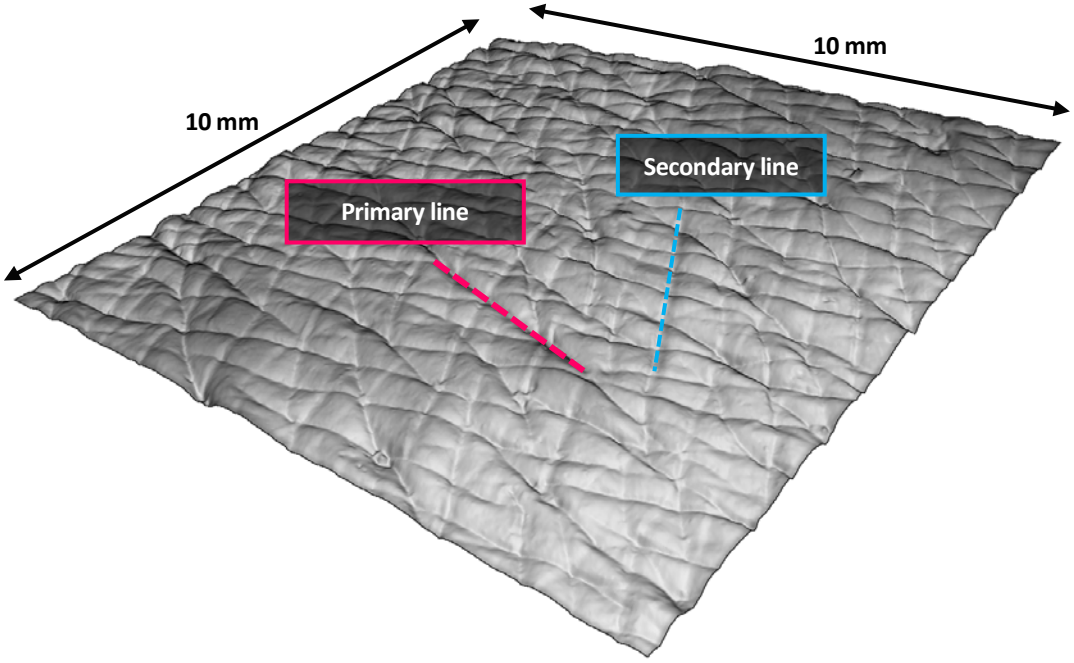

Figure 10. Synthetic image representing the typical microrelief of the skin surface (ridges and furrows), reconstructed from laser scanning profilometry of a silicone replica of a human volar forearm skin patch (40-years old healthy male subject). The acquisition features a 400 x 400 grid of points that was fitted to a NURBS surface.

1.13 Skin wrinkles and the *stratum corneum*

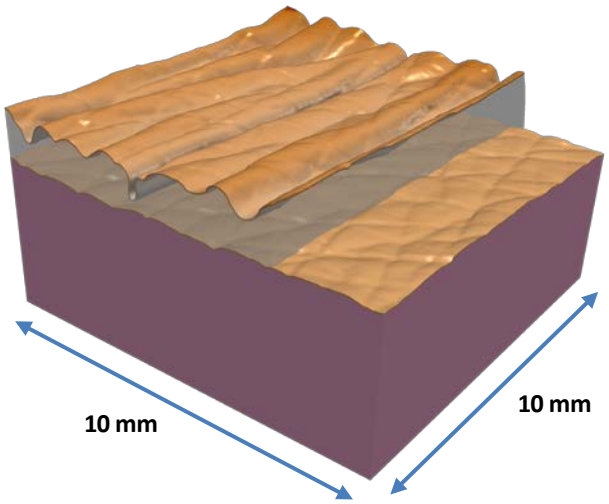

Figure 11. Anatomically-based bi-layer finite element model of human skin featuring a 20 microns-thick *stratum corneum* (top) and a 2.6 mm thick epidermal-dermal substrate, in its undeformed and deformed configurations. In-plane compression of the skin was simulated to trigger wrinkle formation using a robust path-following solving procedure. Young's modulus of the *stratum corneum* is 400 times that of the underlying thicker layer (0.6 MPa). Adapted from Limbert and Kuhl [85].

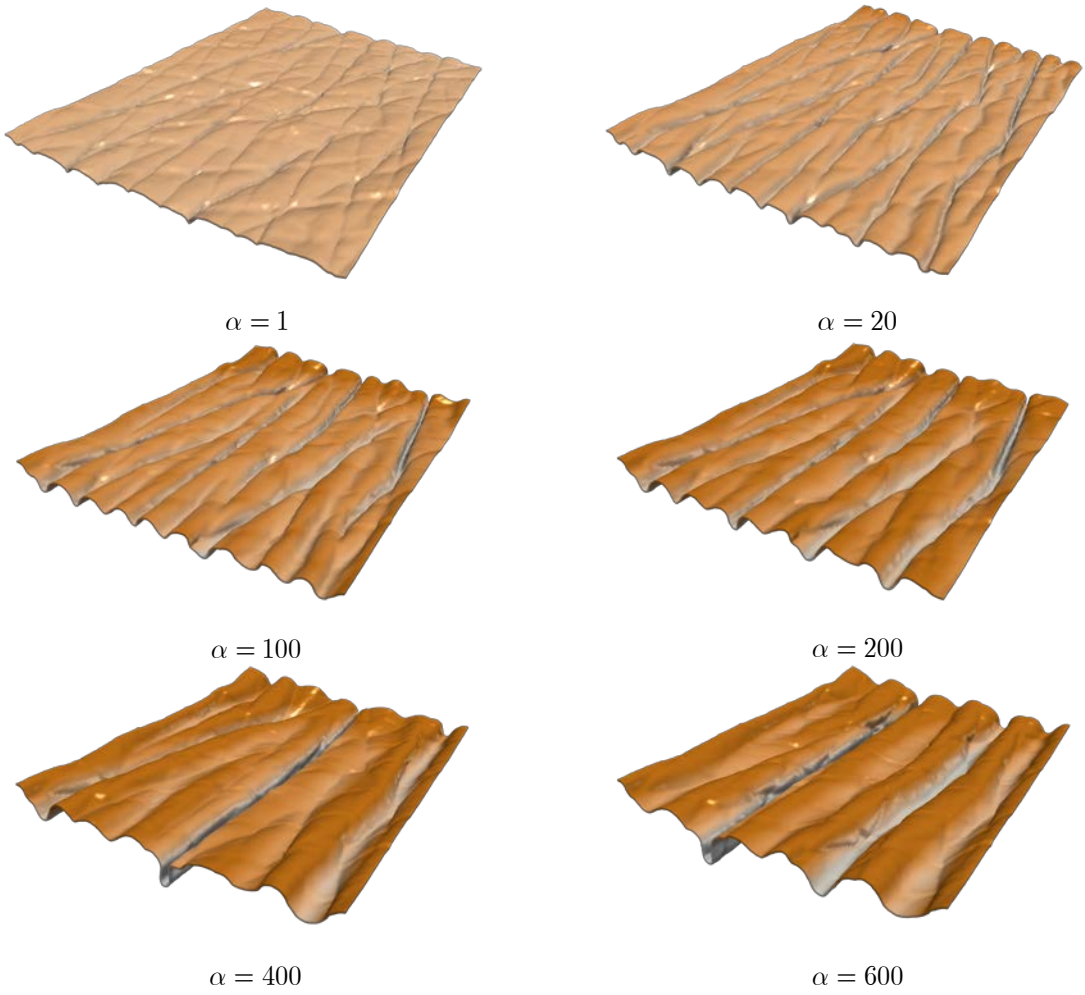

Figure 12. Plot of the deformed stratum corneum layer as a function of the ratio of ground state Young's moduli of the stratum corneum (20 microns-thick) and underlying substrate (0.6 MPa for the substrate) α . Both layers were modelled as neo-Hookean solids and subjected to 25% in-plane compression. This is the same finite element model depicted on **Figure 11**. Adapted from Limbert and Kuhl [85].

2. References

[1] Holzapfel, G.A. 2000 *Nonlinear Solid Mechanics. A Continuum Approach for Engineering*. Chichester, UK, John Wiley & Sons; 470 p.
[2] Belytschko, T., Liu, W.K. & Moran, B. 2000 *Nonlinear Finite Elements for Continua and Structures*. Oxford, Wiley.
[3] Zöllner, A.M., Holland, M.A., Honda, K.S., Gosain, A.K. & Kuhl, E. 2013 Growth on demand: Reviewing the mechanobiology of stretched skin. *J Mech Behav Biomed Mater* **28**, 495-509.
[4] Curnier, A., He, Q.-C. & Zysset, P. 1994 Conewise linear elastic materials. *J Elast* **37**, 1-38.
[5] Holzapfel, G.A. & Ogden, R.W. 2016 On fiber dispersion models: exclusion of compressed fibers and spurious model comparisons. *J Elast*, 1-20.
[6] Lanir, Y. 1983 Constitutive equations for fibrous connective tissues. *J Biomech* **16**, 1-22.
[7] Gasser, T.C., Ogden, R.W. & Holzapfel, G.A. 2006 Hyperelastic modelling of arterial layers with distributed collagen fibre orientations. *J Roy Soc Inter* **3**, 15-35.
[8] Alastrué, V., Martínez, M.A., Doblaré, M. & Menzel, A. 2009 Anisotropic micro-sphere-based finite elasticity applied to blood vessel modelling. *J Mech Phys Solids* **57**, 178-203.
[9] Holzapfel, G.A., Niestrawska, J.A., Ogden, R.W., Reinisch, A.J. & Schriefl, A.J. 2015 Modelling non-symmetric collagen fibre dispersion in arterial walls. *J Roy Soc Inter* **12**.
[10] Sáez, P., Alastrué, V., Peña, E., Doblaré, M. & Martínez, M.A. 2012 Anisotropic microsphere-based approach to damage in soft fibered tissue. *Biomech Model Mechanobiol* **11**, 595-608.
[11] Ogden, R.W. 2016 Nonlinear continuum mechanics and modelling the elasticity of soft biological tissues with a focus on artery walls. In *Lecture Notes from the Summer School "Biomechanics: trends in Modeling and Simulation", September, 2014, Graz, Austria* (ed. G.A.a.O. Holzapfel, R. W.). Heidelber, Springer.
[12] Winitzki, S. 2003 Uniform Approximations for Transcendental Functions. In *Computational Science and Its Applications — ICCSA 2003: International Conference Montreal, Canada, May 18–21, 2003 Proceedings, Part I* (eds. V. Kumar, M.L. Gavrilova, C.J.K. Tan & P. L'Ecuyer), pp. 780-789. Berlin, Heidelberg, Springer Berlin Heidelberg.
[13] Flory, P.J. 1969 *Statistical mechanics of chain molecules*. Chichester-New York, John Wiley & Sons.
[14] Kuhl, E., Garikipati, K., Arruda, E. & Grosh, K. 2005 Remodeling of biological tissue: Mechanically induced reorientation of a transversely isotropic chain network. *J Mech Phys Solids* **53**, 1552-1573.
[15] Kratky, O. & Porod, G. 1949 Röntgenuntersuchungen gelöster Fadenmoleküle. *Rec Trav Chim Pays-Bas Belg* **68**, 1106-1122.
[16] Bischoff, J.E., Arruda, E.A. & Grosh, K. 2002 A microstructurally based orthotropic hyperelastic constitutive law. *J Appl Mech* **69**, 570-579.
[17] Bischoff, J.E., Arruda, E.M. & Grosh, K. 2004 A rheological network model for the continuum anisotropic and viscoelastic behavior of soft tissue. *Biomech Model Mechanobiol* **3**, 56-65.
[18] Garikipati, K., Arruda, E.M., Grosh, K., Narayanan, H. & Calve, S. 2004 A continuum treatment of growth in biological tissue: the coupling of mass transport and mechanics. *J Mech Phys Solids* **52**, 1595-1625.
[19] Flynn, C. & McCormack, B.A.O. 2008 A simplified model of scar contraction. *J Biomech* **41**, 1582-1589.
[20] Flynn, C.O. & McCormack, B.A.O. 2009 A three-layer model of skin and its application in simulating wrinkling. *Comput Meth Biomech Biomed Eng* **12**, 125-134.
[21] Kuhl, E. & Holzapfel, G.A. 2007 A continuum model for remodeling in living structures. *J Mater Sci* **42**, 8811-8823.
[22] Kuhn, W. 1936 Beziehungen zwischen Molekühlgrösse, statistischer Molekülgestalt und elastischen Eigenschaften hochpolymerer Stoffe. *Kolloid-Zeitschrift,* **76**, 258-271.
[23] Arruda, E.M. & Boyce, M.C. 1993 A three-dimensional constitutive model for the large stretch behavior of rubber elastic-materials. *J Mech Phys Solids* **41**, 389-412.
[24] Cohen, A. 1991 A Padé approximant to the inverse Langevin function. *Rheol. Acta* **30**, 270-273.
[25] Nguessong, A.N., Beda, T. & Peyraut, F. 2014 A new based error approach to approximate the inverse langevin function. *Rheol. Acta* **53**, 585-591.
[26] Jedynak, R. 2015 Approximation of the inverse Langevin function revisited. *Rheol. Acta* **54**, 29-39.
[27] Marchi, B.C. & Arruda, E.M. 2015 An error-minimizing approach to inverse Langevin approximations. *Rheol. Acta* **54**, 887-902.
[28] Darabi, E. & Itskov, M. 2015 A simple and accurate approximation of the inverse Langevin function. *Rheol. Acta* **54**, 455-459.
[29] Flynn, C., Rubin, M.B. & Nielsen, P. 2011 A model for the anisotropic response of fibrous soft tissues using six discrete fibre bundles. *Int J Numer Meth Bio* **27**, 1793-1811.

[30] Limbert, G. 2011 A mesostructurally-based anisotropic continuum model for biological soft tissues--Decoupled invariant formulation. *J Mech Behav Biomed Mater* **4**, 1637-1657.
[31] Bischoff, J.E., Arruda, E.M. & Grosh, K. 2002 Finite element simulations of orthotropic hyperelasticity. *Finite Elem. Anal. Des.* **38**, 983-998.
[32] Lanir, Y. & Fung, Y.C. 1974 Two-Dimensional Mechanical Properties of Rabbit Skin—II: Experimental Results. *J Biomech* **7**, 171-182.
[33] Fung, Y.C. 1981 *Biomechanics: mechanical properties of living tissues*. New York, Springer-Verlag.
[34] Muñoz, M.J., Bea, J.A., Rodríguez, J.F., Ochoa, I., Grasa, J., Pérez del Palomar, A., Zaragoza, P., Osta, R. & Doblaré, M. 2008 An experimental study of the mouse skin behaviour: Damage and inelastic aspects. *J Biomech* **41**, 93-99.
[35] Edsberg, L.E., Mates, R.E., Baier, R.E. & Lauren, M. 1999 Mechanical characteristics of human skin subjected to static versus cyclic normal presures. *J. Rehabil. Res. Dev.* **36**.
[36] Ehret, A.E. & Itskov, M. 2009 Modeling of anisotropic softening phenomena: Application to soft biological tissues. *International Journal of Plasticity* **25**, 901-919.
[37] Ehret, A.E., Hollenstein, M., Mazza, E. & Itskov, M. 2011 Porcine dermis in uniaxial cyclic loading: sample preparation, experimental results and modeling. *Journal of Mechanics of Materials and Structures* **6**, 1125-1135.
[38] Li, W. & Luo, X.Y. 2016 An invariant-based damage model for human and animal skins. *Ann Biomed Eng* **44**, 3109-3122.
[39] Volokh, K.Y. 2007 Prediciton of arterial failure based on a microstructural bi-layer fiber-matrix model with softening. *Proceeding of the Amse Summer Bioengineering Conference - 2007*, 129-130
1075.
[40] Volokh, K.Y. 2011 Modeling failure of soft anisotropic materials with application to arteries. *J Mech Behav Biomed Mater* **4**, 1582-1594.
[41] Volokh, K.Y. 2014 On irreversibility and dissipation in hyperelasticity with softening. *Journal of Applied Mechanics, Transactions ASME* **81**.
[42] Yang, W., Sherman, V.R., Gludovatz, B., Schaible, E., Stewart, P., Ritchie, R.O. & Meyers, M.A. 2015 On the tear resistance of skin. *Nat Commun* **6**, 6649.
[43] Mazza, E., Papes, O., Rubin, M.B., Bodner, S.R. & Binur, N.S. 2005 Nonlinear elastic-viscoplastic constitutive equations for aging facial tissues. *Biomech Model Mechanobiol* **4**, 178-189.
[44] Mazza, E., Papes, O., Rubin, M.B., Bodner, S.R. & Binur, N.S. 2007 Simulation of the aging face. *J Biomech Eng* **129**, 619-623.
[45] Rubin, M.B. & Bodner, S.R. 2002 A three-dimensional nonlinear model for dissipative response of soft tissue. *Int J Solids Struct* **39**, 5081-5099.
[46] Weickenmeier, J. & Jabareen, M. 2014 Elastic–viscoplastic modeling of soft biological tissues using a mixed finite element formulation based on the relative deformation gradient. *Int J Numer Meth Bio* **30**, 1238-1262.
[47] Weickenmeier, J., Jabareen, M. & Mazza, E. 2015 Suction based mechanical characterization of superficial facial soft tissues. *J Biomech* **48**, 4279-4286.
[48] Taber, L.A. 1995 Biomechanics of growth, remodeling and morphogenesis. *Applied Mechanics Review* **48**, 487-545.
[49] Epstein, M. 2015 Mathematical characterization and identification of remodeling, growth, aging and morphogenesis. *J Mech Phys Solids* **84**, 72-84.
[50] Neumann, C.G. 1959 The expansion of an arrea of skin by progressive distension of a subcutaneous balloon; us eo fthe method for securing skin for subtotal reconstruction of the ear. *Plastic and Reconstructive Surgery* **19**, 124-130.
[51] Socci, L., Pennati, G., Gervaso, F. & Vena, P. 2007 An axisymmetric computational model of skin expansion and growth. *Biomech Model Mechanobiol* **6**, 177-188.
[52] Rodriguez, E.K., Hoger, A. & McCulloch, A.D. 1994 Stress-dependent finite growth in soft elastic tissues. *J Biomech* **27**, 455-467.
[53] Lubarda, V.A. & Hoger, A. 2002 On the mechanics of solids with a growing mass. *Int J Solids Struct* **39**, 4627-4664.
[54] Menzel, A. & Kuhl, E. 2012 Frontiers in growth and remodeling. *Mech Res Commun* **42**, 1-14.
[55] Buganza Tepole, A., Ploch, C.J., Wong, J., Gosain, A.K. & Kuhl, E. 2011 Growing skin: A computational model for skin expansion in reconstructive surgery. *J Mech Phys Solids* **59**, 2177-2190.
[56] Kuhl, E. & Steinmann, P. 2003 Theory and numerics of geometrically non-linear open system mechanics. *Int J Numer Meth Eng* **58**, 1593-1615.

[57] Buganza Tepole, A., Gosain, A.K. & Kuhl, E. 2012 Stretching skin: The physiological limit and beyond. *Int. J. Non-Linear Mech.* **47**, 938-949.
[58] Zöllner, A., Buganza Tepole, A., Gosain, A.K. & Kuhl, E. 2012 Growing skin: tissue expansion in pediatric forehead reconstruction. *Biomech Model Mechanobiol* **11**, 855-867.
[59] Zöllner, A.M., Buganza Tepole, A. & Kuhl, E. 2012 On the biomechanics and mechanobiology of growing skin. *J Theor Biol* **297**, 166-175.
[60] Buganza-Tepole, A., Gart, M., Purnell, C., Gosain, A. & Kuhl, E. 2015 Multi-view stereo analysis reveals anisotropy of prestrain, deformation, and growth in living skin. *Biomech Model Mechanobiol* **14**, 1007-1019.
[61] Buganza Tepole, A., Gart, M., Gosain, A.K. & Kuhl, E. 2014 Characterization of living skin using multi-view stereo and isogeometric analysis. *Acta Biomater* **10**, 4822-4831.
[62] Xu, F. & Lu, T. 2011 *Introduction to Skin Biothermomechanics and Thermal Pain*. Heidelberg Dordrecht London New York, Springer; 414 p.
[63] Ulrich, D., Noah, E.-M., Fuchs, P. & Pallua, N. 2001 Burn injuries caused by air bag deployment. *Burns* **27**, 196-199.
[64] Sulzberger, M.B., Cortese, T.A., Fishman, L. & Wiley, H.S. 1966 Studies on blisters produced by friction. I. Results of linear rubbing and twisting technics. *J Invest Dermatol* **47**, 456-465 contd.
[65] Knapik, J.J., Reynolds, K.L., Duplantis, K.L. & Jones, B.H. 1995 Friction blisters. Pathophysiology, prevention and treatment. *Sports Medicine* **20**, 136-147.
[66] Gefen, A. 2011 How do microclimate factors affect the risk for superficial pressure ulcers: A mathematical modeling study. *J Tissue Viability* **20**, 81-88.
[67] McBride, A., Bargmann, S., Pond, D. & Limbert, G. 2016 Thermoelastic modelling of the skin at finite deformations. *Journal of Thermal Biology* **62**, 201-209.
[68] Khunger, N., Molpariya, A. & Khunger, A. 2015 Complications of tattoos and tattoo removal: stop and think before you ink. *Journal of Cutaneous and Aesthetic Surgery* **8**, 30-36.
[69] Kuperman-Beade, M., Levine, V.J. & Ashinoff, R. 2001 Laser removal of tattoos. *American Journal of Clinical Dermatology* **2**, 21-25.
[70] Choudhary, S., Elsaie, M.L., Leiva, A. & Nouri, K. 2010 Lasers for tattoo removal: a review. *Lasers in Medical Science* **25**, 619-627.
[71] Ross, J.R. & Matava, M.J. 2011 Tattoo-induced skin "burn" during magnetic resonance imaging in a professional football player: a case report. *Sports Health* **3**, 431-434.
[72] Kreidstein, M.L., Giguere, D. & Freiberg, A. 1997 MRI Interaction with Tattoo Pigments: Case Report, Pathophysiology, and Management. *Plastic and Reconstructive Surgery* **99**, 1717-1720.
[73] Kenney, W.L., DeGroot, D.W. & Alexander Holowatz, L. 2004 Extremes of human heat tolerance: life at the precipice of thermoregulatory failure. *Journal of Thermal Biology* **29**, 479-485.
[74] Schar, C. 2016 Climate extremes: The worst heat waves to come. *Nature Clim. Change* **6**, 128-129.
[75] Defense, U.D.o. 2016 Active Denial Technology. (DOE.
[76] Nelson, D.A., Walters, T.J., Ryan, K.L., Emerton, K.B., Hurt, W.D., Ziriax, J.M., Johnson, L.R. & Mason, P.A. 2003 Inter-species extrapolation of skin heating resulting from millimeter wave radiation: modelling and experimental results. *Health Physics* **84**, 608-615.
[77] Pennes, H.H. 1948 Analysis of tissue and arterial blood Temperatures in the resting human forearm. *Journal of Applied Physiology* **1**, 93-122.
[78] Piérard, G.E., Hermanns, J.F. & Lapière, C.H. 1974 Stéréologie de l'interface dermo-épidermique. *Dermatologica* **149**, 266-273.
[79] Piérard-Franchimont, C. & Piérard, G.E. 1987 Assessment of aging and actinic damages by cyanocrylate skin surface strippings. *Am J Dermopathol* **9**, 500-509.
[80] Setaro, M. & Sparavigna, A. 2001 Irregularity skin index (ISI): a tool to evaluate skin surface texture. *Skin Res Technol* **7**, 159-163.
[81] Lévêque, J.L. 1999 EEMCO guidance for the assessment of skin topography. *J Eur Acad Derm Vener* **12**, 103-114.
[82] Lévêque, J.L. & Audoly, B. 2013 Influence of Stratum Corneum on the entire skin mechanical properties, as predicted by a computational skin model. *Skin Res Technol* **19**, 42-46.
[83] Hashimoto, K. 1974 New methods for surface ultrastructure:comparative studies of scanning electron microscopy, transmission electron microscopy and replica method. *International Journal of Dermatology* **13**, 357-381.
[84] Quatresooz, P., Thirion, L., Piérard-Franchimont, C. & Piérard, G.E. 2006 The riddle of genuine skin microrelief and wrinkles. *International Journal of Cosmetic Science* **28**, 389-395.
[85] Limbert, G. & Kuhl, E. 2017 On skin microrelief and the emergence of expression micro-wrinkles. *Soft Matter*, submitted.